ASSESSING THE ULTRAVIOLET OPTICAL SCREENING TOOL FOR DELINEATING AN IN-SITU, WATER-COVERED, CONTAMINATED SEDIMENT LAYER

by

Kirklyn Barry Davidson

Submitted in partial fulfilment of the requirements
for the degree of Master of Applied Science

at

Dalhousie University
Halifax, Nova Scotia
August 2020

Table of Contents

List of Tables

List of Figures

Abstract

A stabilization lagoon in Pictou County, NS, has been receiving industrial wastewater for the past 50+ years and is slated for remediation. Conventional sampling has identified a layer of black effluent influenced sediment contaminated with dioxins and furans overlying an uncontaminated grey estuarine influenced sediment. In this thesis, laboratory and field testing on the sediments are presented as a proof of concept for a unique application of the Ultraviolet Optical Screening Tool (UVOST).

This research presents an alternative use for the UVOST; the ability to delineate the spatial distribution of an organic-rich, unconsolidated, water-covered sediment, contaminated with dioxins, furans, and elevated metals. The results of this study indicate that the UVOST can be utilized at freshwater aquatic sites to delineate an organic-rich sediment which overlays a clastic sediment layer. The resolution of the acquired data was shown to provide multiple surface elevations (i.e. water and sediment layers) simultaneously.

List of Abbreviations Used

ASD: Analytical Spectral Devices

BEIS: Black Effluent Influenced Sediment

BSHL: Boat Harbour Stabilization Lagoon

CCME: Canadian Council of Ministers of the Environment

DI: Deionization

DNAPL: Dense non-aqueous phase liquid

DO: Dissolved Oxygen

ESA: Environmental Site Assessment

GEIS: Grey Estuarine Influenced Sediment

HDPE: High-density polyethylene

HRSC: High Resolution Site Characterization

ISQG: Interim Sediment Quality Guideline

LIF: Light Induced Fluorescence

LOD: Limit of Detection

NAPL: Non-aqueous phase liquid

NIRS: Near Infrared Spectrometer

PAH: Polycyclic aromatic Hydrocarbon

PEL: Probable Effects Level

PHC: Petroleum Hydrocarbon

QA/QC: Quality Control and Quality Assurance

RE: Reference Emitter

STDEV: Standard deviation

SQG: Sediment Quality Guideline

TDS: Total Dissolved Solids

UV: Ultraviolet

UVOST: Ultraviolet Optical Screening Tool

VOC: Volatile Organic Compound

%RE: Percent Reference Emitter

Acknowledgements

Over the course of this thesis these last two years I have received support from countless individuals. First and foremost, I would like to thank my supervisor Craig Lake and co-supervisor Ian Spooner for their time and dedication to their students. Without both of their guidance, and the opportunities they have provided, I would not find myself in the position I do today, so thank you.

I would like to acknowledge my colleagues Baillie Holmes and Hayden Tackley for their support during my research. These individuals assisted me with sample collections, thesis edits, and were always there to support me in whatever way was needed.

Within Dalhousie's Civil department, I would also like to give a special thanks to June Ferguson, Terra Chartrand and Paula Zwicker for all of their assistance. Each of you was always willing to lend, and always did so with a big smile, which is appreciated!

I would like to give a special thanks to SCG Industries team whom I worked alongside with during the course of this research. Without the support of this crew, this project would not have been possible.

Last but not least, I would like to thank all of my family for the support that they have given me throughout the years. Between the moral support, humor relief, and them continuously cheering me on, they have helped me get to where I am today. Thank you for everything.

Chapter 1 Introduction

1.1 Opening Statement

Prior to its conversion into a stabilization lagoon, Boat Harbour (Pictou County, NS) was an estuary (Davidson, 2018; Holmes, 2018; Spooner and Dunnington, 2016). Since 1967, the operation of a kraft pulp and paper effluent treatment facility has resulted in the deposition of a black effluent influenced sediment (BEIS) (~26cm; Alimohammadi et al., 2020; Spooner and Dunnington, 2016; Davidson, 2018; Holmes, 2018) over top of a grey estuarine influenced sediment (GEIS) which was present prior to the introduction of effluent from the treatment facility. This BEIS layer is known to be contaminated with elevated concentrations of heavy metals, as well as organic contaminants such as dioxins and furans (GHD Limited, 2018a; Holmes, 2018; Hoffman et al., 2019; Hoffman et al., 2017). At the time of this thesis, the site is slated to be remediated. The driver of this remediation is the Boat Harbour Act which was passed in 2015 as the result of a breach in the kraft pulp and paper mills effluent pipeline which allowed effluent to pump directly into Pictou Harbour. The remediation project is focused on the removal of the entire BEIS layer and the return of the stabilization lagoon to its former state as an estuary by leaving only the GEIS on the basin floor. Being able to accurately assess the thickness of a contaminated sediment layer such as this (i.e. large area, under water) is integral to the development of remediation approaches and project costs. The development of an in-situ test that can rapidly, yet effectively, establish contaminated sediment thickness is the focus of this research.

In this thesis, SCG Industries Limited acted as a research partner in the development of a specific application to accurately measure the in-situ BEIS thickness using the

Ultraviolet Optical Screening Tool (UVOST). The UVOST is equipped for light and conductivity detection allowing for a real-time multivariable analysis of sediment. Traditionally the UVOST is used for the assessment of soils impacted by hydrocarbon contamination. Since the UVOST is capable of measuring the fluorescence signature emitted by fluorophores in sediment, the focus of this work is to assess the potential to delineate the boundaries between different layers in this effluent receiving pond using the UVOST. The fluorescence signatures produced by these two different materials and overlying water are investigated in this thesis. By defining the boundaries of various mediums, the ability of the UVOST to accurately determine the BEIS's thickness has been examined.

1.2 Fluorescence Overview

Fluorescence is defined as the emission of light from a substance in response to the application of energy (Guilbault, 1990; Lakowicz, 2006). On average, light travels at 30 cm per nanosecond. However, the fluorescence emission of a given substance can often have a sub-nanosecond lifespan (Lakowicz, 2006). The short lifespans require sophisticated optical and electronic measurement techniques to examine these emissions for practical use. Techniques to measure fluorescence emissions are becoming increasingly prevalent across a variety of disciplines, particularly in the field of environmental monitoring (Bero et al., 1995; Bidmanova et al., 2016; Christensen et al., 2005; Guilbault, 1990; Hudson et al., 2007; Kallithrakas-Kontos et al., 2016; Kotzick and Niessner, 1996; Lakowicz, 2006).

Fluorescence is a subcategory of the phenomena known as luminescence, which refers to an excitation of the molecular state within a compound (Becker, 1969; Guilbault, 1990; Lakowicz, 2006). This excitation occurs as an emission of light being defined as

either fluorescence or phosphorescence. Fluorescence is the primary focus of this thesis due to its use in environmental monitoring. At the atomic level, fluorescence is dependent on the excitation of singlet states, the state in which no electrons are unpaired (Figure 1). When light is applied to an atom, an electron in its ground state (i.e. lowest energy state) becomes excited and moves to a higher orbital state (Lakowicz, 2006). The rapid decay of a fluorescent emission is caused by the return of the electron within the excited orbital to the ground state. This results in the emission of energy (in the form of a photon) which is responsible for the light emitted from the substance of interest.

To show what occurs during fluorescence, the following stages (1-6) (Figure 1) can be followed, which represent a simplified version of a Jablonski Diagram (Figure 2). Step 1 depicts energy in the form of light being introduced to an atom (Step 2) which has its electrons currently in the ground state (S0) (Figure 1). After light interacts with the atom, the light is absorbed by the atom (Step 3), thus exciting its electrons (Step 4) into a higher state (either S1 or S2). The absorption of the energy (Step 4) is depicted by the solid black arrow showing the movement of the electron (e^-) from its ground state (S0) to a higher state (in this case S2) (Figure 1). When an electron becomes excited (Step 4), it rapidly returns to its ground state by releasing energy (Step 5). This release of energy produces light (Step 5) in the form of a released photon which is known as fluorescence. The fluorescence results in the return of the electron from S2 back to its ground state (S0) (Step 6).

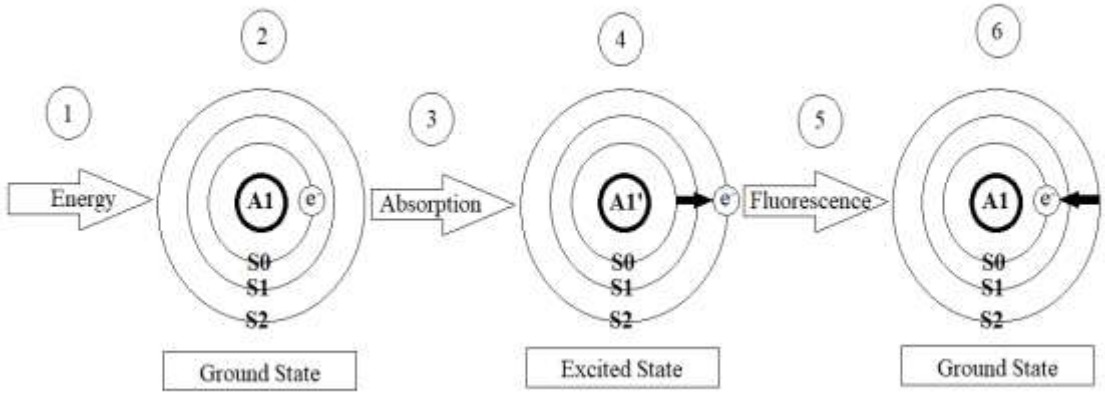

Figure 1: Simplified process of an atom fluorescing (modified from Lakowicz (2006)).

The Jablonski diagram shows the state of an electron within an atom, as depicted by S_0, S_1, and S_2 (Figure 2). These are comparable to the electron states S0, S1, and S2 (Figure 1), with both S0 and S_0 representing the ground state of the electron within the atom. At each of these states, it is possible for an electron to exist in a multitude of vibrational energy levels (horizontal lines, Figure 2) (Lakowicz, 2006). These energy levels are annotated as 0, 1, and 2, to the right of each state (S_0, S_1, and S_2), with 0 (the bolded line) being considered the lowest vibrational energy level of each state. The transitional stages of this processes (depicted by the horizontal lines in Figure 2), beginning with absorption (hV_A) result in either the phosphorescence of the atom (hV_P), or the fluorescence of the atom (hV_F) (Guilbault, 1990; Jabłoński, 1935; Lakowicz, 2006). The UVOST is

capable of detecting these compounds which fluoresce and are known as fluorophores (Becker, 1969; Guilbault, 1990; Lakowicz, 2006; Martin and St. Germain, 2008).

.

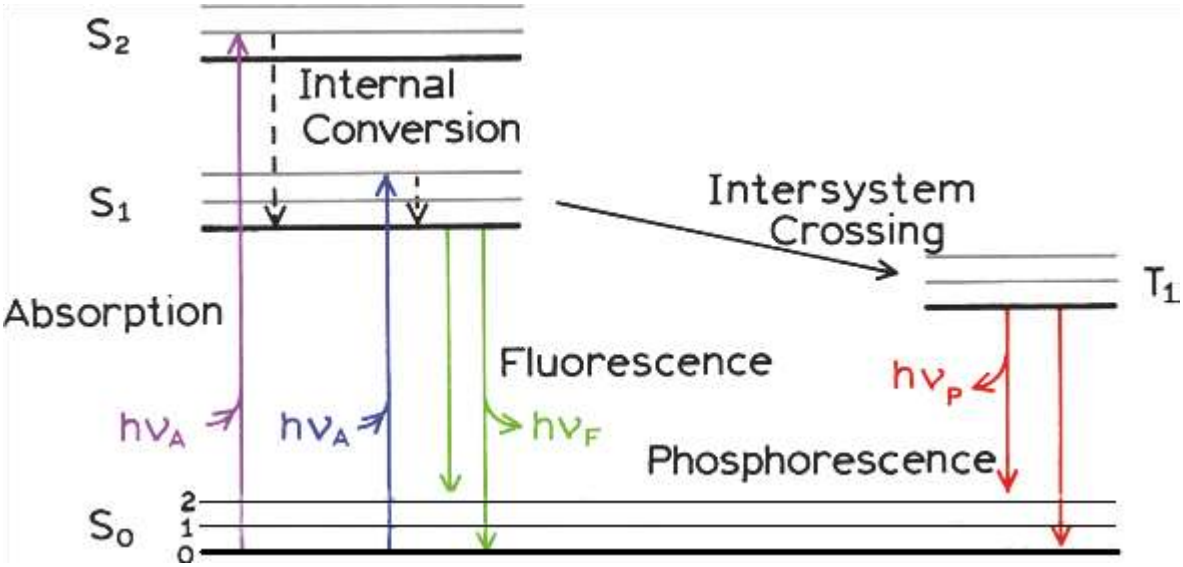

Figure 2: Jablonski Diagram (from Lakowicz, 2006).

1.2.1 Fluorophores and Quenchers

In general, fluorescence occurs frequently in aromatic compounds such as polycyclic aromatic hydrocarbons (PAHs), an example of a fluorophore (Martin and St. Germain, 2008). The process begins with the absorption of light by the fluorophore. The electrons within the fluorophore then become excited and achieve a higher state, moving from the ground state (S_0) to a higher state (S_1 or S_2) (Becker, 1969; Guilbault, 1990; Lakowicz, 2006). While doing so, the vibrational energy level within each state can also increase. Molecules which absorb light will have their vibrational state rapidly decay to the lowest vibrational level of S_1. This process is known as internal conversion and is typically completed before emission occurs (Guilbault, 1990; Jabłoński, 1935; Lakowicz, 2006; Verhoeven, 1996). As a result of this process, emission which occurs during fluorescence typically begins at the lowest vibrational energy level of S_1.

After the vibrational energy of the higher state decreases to the lowest energy state of S_1, the electron moves back to its original state, releasing a photon in the process. The release of this photon equates to a release of energy which results in a pulse of light otherwise known as fluorescence (Lakowicz, 2006; Verhoeven, 1996). In certain cases, and with dependent energy inputs, a molecule which has its electrons in the S_1 state can undergo a spin conversion of its electron (Lakowicz, 2006). This process transfers an electron from the singlet state to the triplet state at T_1 (Figure 2). The difference between the singlet state and triplet state can be seen in Figure 3. Phosphorescence occurs when there is an emission from T_1 which returns the electron to the S_0 state. This process is known as intersystem crossing (Verhoeven, 1996). Phosphorescence is often a much slower process then fluorescence (Lakowicz, 2006).

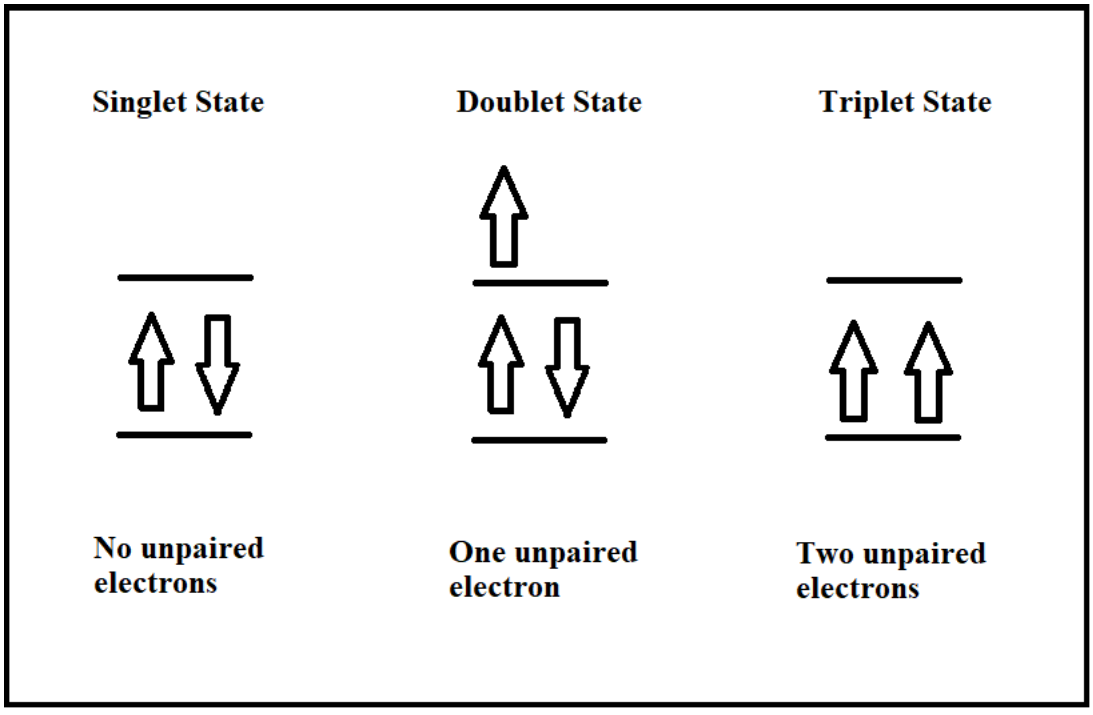

Figure 3: Examples of the varying states of electrons in an atom (modified from Burrows et al. (2008) and Schaller (2020)).

When examining the fluorescence of a fluorophore, fluorescence quenching can occur. Quenching is the process by which the intensity of fluorescence decreases. This process of fluorescence quenching can be caused by a number of factors. One cause of fluorescence quenching is collisional quenching. This occurs when an excited fluorophore collides with a separate molecule (the quencher) within the same solution. The collision of these two molecules can deactivate the fluorophore, thus rendering it unable to fluoresce through loss of energy during the collision. Some common examples of possible quenchers include halogens, amines, oxygen, and molecules which are electron deficient. It is important to note that the molecules themselves are not altered at all by the quenching process. There is simply an exchange of energy between the two molecules (Lakowicz, 2006).

In addition to collisional quenching, fluorophores may be quenched in many other ways. Another process known as static quenching occurs when fluorophores interact with other substances within the mixture of interest and create complexes which are nonfluorescent by-products. This method of quenching occurs when a molecule is in its ground state and therefore quenching is not dependent on molecular collisions (Lakowicz, 2006). Other methods of quenching can be much more trivial. An example of this would be the attenuation of the light source being introduced to the fluorophore, thus disrupting the process of fluorescence (Lakowicz, 2006). Multiple examples of fluorophores and their potential quenchers are presented below (Table 1).

Table 1: Examples of fluorescent quenchers and their associated fluorophores (modified from Lakowicz (2006)).

Quenchers	Typical fluorophore
Acrylamide	Tryptophan, pyrene, and other fluorophores
Amines	Anthracene, perylene
Amines	Carbazole
Amine anesthetics	Perylene, anthroyloxy probes
Bromate	*Not described
Bromobenzene	Many fluorophores
Carbon disulfide	Laser dyes, perylene
Carboxy groups	Indole
Cesium (Cs+)	Indole
Chlorinated compounds	Indoles and carbazoles
Chloride	Quinolinium, SPQ
Cobalt (Co2+)	NBD, PPO, Perylene
Dimethylformamide	Indole
Disulfides	Tyrosine
Ethers	9-Arylxanthyl cations
Halogens	Anthracene, naphthalene, carbazole
Halogen anesthetics	Pyrene, tryptophan
Hydrogen peroxide	Tryptophan
Iodide	Anthracene
Imidazole, histidine	Tryptophan
Indole	Anthracene, pyrene, cyanoanthracene
Methylmercuric chloride	Carbazole, pyrene
Nickel (Ni2+)	Perylene
Nitromethane and nitro compounds	Polycyclic aromatic hydrocarbon
Nitroxides	Naphthalene, PAH, Tb3+, anthroyloxy probes
NO (nitric oxide)	Naphthalene, pyrene
Olefins	Cyanonaphthalene, 2,3-dimethylnaphthalene, pyrene
Oxygen	Most fluorophores
Peroxides	Dimethylnaphthalene
Picolinium nicotinamide	Tryptophan, PAH
Pyridine	Carbazole
Silver (Ag+)	Perylene
Succinimide	Tryptophan
Sulfur dioxide	Rhodamine B
Thallium (Tl+)	Naphthylamine sulfonic acid
Thiocyanate	Anthracene, 5,6-benzoquinoline
Xenon	*Not described

1.2.2 Steady State and Time Resolved Measurements

When examining technologies which measure fluorescence, there are two distinct types; steady state and time resolved measurements (Becker, 1969; Guilbault, 1990; Lakowicz, 2006). The most commonly used type is steady state because of the nanosecond timescale in which fluorescence occurs (Lakowicz, 2006). Steady state measurements are taken with the sample being constantly illuminated and observed for the entirety of the illumination. During the process, a beam of light is continuously applied to the sample and both the intensity and wave spectrum of the emission are recorded (Lakowicz, 2006). The illumination results in a steady state, which is reached almost as soon as the sample is subjected to light (Lakowicz, 2006). The time resolved method is used to measure either anisotropy decays or intensity decays of samples. The time resolved method relies on the sample being subjected to a discrete pulse of light in which the duration of the pulses is set to be less than the known decay time of the sample of interest (Lakowicz, 2006). For this measurement to be taken, high speed detection systems which are capable of recording anisotropy or intensity measurements on a nanosecond timescale are required. The UVOST utilizes the time resolved method to analyze fluorescence within samples.

1.3 UVOST Technology

1.3.1 General

Dakota Technologies (Fargo, North Dakota, USA) is the developer of the "Ultraviolet Optical Screening Tool" (UVOST). This device uses push probe technology and is able to rapidly detect polycyclic-aromatic hydrocarbons (PAHs) within non-aqueous phase liquids (NAPL). This tool is capable of collecting time-resolved fluorescence measurements from a sample. PAHs such as light petroleum distillates (gasoline, diesel,

kerosene, motor oil, cutting fluids, hydraulic fluids) are within the instruments range of detection and can be identified as the push probe's primary sensor passes through the sediment of interest. The UVOST's range of detection begins to diminish, however, as the molecular structure of the PAHs become larger in form. PAHs such as coal tar, creosote, and bunker oils are not detected as accurately as smaller PAHs, resulting in signatures which may be difficult to interpret (St. Germain, 2019). Compounds which are characterized as polychlorinated biphenyls, chlorinated dense non-aqueous phase liquids (DNAPL), and aqueous phase PAHs are outside of the UVOST's detection range. Common field applications of the UVOST often involve fuel storage sites which have experienced some form of leakage. These sites include pipelines, refineries, and fueling stations, as well as tailing ponds (St. Germain, 2019).

1.3.2 UVOST Operation

A hydraulically pushed probe allows for the collection of both conductivity and optical data simultaneously. The base design of the UVOST system (left) and UVOST probe are shown below in Figure 4. In operation, the UVOST utilizes a 308 nm xenon chloride laser to send a pulse of light through a fiber optic cable and into the soil via a sapphire window on the side of the probe (Figure 4, right). This sapphire window is set between the sample and the fiber optical cable to maintain the integrity of the cable. The UV light which is emitted from the fiber optic cable is absorbed and re-emitted from the sample of interest. The pulse of light emitted by the UVOST interacts with the molecules outside of the sapphire window (i.e. in the soil). These molecules absorb the light energy, which excites their electrons from the ground state to a higher state. These electrons in the higher state rapidly move back to the ground state and release energy in the form of light

as a by-product of this process. The light which is re-emitted (or fluoresced) is detected by a secondary optical cable and is interpreted using proprietary software after the light passes through a series of 4 nm cut-off filters. The cut off filters create a time delay so that all waveforms can be received at the same time. The delay allows for the data to be analyzed as a 2D waveform instead of a 3D waveform for the purposes of interpretation (Martin and St. Germain, 2008).

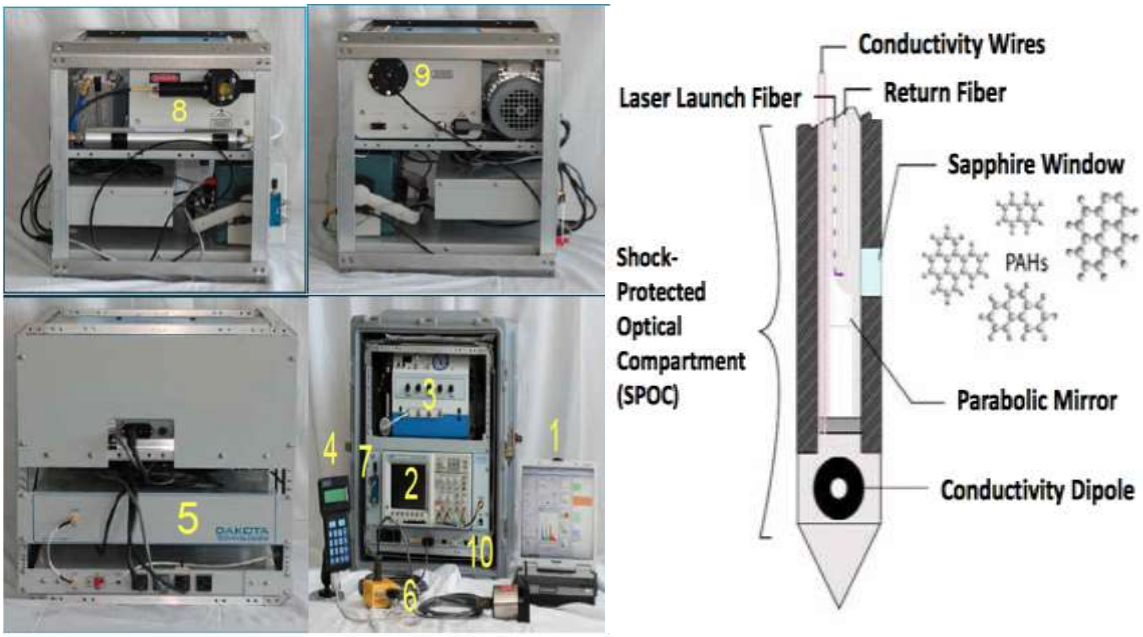

Figure 4: External components of the Ultraviolet Optical Screening Tool (UVOST) by Dakota Technologies; control computer (1); oscilloscope (2); laser (3); remote display (4); emission detection module (5); breakout box (6); fiber I/O (7); launch assembly (8); fiber-based trigger (9); e-deck (10) (from Martin and St. Germain, 2008) (left) and the UVOST probe and its components (Creaden, 2015) (right).

To normalize the data so it can be compared to other samples, a compound known as the reference emitter (RE) was used. The RE is a hydrocarbon blend of known concentrations, which is provided by Dakota Technologies. It is the normalizing standard which is used with all UVOST devices (St. Germain, 2019). Using this standard RE enables the comparison of the data with a known compound for further assessment. Variations in signal strength sent to the sample are accounted for during the normalization process. The

fluorescence intensity of samples collected using the UVOST are measured as a function of %RE.

Data collected during a UVOST operation is both qualitative and semi-quantitative. The UVOST has a limit of detection between 10-500 ppm for compounds it was designed to investigate (petroleum fuels and various lubricants). When assessing returned data, the software calculates the areas beneath the wavelength curves that are generated. The wavelengths of interest for the UVOST are the 350 nm (blue), 400 nm (green), 450 nm (orange), and 500 nm (red) wavelengths. Varying combinations of these colours are used to generate the colour fill used in the graphs produced during the software analysis. These graphs plot the sample with respect to %RE and show fluorescence intensities at each sampled point.

1.3.3 UVOST False Positives and Negatives

When using the UVOST, there are several false positives and false negatives that can be detected by the tool. False positives detected by the UVOST make the %RE signal strength appear stronger. In this thesis, the organic matter in the BEIS produces a "beneficiary" false positive. By contrast, false negatives show a lower %RE signal than expected. Examples of both false positives and false negatives can be seen below (Table 2 and Table 3). These signals can range from very weak (>1 %RE) to strong (>10 %RE) based on the composition of the compound providing the false return.

Table 2: False positive examples (modified from Martin and St. Germain, 2008).

UVOST False Positives				
Compound	Signal Strength			
	Very weak (>1% RE)	Weak (1-3% RE)	Medium (3-10% RE)	Strong (>10% RE)
Sea shells		✓	✓	
Paper			✓	✓
Peat/meadow mat		✓	✓	
Calcite/calcareous sands		✓	✓	
Asphalt	✓			
Stiff/viscous tars		✓		
Certain soils		✓		
Tree roots		✓	✓	
Sewer lines			✓	✓
Coal	✓			
Quicklime		✓		

Table 3: False negative examples (modified from Martin and St. Germain, 2008).

UVOST False Negatives				
Compound	Signal Strength			
	Very weak (>1% RE)	Weak (1-3% RE)	Medium (3-10% RE)	Strong (>10% RE)
Weathered fuels (especially gasoline)		✓	✓	
Aviation gasoline		✓		
Coal tars	✓			
Creosotes	✓			

1.3.4 UVOST QA/QC Procedures

Accuracy, precision, and reliability of data collected during the operation of a UVOST is maintained by following the guidelines of the manufacturer. The tool is calibrated by taking a sample of both the RE and background (in air). To collect background data, the sapphire window is wiped clean (without any physical sample present), and the UVOST software is initiated by running the 'collect background' function. External light can affect this reading, so care must be taken to minimize light exposure on the sapphire window during background data collection. When calibrating background levels, readings

must be maintained below 5 mV to ensure the best quality data is collected during operation. Initial RE data is collected by placing the RE on the sapphire window and running the 'collect RE' function in Dakota Technologies proprietary software. Following this step, the RE intensity of the UVOST must be adjusted so that the area under the curve is equal to 10000 +/- 1000 pVs. The intensity is adjusted using the "launch adjust" knob, with the results of each adjustment being displayed on the oscilloscope. This calibration must be conducted prior to each sample, and after every 30 min of continuous operation, to account for factors such as the aging of the tool, differences in the length of fiber optical cables used, and changes in the energy levels which are being emitted from the laser. Without such re-calibration, %RE signals may not remain consistent. While sampling, a consistent penetration speed of 2 cm/s or less must be maintained for optimal data collection. If penetration speeds exceed 2 cm/s, gaps in the dataset may result. This can cause a "blurring" effect resulting from missing data points and can lead to poor interpretation of the sample of interest.

The UVOST lacks a method of direct measurement of depth during sediment sampling and as such requires an accurate external source to do this. A string pot (potentiometer) can be attached to the UVOST rod deployment station for the purpose of this monitoring, but must consistently be checked for accuracy of measurement, as well as physical state (wearing).

1.3.5 Case Study of a Typical UVOST Application

Wagner and Barker (2019) present a case study of the UVOST in a typical application. It is to be noted that the ultraviolet optical screening tool was designed for delineating PAHs, and as such, most of the literature is reflective of this. Wagner and

Barker (2019) examined the legacy of PAHs at both military and industrial sites underlain with permafrost in the Alaskan Arctic and along the Arctic Ocean coast. This study examined 143 vertical UVOST logs at two sites of interest, the first being an airstrip site and the second being a powerhouse station. The logs were then compared to one another, and results were plotted to discover the source of the spill. Both sites had an accumulation of PAHs on both the surface and subsurface, with a vertically heterogenous distribution throughout (Wagner and Barker, 2019). When comparing the samples horizontally however, the %RE readings ranged from 0-82.7 %RE. The highest reading was at the original spill site at each location. Wagner and Barker (2019) concluded that the variation in intensities can be attributed to the initial source of the spills and that their work could be applied when investigating local bodies of water.

1.4 Research Question

At pulp and paper treatment facilities where organic-rich, water-covered sediment is present and requires remediation, it is often costly and time-consuming to obtain large numbers of samples to delineate the thickness and distribution of the contaminated sediment from underlying sediments. The purpose of this thesis is to explore a potential approach to this problem by answering the following question: can UVOST technology be used to delineate an organic-rich, water-covered, contaminated sediment layer, where hydrocarbons are not the main contaminant of concern? The objective of the study is to evaluate a cost and time effective method with the potential to obtain accurate volume estimates of an organic-rich sediment by delineating multiple mediums. The working hypothesis of this study is that the difference in composition of organic sediment will result in the production of unique fluorescent signatures which can be used to delineate changing

sediment stratigraphy. To investigate this research question, this thesis has been organized in the following manner:

Chapter 2: Site Background: This chapter provides a summary of the BHSL where the UVOST has been applied. Topics which have been examined include local geology, sediments of interest within the BHSL, as well as previous research conducted at the BHSL.

Chapter 3: Methods: The development of a qualitative method of medium interpretation is presented. A four-phase proof-of-concept, from the initial to final stages of the development of the interpretation method is outlined. These four phases include sediment collection techniques, methods of differentiating organics within the various sediments, and the interpretation and development of methods used during both laboratory and field trails.

Chapter 4: Results and Discussion: This chapter details results collected for each of the four phases of the proof-of-concept investigation. Water quality parameters, compiled results of organics analysis, and UVOST data from both the laboratory and field trials are presented. Discussed during the presentation of laboratory and field trials are the methods which were developed as part of the interpretation and delineation of multiple mediums within the BHSL.

Chapter 5: Summary and Conclusion: In this chapter, the results of this thesis with relation to the research question are summarized. Inherent knowledge gaps in the literature are noted and future recommendations to bridge such knowledge gaps are suggested.

Chapter 2 Site Background

2.1 Boat Harbour Effluent Treatment Facility

The Boat Harbour effluent treatment facility and its various component are illustrated in Figure 5. The primary contributors (in terms of volume) to the wastewater effluent since the opening of the facility in 1967 is wood pulp, as well as the effluent from a chloralkali plant which was active from 1971 to 1992. Effluent moves through six locations (A to F of Figure 5) before it discharges to the marine environment at location F. Effluent is pumped from Abercrombie Point (Figure 5, A) through an underwater pipeline (B) and is discharged through an open air channel to the twin settling basins(C). The effluent then flows through an outlet and into a series of the aeration ponds (D). Nutrients are added to the effluent to promote bacterial growth and degradation. The effluent then flows to the stabilization lagoon (E), where further sedimentation occurs prior to discharge at location F. The stabilization lagoon (E), referred to as the Boat Harbour Stabilization Lagoon (BHSL) in this thesis, is the location which was assessed in this study.

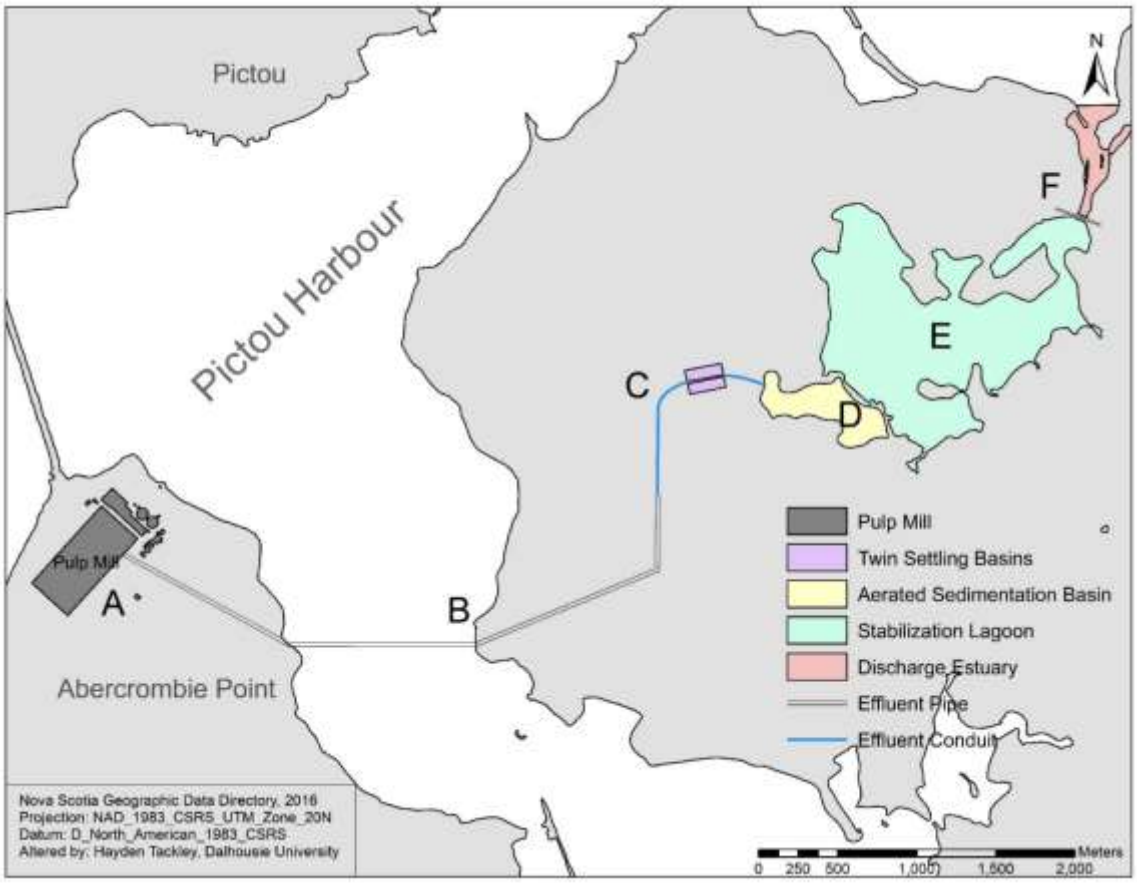

Figure 5: Boat Harbour effluent treatment facility (South of the Pictou Landing First Nation (PLFN)) and its components (A-F) (from Tackley, 2019).

2.1.1 Local Geology Near the Treatment Facility

In the general vicinity of the BHSL, the majority of surficial sediment is comprised of the Tony River Till and forms a hummocky ground moraine (Quaternary in age). These sediments consist of deposits of gravel, sand and fine grained material, which range from 2 to 25 m thick (Davidson, 2018; GHD Limited, 2018a; Holmes, 2018b; JWEL and Beak, 1992; Stea et al., 1992). The western portion of the site (Figure 5, C) differs in that it is overlain by the Silty Till Plain (Quaternary age), which has been described by GHD Limited (2018a) as a silty till with compact materials from both distal and local sources, and ranging from 3-30 m thick (Stea et al., 1992). The regional bedrock consists of

Pennsylvanian-aged sedimentary rocks (Davidson, 2018; GHD Limited, 2018a; Holmes, 2018; JWEL and Beak, 1992; Stea et al., 1992). The bedrock has been structurally deformed and shows east-west trending ridge and valley structures. The local rocks belong to the Pictou Group (Cape John, Tatamagouche, and Balfron Formations) and consist of red and grey fluvial sandstone (non-marine), shale, mudstone, and conglomerate, and lacustrine limestone (Davidson, 2018; GHD Limited, 2018a; Holmes, 2018; JWEL and Beak, 1992; Stea et al., 1992)

2.1.2 Surficial Soils Found Within the Stabilization Lagoon

Song (2020), Alimohammadi et al (2019), Davidson (2018), Holmes (2018) and Spooner and Dunnington (2016) have collected multiple gravity and percussion core samples from the BHSL of both the BEIS and GEIS. The sediment contained within the BHSL has been found to generally consists of two facies. These facies are visually and chemically distinct from one another (Figure 6). The basal facies (labelled as "1" on Figure 6) consists of GEIS that contains traces of marine fauna. The overlying facies (labelled as "2" on Figure 6) consists of highly organic BEIS which has been anthropogenically influenced (i.e. derived from pulp mill effluent) (Hoffman et al., 2019).

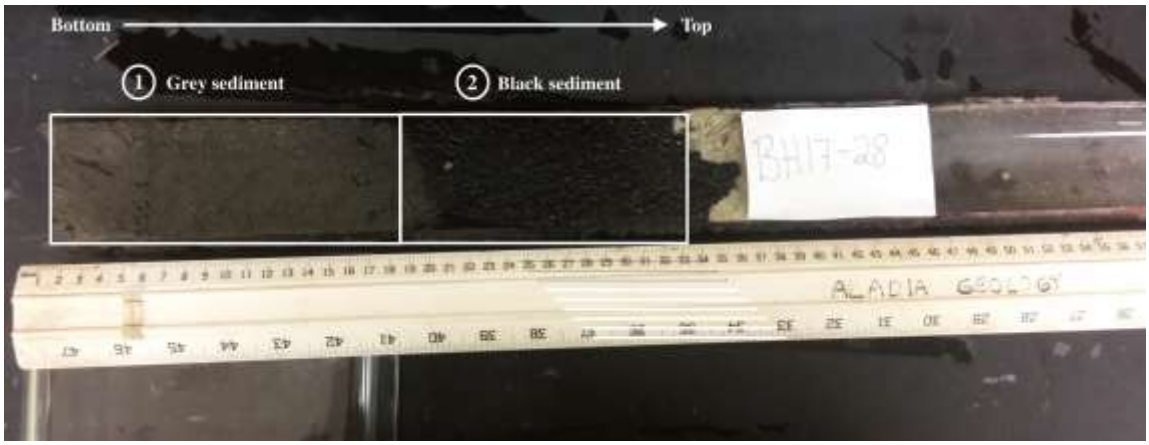

Figure 6: BH17-28 Boat Harbour Sediment core; sediment types 1) GEIS (bottom); 2) BEIS (top) (from Davidson, 2018).

2.2 BEIS Properties

Spooner and Dunnington (2016), Holmes (2018), Tackley (2019), and Alimohammadi et al. (2019) have characterized the physical and chemical characteristics of the BEIS found in the BHSL. The geotechnical water content of the BEIS was reported by Tackley (2019) as approximately 1180%, and the solids content 7.8%. Alimohammadi et al. (2019) measured the range of the geotechnical water content throughout BEIS gravity cores and found that it varied from 3200% near the top of the BEIS-water interface to 500% at the BEIS-GEIS. The solids content found throughout sediment gravity cores was noted to range from 2% near the top of the BEIS-water interface, to 12% at the BEIS-GEIS interface (Alimohammadi et al., 2019).

2.2.1 Thin Section Analysis

Thin section analysis conducted by Holmes (2018) indicated that the BEIS consisted largely of coarse (0.5-1 mm diameter) to fine ($1/64^{th}$-$1/128^{th}$ mm diameter) sized organic material with some inorganic sediment intermixed. A 40x magnified thin section shows detailed sediment association (Figure 7). Ostracod shells were present only near the BEIS-GEIS interface. This was the only indication of benthic activity that was reported by Holmes (2018).

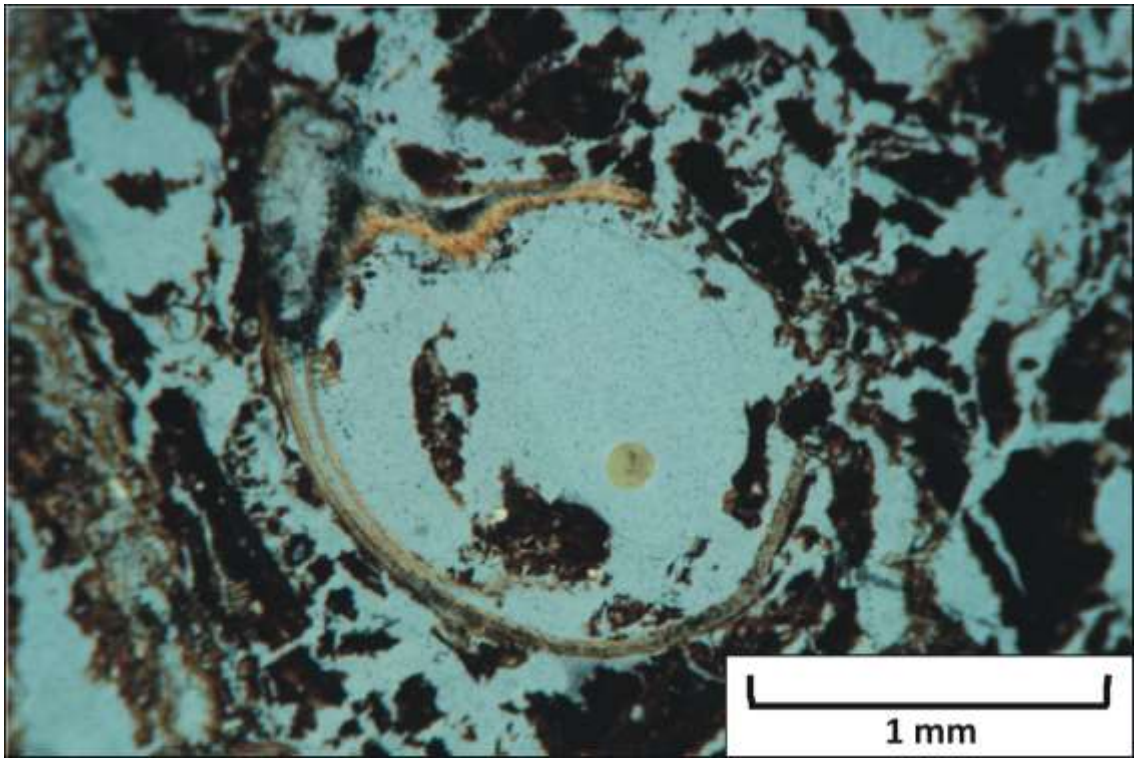

Figure 7: "Microscope image taken at 40x from a thin-section that was obtained from the BEIS 24 – 33 cm down core, just above the GEIS contact. An ostracod shell is shown directly in the centre, surrounded by organic detritus." (from Holmes, 2018).

2.2.2 Origin of Organics

Alimohammadi et al. (2019) determined that the BEIS was composed of 25-31% organic carbon. Holmes (2018) conducted total C, total N, and stable isotope analysis on 14 BEIS samples collected within Boat Harbour's stabilization lagoon (Figure 8). Total C/N values ranged between 10-20, and the average of $\delta^{13}C$ values were approximately -28 % (± 1 %). These results indicate that the organic matter within the BEIS was derived largely from a terrestrial source (Holmes, 2018). This classification of the BEIS indicates that the organic inputs within the stabilization lagoon are lignin rich and protein poor (Brodie et al., 2011; Holmes, 2018). It was also noted that the "top" samples from the stabilization lagoon's BEIS on average contained organics with higher $\delta^{13}C$ values (Holmes, 2018). The $\delta^{13}C$ values from the BEIS indicated that the organics found within

the sedimentary basin are largely composed of C_3 plant matter (Holmes, 2018). C_3 plant matter is dominantly found in terrestrial plants which have adapted to temperate regions (Brodie et al., 2011; Holmes, 2018). This type of plant material is consistent with the biomass commonly utilized at this type of pulp and paper facility (Pettersen, 1984; Sawidis et al., 2011; Tackley, 2019).

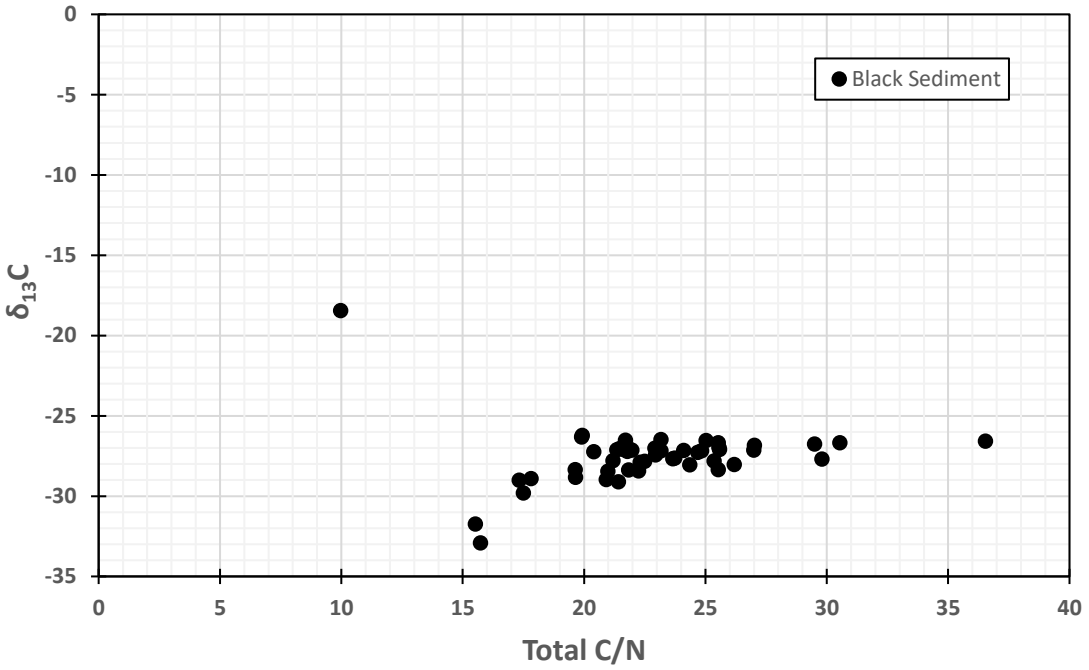

Figure 8: Total C/N vs. $\delta^{13}C$ plot of Boat Harbour's BEIS (modified from Holmes (2018).

The values shown in Table 4 were used to classify the provenance of both the BEIS and GEIS organics as being; freshwater (C/N ratio of 11-17 and $\delta^{13}C$ values between -24.9% to -32.5%), marine (C/N ratio of 4-42 and $\delta^{13}C$ values greater than -23%), or terrestrial (C/N ratio of 5-11 and 17-58 as well as $\delta^{13}C$ values between -24.9%--32.5%) in origin (Davidson, 2018; Galimov, 2012; Holmes, 2018; Mackie et al., 2005; Meyers and Lallier-Vergès, 1999).

Table 4: Classification Scheme for C/N and $\delta^{13}C$ Analysis (from Davidson, 2018).

C/N versus $\delta^{13}C$		
Total C/N	**$\delta^{13}C$ (%)**	**Provenance**
11-17	-24.9% to -32.5%	Freshwater Aquatics
4-42	>-23%	Marine
5-11 and 17-58	-24.9%--32.5%	Terrestrial

2.2.3 BEIS Thickness

Alimohammadi et al. (2019) created an isopach map using the data collected from sediment gravity cores taken throughout the BHSL (Figure 9). This map was developed by interpolating thicknesses between sampling points, which aided in a visualization of the extent and thickness of the BEIS throughout the BHSL. Current volume estimates suggest there is approximately 577,000 m^3 of BEIS in the basin (GHD Limited, 2018b). For large projects such as the BHSL, this volume estimate can be a primary factor when determining the total cost of a remediation operation. As such, a rapid and reliable method for making accurate volume estimates of the BEIS is focus of this thesis.

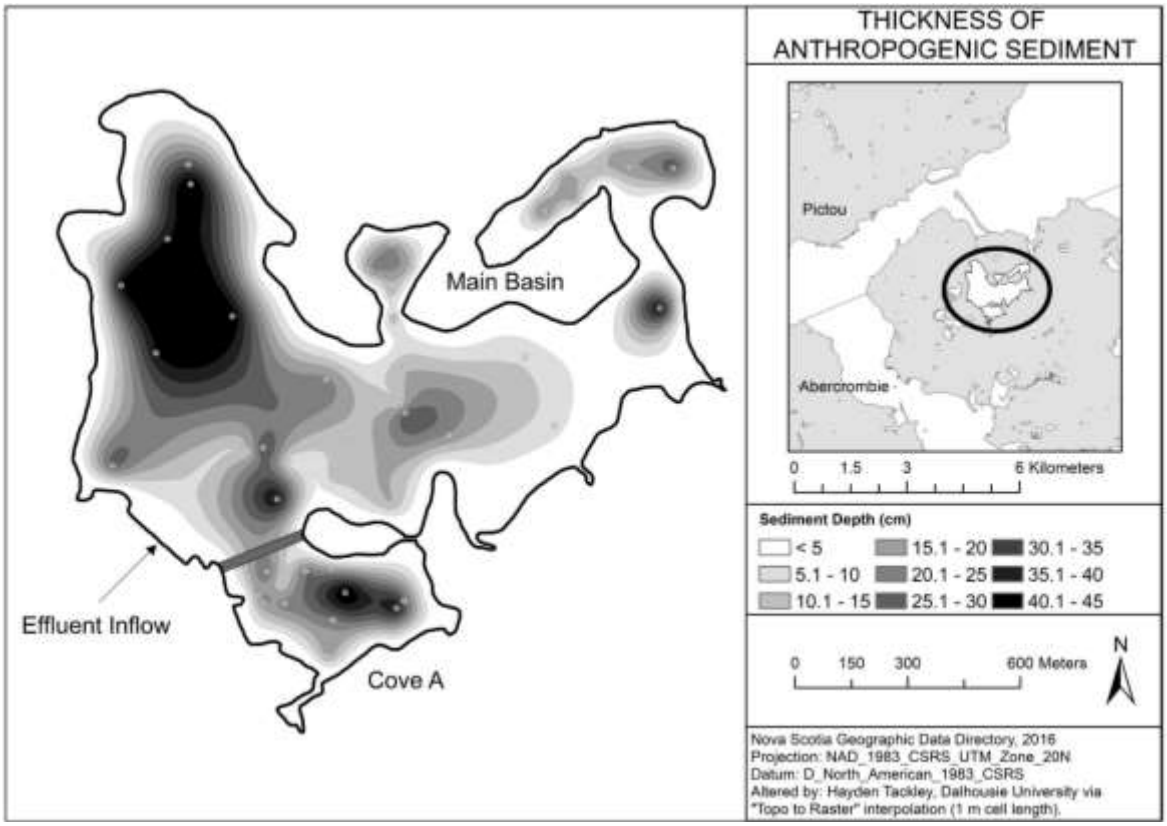

Figure 9: Isopach thickness map of the BEIS (from Alimohammadi et al., 2019).

2.3 GEIS Properties

Spooner and Dunnington (2016), Davidson (2018), and Song (2020) characterized the chemical and physical properties of the GEIS. Spooner and Dunnington (2016) described GEIS as a "basal, dense, grey-brown sediment" and Davidson (2018) described GEIS as consisting of dominantly silt sized particles. Chemical analysis of the bulk geochemistry of the GEIS indicated elevated levels of Ti, K, Rb, Y, Zr, and Nb. This is indicative of an estuarine depositional environment (Spooner and Dunnington, 2016). Song (2020) analyzed the moisture content and density of the GEIS) (Figure 10, 11). The moisture content above the BEIS-GEIS contact was noted to decrease rapidly with depth. Results from the BEIS-GEIS interface and below indicate a consistent moisture content of approximately 200% which in some samples decreased with depth (Song, 2020). This

decrease was thought to have been caused by the coarsening of the GEIS with depth (Song, 2020). The bulk density of the GEIS averaged 1.2g/cm^3 and increased with depth (Song, 2020). Song (2020) concluded that this was likely caused by the sedimentological nature of the GEIS (coarsening with depth).

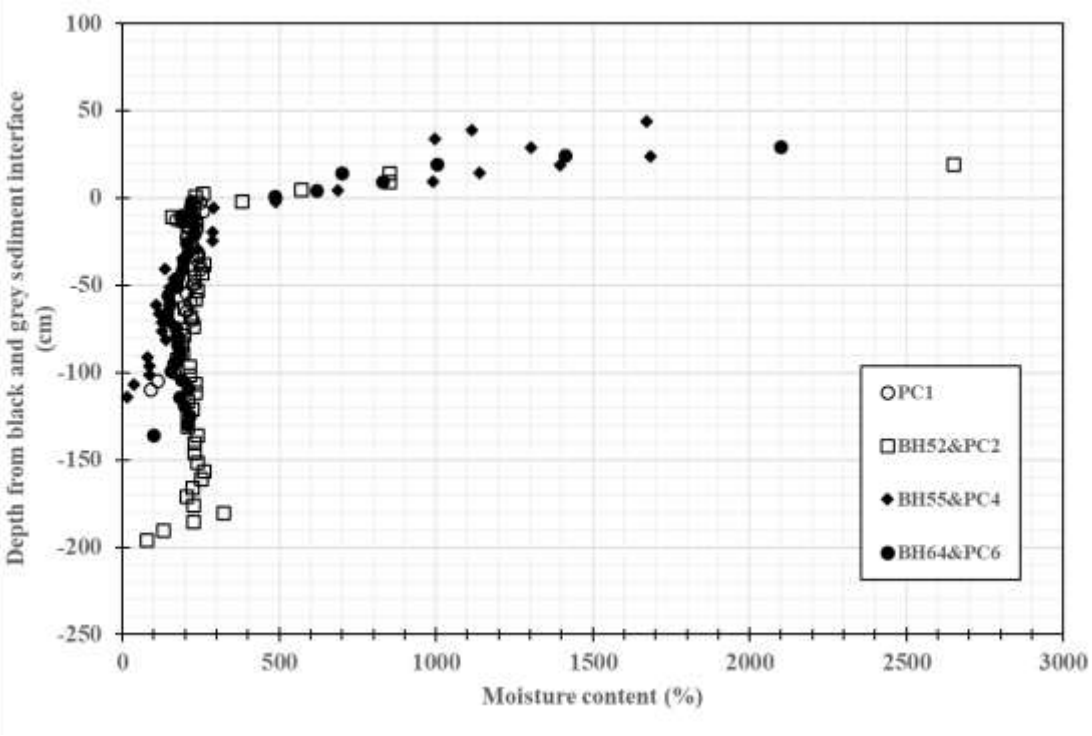

Figure 10: Moisture content of GEIS analysis (from Song, 2020).

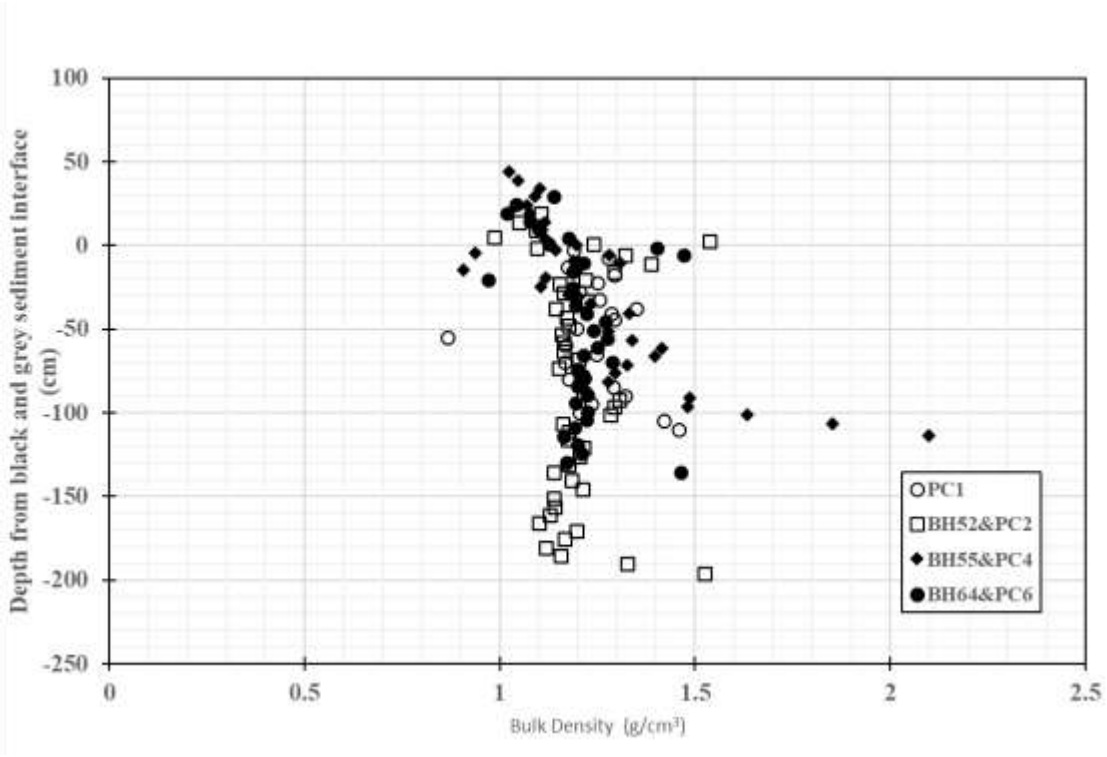

Figure 11: Bulk density analysis of GEIS (from Song, 2020).

The GEIS exhibited low hydraulic conductivity of 3.3×10^{-9} m/s to 9.0×10^{-9} m/s (Song, 2020). Song (2019) connected the hydraulic conductivity to the salinity profile of the sediment (Figure 12) with the hypothesis that the profile was "initiated at the time of the installation of the BHSL. The salinity profile shows increasing salinity with depth throughout the GEIS which appears to stabilize (equilibrate) at around 50 cm below the BEIS-GEIS interface (Song, 2020).

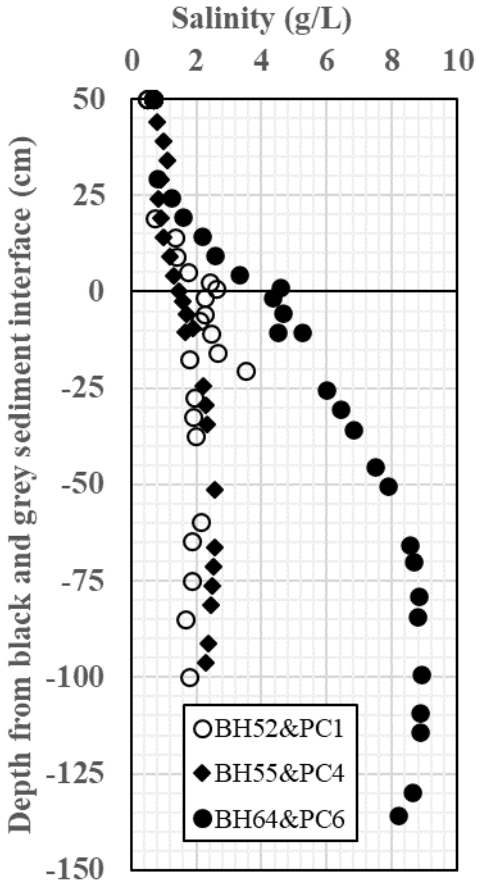

Figure 12: Salinity profile of Boat Harbour sediment cores (from Song, 2020).

2.3.1 Clast Size Analysis

A stratigraphic examination of percussion core results (sample locations shown on Figure 13) show a fining upward trend of grain sizes in the GEIS (Davidson, 2018). The sediments were analyzed using the Wentworth classification system (Appendix A) (Wentworth, 1922). There is an apparent size transition of the sediment from being dominantly sand sized particles, to dominantly silt sized particles as you get closer to the BEIS interface. The sand sized particle content of the GEIS decreases from 74.3% to 9.7% (Table 5). The silt and clay, however, increased from 18.7% and 7.0% to 51.3% and 39%, respectively.

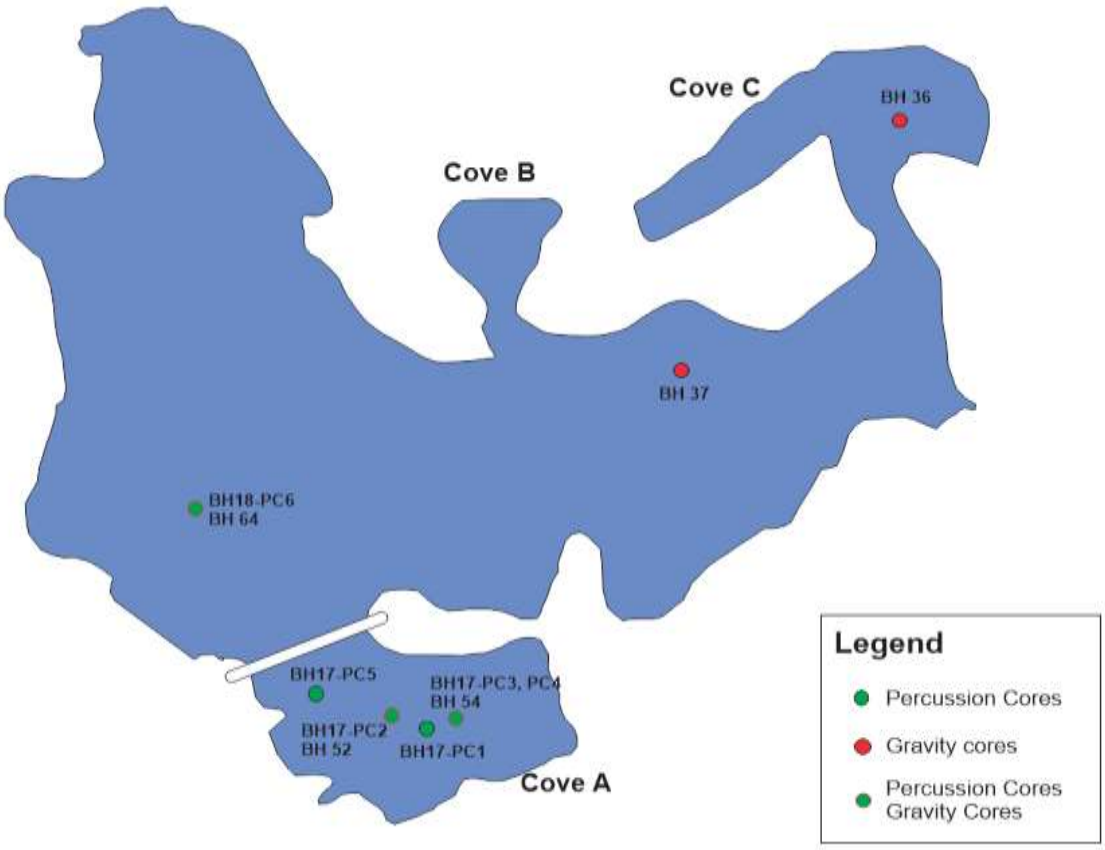

Figure 13: Percussion core locations (from Davidson, 2018; Song, 2020).

Table 5: Percussion core (BH17-PC1 (Figure 13)) clast size analysis using the Wentworth classification system (Davidson, 2018).

Geological Clast Size Results				
BH17-PC1 (Figure 13) Sample Information		Size classification (%)		
Sample No.	Depth from contact (cm)	Sand % (< 2mm)	Silt % (<1/16mm)	Clay % (< 1/256mm)
1	41.3-47.3	9.7	51.3	39.0
2	92.3-97.3	34.3	44.4	21.4
3	107.3-112.3	74.3	18.7	7.0

A geotechnical examination of the GEIS was conducted by Song (2020). Results were collected from six percussion cores taken from Boat Harbour (Figure 13) and are summarized (Figure 14).

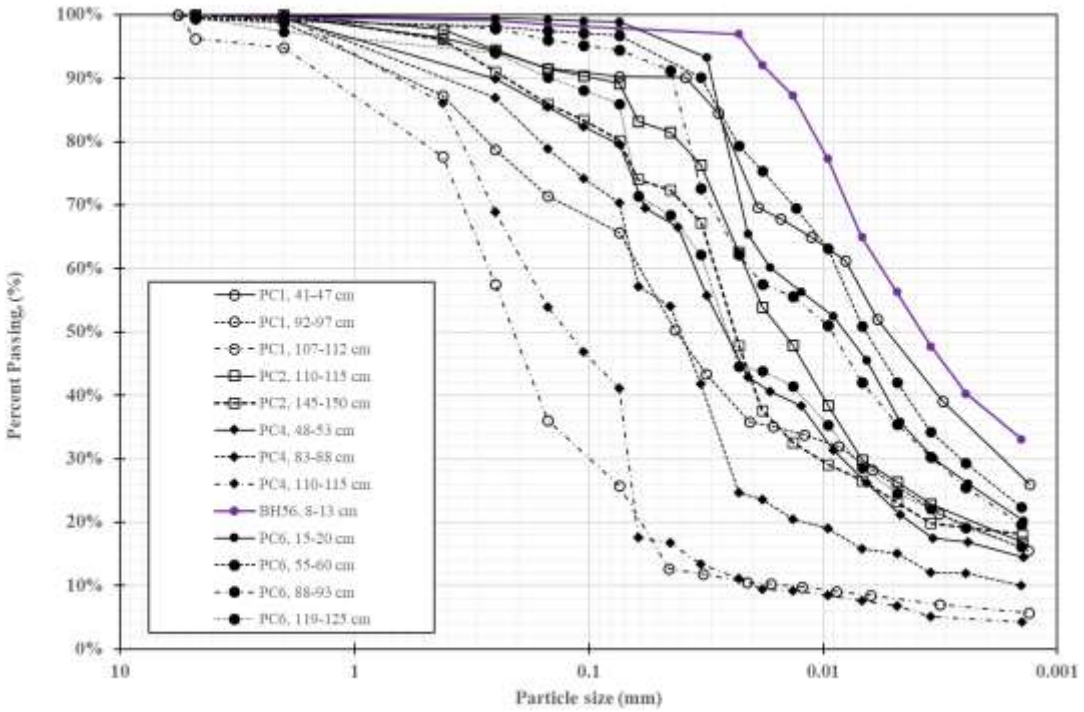

Figure 14: GEIS particle size distribution summary (from Song, 2020).

Percussion core results indicate that more than 70% of the samples consisted of silt and clay sized particles (Song, 2020). Percussion cores of the GEIS were noted to gradually increase to coarse grained sediment with depth, and show a fining upward trend as previously(Davidson, 2018; Song, 2020).

2.3.2 Thin Section Analysis

The thin section analysis conducted by Davidson (2018) found the same trend as that of the clast size analysis. A fining upward sequence was observed, with quartz content decreasing from 70% to 7% of the total sample (Table 6). Although silt and clay fractions within the thin sections were not distinguished, a general decreasing concentration trend with depth was observed. The sediment is, in general, texturally immature, and the grains are subangular with low sphericity (Davidson, 2018).

Table 6: Percussion core (BH17-PC1) thin section analysis (modified from Davidson (2018).

Thin Section Analysis			
Sample	Composition (%)		
Depth from contact (cm)	Quartz	Feldspar	Silt and Clay
(8 - 15)	7	0	93
(15 - 22)	10	0	90
(35 - 42)	30	1	69
(47 - 54)	40	2	58
(59 - 66)	40	2	58
(69 - 76)	50	10	40
(79 - 85)	60	10	30
(88 - 94)	70	0	30

2.3.3 Organism Identification

The macrofauna identified by Davidson (2018) originate from a marine environment. These species are commonly found within the Minas Basin and indicate that the sediment at Boat Harbour support an ecological community consistent with a meso tidal estuarine environment (Bromley, 1985). The marine fauna found within Boat Harbour's GEIS have previously been identified as *Mercenaria mercinaria* (Linnaeus, 1758), *Spisula solidissima* (Dillwyn, 1817), *Ensis directus* (Conrad, 1843), *Littorina littorea* (Linnaeus, 1758), and *Mytilus edulis* (Linnaeus, 1758) (Figure 15).

Figure 15: "Marine fauna found within the GEISs of the BSHL. From left to right, *Mercenaria mercinaria* (Linnaeus, 1758), *Spisula solidissima* (Dillwyn, 1817), *Ensis directus* (Conrad, 1843), *Littorina littorea* (Linnaeus, 1758), and *Mytilus edulis* (Linnaeus, 1758)" (from Davidson, 2018).

2.3.4 Origin of Organics

Song (2020) indicated that the GEIS is composed of approximately 1.5% organic carbon. Davidson (2018) reported total C, total N, and stable isotope analysis for 16 GEIS samples collected within the BHSL. These results were compared to the classification scheme used by Galimov (2012), Mackie et al (2005), and Meyers and Lallier-Vergès (1999) (Appendix A) to further characterize the provenance the GEIS's organics.

GEIS samples were collected from both the top (just below the BEIS-GEIS interface) and bottom of each sediment core. Total C/N results were plotted against $\delta^{13}C$ (%) values processed during the stable isotope analysis (Figure 16) (Davidson, 2018). The organics within the GEIS had total C/N values which ranged from 8-12 throughout the stabilization lagoon (Figure 16) (Davidson, 2018). The GEIS $\delta^{13}C$ values were less than -23% and ranged from -23% to -16%. Total C/N values plotted between the 4-42 range, and

$\delta^{13}C$ values were greater than -23%. Davidson (2018) concluded that the organic matter within the GEIS was derived largely from a marine source.

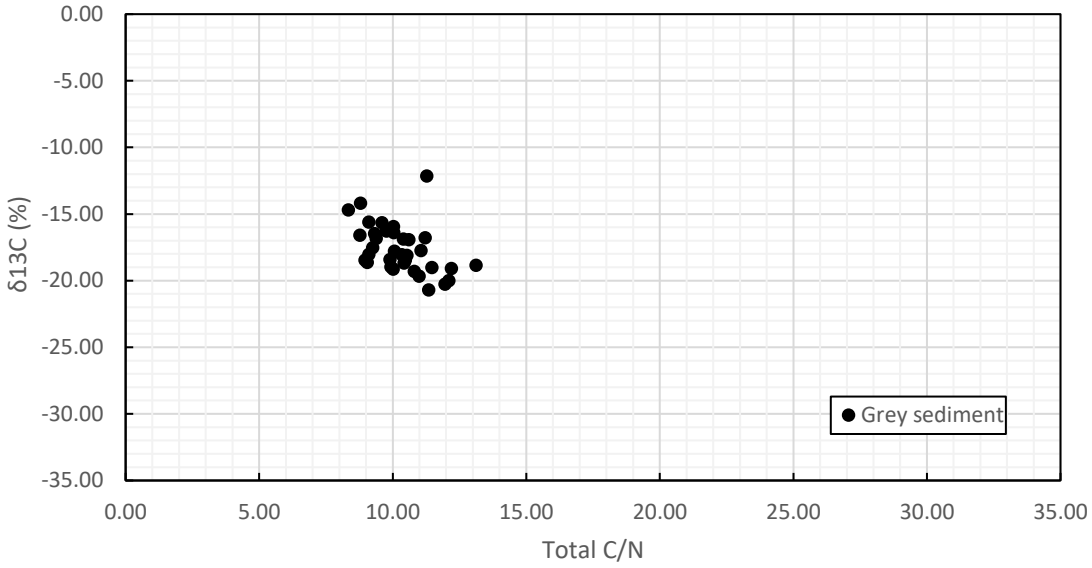

Figure 16: Total C/N versus δ13C in GEIS (modified from Davidson (2018).

2.4 Contaminants of Concern Within Surficial Sediments of the BHSL

Hoffman et al (2017) and Walker et al (2016) conducted a spatiotemporal assessment of the contaminated sediment within the BSHL. The objective of this work was to better understand historical sediment characteristics of the BHSL. This was done by examining 103 sediment samples which had been taken over the last ~quarter century from 1992-2015 (Figure 17) (Hoffman et al., 2017; Walker et al., 2016).

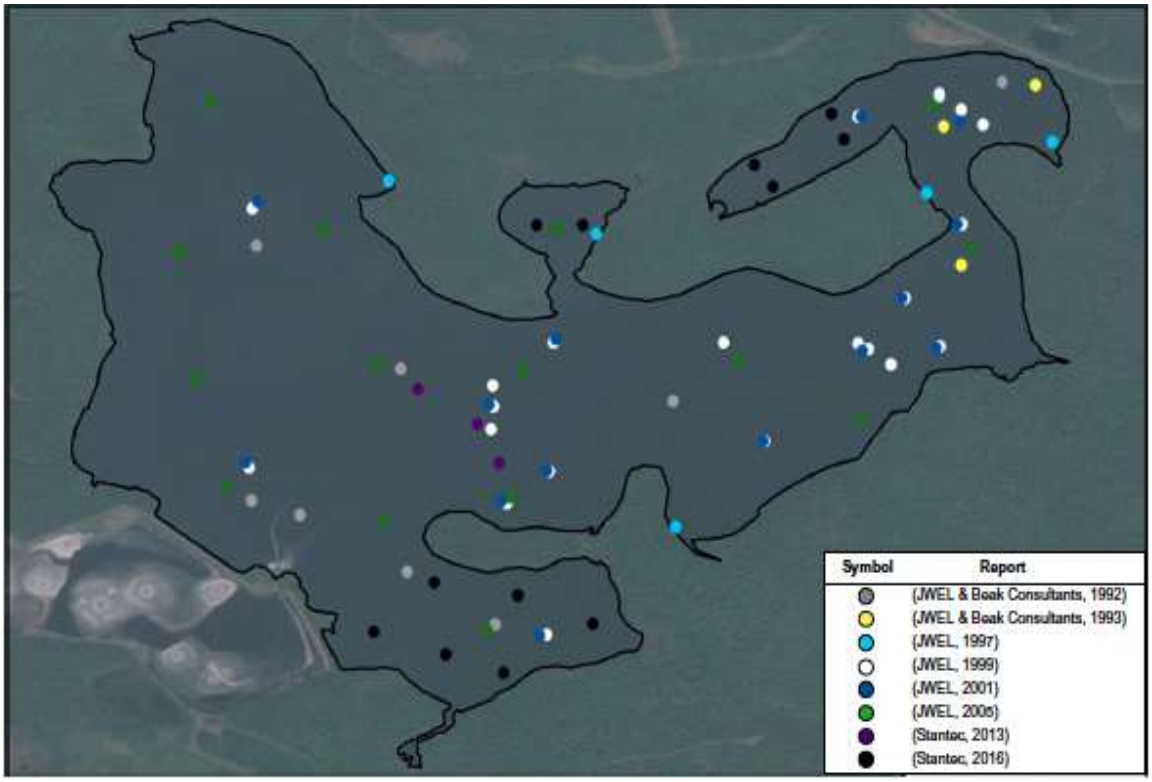

Figure 17: Spatiotemporal distribution of 103 sediment sample sites within Boat Harbour (1992-2015) (from Hoffman et al., 2017; Walker et al., 2016).

The sediment is impacted by both organic, and inorganic pollutants which include metals, metalloids, PAH's, dioxins, and furans (Hoffman et al., 2017; Walker et al., 2016). Hoffman et al (2017) and Walker et al (2016) compared metal and metalloid concentrations to Canadian freshwater and marine sediment quality guidelines (SQGs). Multiple exceedances were noted for both freshwater and marine sediment guidelines (Table 7). The metals Cd, Cr, Cu, Pb, Hg, and Zn often exceeded Canadian SQGs in the contaminated sediment for both freshwater and marine ecosystems. Metals which exceeded freshwater probable effect levels (PELs) include As, Cd, Cr, Pb, Hg, and Zn. Metals which exceeded marine PELs include Cd, Cu, Hg, and Zn. Hoffman et al (2017) and Walker et al (2016) suggested that the metal enrichment within the sediment is likely related to the pulp mill effluent. Both authors pointed out, however, that elevated levels of Hg may be related to

coal combustion and a local chlor-alkali plant which operated and discharged effluent into the BHSL between 1971 and 1992 (Hoffman et al., 2017; Walker et al., 2016). These two processes are known to contribute to elevated levels of Hg in surficial sediments (Gagnon et al., 1997; Garron et al., 2005; Gobeil & Cossa, 1993; Parsons & Cranston, 2006; United Nations Environment Programme (UNEP), 2008; Walker, 2016a, 2016b; Wilson & Travers, 1976).

Table 7: Canadian Council of Ministers of the Environment (CCME) Freshwater and marine sediment quality guideline exceedances for Boat Harbour's contaminated sediment (n = total sediment samples) (modified from Hoffman et al (2017) and Walker et al (2016)).

Parameter	Freshwater				Marine			
	ISQG		PEL		ISQG		PEL	
	SQG limit	Number of exceedances (%)	SQG limit	Number of exceedances (%)	SQG limit	Number of exceedances (%)	SQG limit	Number of exceedances (%)
As (n = 100)	5.9	59 (59.0)	17	1 (1.0)	7.24	23 (23.0)	41.6	0 (0.0)
Cd (n = 103)	0.6	91 (88.4)	3.5	58 (56.3)	0.7	88 (85.4)	4.2	55 (53.4)
Cr (n = 103)	37.3	58 (56.3)	90	4 (3.9)	52.3	39 (37.9)	160	0 (0.0)
Cu (n = 103)	35.7	58 (56.3)	197	0 (0.0)	18.7	94 (91.3)	108	21 (20.4)
Pb (n = 103)	35	70 (68.0)	91.3	11 (10.7)	30.2	79 (76.6)	112	0 (0.0)
Hg (n = 84)	0.17	68 (81.0)	0.486	53 (63.1)	0.13	70 (83.3)	0.7	43 (51.2)
Zn (n = 103)	123	81 (78.6)	315	55 (53.4)	124	80 (77.7)	271	56 (54.4)

Previous research conducted at the BHSL has focused on the bulk geochemistry of the 2 sediment types present in the stabilization lagoon. Spooner and Dunnington (2016), Holmes (2018), and Davidson (2018) indicated that multiple metals either met, or exceeded, interim sediment quality guidelines (ISQG) for marine and freshwater sediments. Holmes (2018) found that the effluent negatively impacted the bulk geochemistry of the

BEIS and that metal concentrations were higher than in samples taken from nearby, non-impacted lakes. Davidson (2018) indicated that strong geogenic influences were the primary contributor to the bulk geochemistry of the GEIS. Although the GEIS did exceed the ISQGs for various metals, these elevated levels were found to be uninfluenced by the overlying contaminated sediment (Davidson, 2018).

GHD Limited (2017, 2018a, 2018b) Environmental Site Assessment (ESA phase 1 and 2) was conducted by GHD Limited, the primary consult for Nova Scotia Lands' Boat Harbour remediation project (GHD Limited, 2017, 2018b, 2018a). Potential contaminants of concern within the BHSL were noted to be cyanide, chlorate/chlorite, resin and fatty acids, sulphate, and hydrogen sulphide (GHD Limited, 2018a). GHD Limited (2018a) identified several other contaminants of concern, including dioxins and furans, PAHs, VOCs, PHCs, Metals (including mercury), and chlorate/chlorite, which were thought to originate during the kraft pulping process conducted at the associated mill (effluent contributor). Metals within the sediment of the BHSL showed exceedances for both freshwater and marine provincial guidelines (GHD Limited, 2018a). Freshwater metal exceedances included; As, Cd, Cr, Mn, Hg, Se, and Ag, whilst marine metal exceedances included; Cd, Cu, Hg, Ag, and Zn (GHD Limited, 2018a). PAH exceedances of 2-methylnaphthalene, anthracene, fluorene, phenanthrene, and pyrene were noted to exceed both freshwater and marine provincial guidelines within the BSHL (GHD Limited, 2018a). Petroleum hydrocarbon (PHC) exceedances for the fuel oil range (>C10 to C16) and the lubricant oil ranges (>C16 to C21 and >C21 to C32) were noted to exceed both freshwater and marine provincial guidelines within the BSHL (GHD Limited, 2018a). Volatile organic compound (VOC) exceedances of toluene were noted to exceed both freshwater and marine provincial guidelines within the BSHL (GHD Limited, 2018a). Dioxin and furan

exceedances were noted to exceed both freshwater and marine provincial guidelines within the BSHL (GHD Limited, 2018a). Dioxin and furan concentrations exceeded highest effect level, indicating that they pose a sever risk to ecological health (Hoffman et al., 2019).

2.5 Implications for Research

Both Hoffman et al. (2017) and Walker et al. (2016) note from their historical sediment-monitoring data review of Boat Harbour that gaps are still present in our understanding of the spatial (horizontal) and temporal (vertical) nature of the BHSL's contaminated sediment. Hoffman et al. (2017) and Walker et al. (2016) have recommended that more detailed sampling be performed to properly characterize these sediments. GHD Limited's (2018a) Phase 2 ESA further demonstrated the need for more detailed sampling at the BHSL, as a number of guideline exceedances were observed. GHD Limited (2018a) acknowledged that the contamination within the BHSL is generally limited to the overlying BEIS layer. With this in mind, determining an accurate volume estimate of the BEIS is a crucial component of the remediation project. GHD Limited (2018a) suggest that additional sampling is required to accurately delineate the contaminated sediment layer within the stabilization lagoon. By providing an efficient and cost-effective means of delineating the contaminated sediment within the BHSL, more accurate volume, and cost estimates can be derived for project management purposes.

At the BHSL there is clear need for more detailed sampling to be conducted before remediation decisions are made. Of particular interest is the thickness of BEIS. As both sediment types within the BHSL vary significantly in terms of chemical composition, the level of organic carbon content (%), and organic composition (total C/N and $\delta^{13}C$), the UVOST has the potential to gather the detailed stratigraphic discrimination data required

for this project. The BEIS, which contains a higher organic carbon content than the GEIS likely has a higher concentration of compounds with the capability of fluorescing (Alimohammadi et al., 2019; Brodie et al., 2011; Holmes, 2018b; Song, 2020). As the BEIS is derived from a variety of pulped trees, it is lignan rich, and thus contains a known fluorophore (Donaldson, 2013; Donaldson et al., 2018; Holmes, 2018). These fluorophores could facilitate the distinction of each medium within the BHSL using the UVOST. To date, the UVOST has not been used in such an application as it has been designed for the delineation of sites contaminated with hydrocarbons. To assess this potential for a new application of the UVOST, a four-phase testing plan is presented to test the ability of the UVOST to delineate differences in the BEIS and GEIS found within the BHSL.

Chapter 3 Methods

As hypothesized in Chapter 1, it is thought that the quantity and variety of organic compounds in the BEIS will produce a different fluorescence signature than that of the GEIS and that the UVOST has the capability to accurately detect these variations. This chapter presents a four-phase testing plan created to investigate this hypothesis (Figure 18).

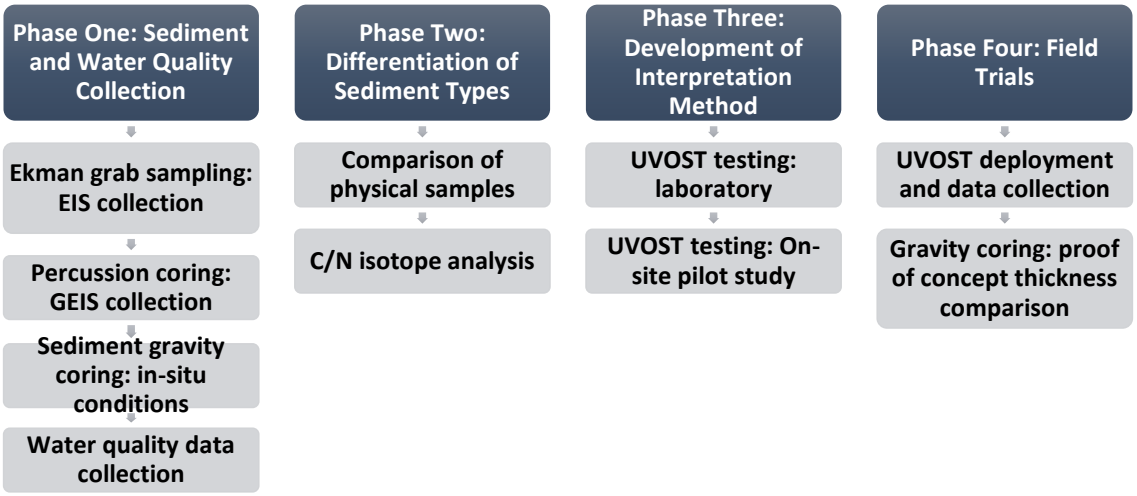

Figure 18: Four phase testing plan to investigate the ability of the UVOST to delineate BEIS thickness.

Phase One: Field-sampling of the BEIS and GEISs for preliminary lab work. In this phase, the processes of sediment and water quality data collection are outlined and presented.

Phase Two: Comparing the differences in organic matter between the two sediments. In this phase the physical characteristics of the sediments and a total C/N and $\delta^{13}C$ isotope analysis are presented and compared based on the previous work of Davidson (2018) and Holmes (2018). Both of these datasets have been compiled for further comparative analysis.

Phase Three: Laboratory testing of the UVOST application on the two sediments. In this phase, the processes conducted during preliminary lab-based trials are outlined. In addition, the procedures involved in a pilot study at the BHSL conducted to develop a method of interpreting the data logs are described.

Phase Four: Field testing of the UVOST application on the two sediments. In this phase, the details of a field test conducted at the BHSL are described to provide a basis for the comparison of the method outlined in phase three. This phase is focused on development of the final methodology of the interpretation of each sediment type.

3.1 Phase one: Sediment and Water Quality Data Collection

To obtain the required volume of sediment needed for preliminary trials, multiple methods of collection were employed at the BHSL on April 16th, 2019. Percussion coring was conducted to collect GEIS samples, while sediment gravity coring was conducted to collect both BEIS and GEIS samples. The contact between the BEIS and GEIS was well preserved in gravity core samples which were used to gauge the thickness of the contaminated layer. Bulk sampling was conducted using an Ekman grab sampler (model 196-815), to collect a larger volume of the BEIS for geochemical analyses. Each sampling technique was selected based on the method's reliability, as well as ability to collect sufficient sample volumes of a given sediment type for phase one, two, and three testing. All samples were collected in close proximity to one another (within 1m) in the BHSL (Figure 19). Water quality parameters were also collected from the water column in the area of the sediment sampling prior to sediment sampling.

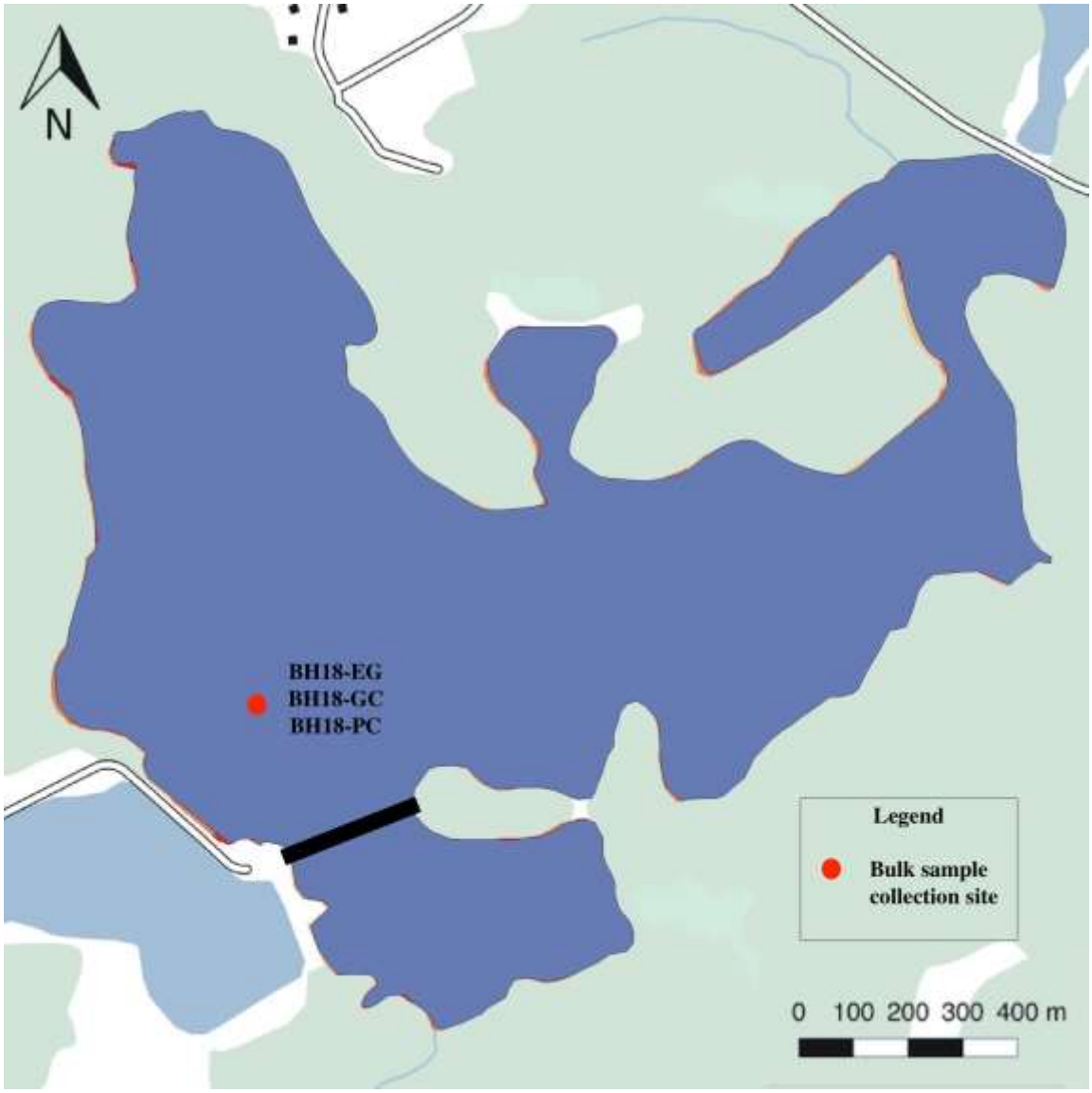

Figure 19: Bulk sediment sampling site for laboratory trials.

3.1.1 Ekman Grab Sampling: BEIS Collection

Samples were taken within the BHSL at the location shown in Figure 19. This location was selected as previous sediment gravity core samples showed that the BEIS at this site was at least 20cm thick, which would allow for the collection of BEIS without GEIS contamination. The sampler was lowered into the water column and triggered for collection once the sampler entered surface of the BEIS. Upon retrieval of the sampler, the jaw mechanism was released, and the sample was collected within a 20L sediment

collection bucket. In total, 20L of the BEIS was collected and sealed for transport back to Dalhousie University. After the sediment was transported to Dalhousie University, the 20L container was refrigerated, before being taken to SCG Industries Limited (St. John, NB, Canada) for UVOST analysis.

3.1.2 Percussion Coring: GEIS Collection

To obtain large samples of GEIS from the BHSL, percussion coring was conducted from a floating raft. Core barrels constructed from PVC piping (3m long, 75 mm diameter) fitted with custom core catchers were used to collect 4 percussion cores (Figure 19). Cores were collected by manually driving the core barrels into the underlying sediment until refusal. Retrieved cores were sealed and transported to the shore for further processing where holes were drilled into the sides of the core barrels to drain the overlying water from the cores and to find the BEIS/GEIS interface contact. The interface was marked, and core barrels were cut 50 mm below the interface, so as to avoid contamination of the GEIS due to core deformation (Spooner and Dunnington, 2016). Processed cores were sealed, transported to Dalhousie University labs, and then extruded into a 20L sediment collection bucket pail using a vertical extrusion device. The 20L bulk GEIS sample was then refrigerated prior to being transported to SCG Industries Limited. for further analysis.

3.1.3 Sediment gravity coring

Intact sediment cores were collected using a Glew gravity coring device (Figure 19) (Glew, 1989). Figure 20 shows a rendering of the Glew gravity coring device along with an attached core. Collection and sealing protocols used by Spooner and Dunnington (2016), Holmes (2018), and Davidson (2018) were used in this study. Sediment gravity cores were sealed with bentonite clay on site to stabilize the sediment for transport. Sediment cores

were placed upright in a core stabilization container and were transported to Dalhousie University. After transport, the collected cores were refrigerated before being taken to SCG Industries Limited. for visual analysis.

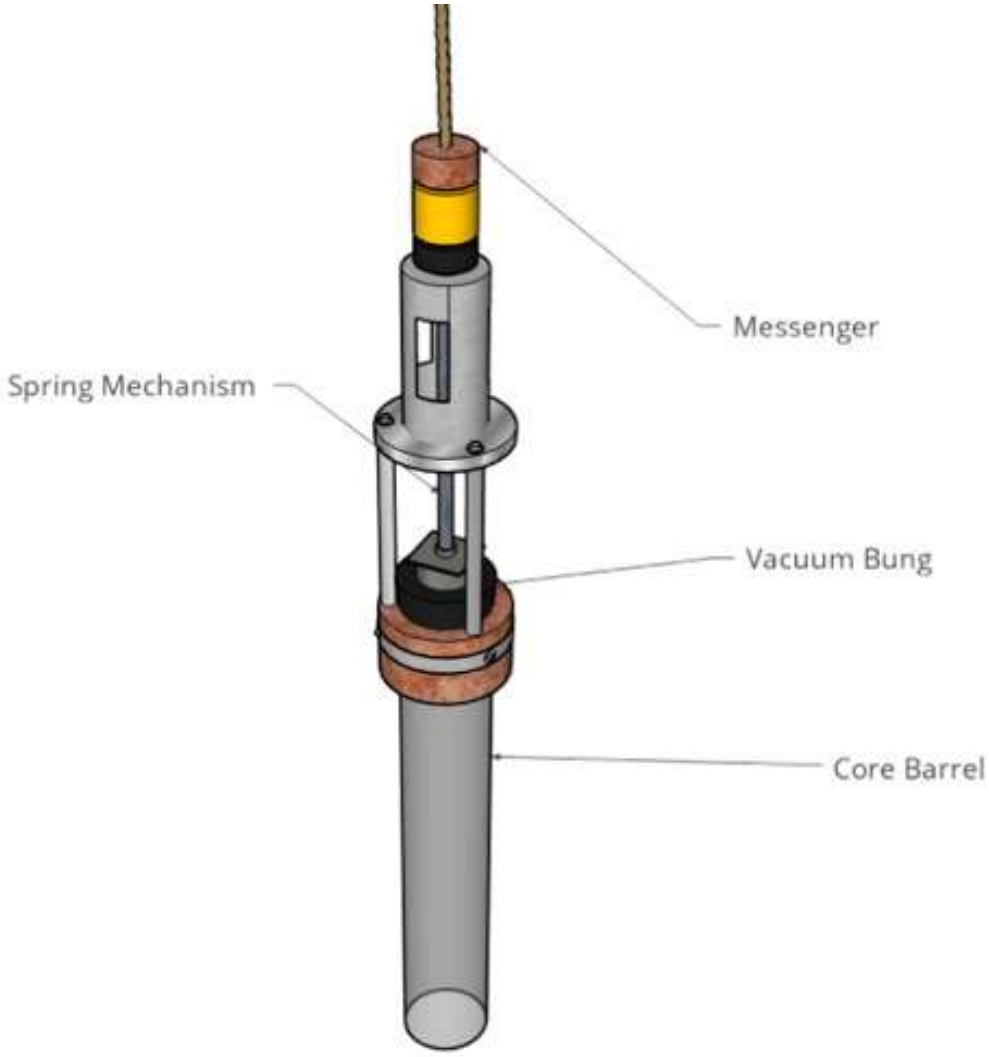

Figure 20: Rendering of the Glew gravity coring device.

3.1.4 Water Quality Data Collection

Water quality measurements were taken using and a YSI Professional Plus (Pro Plus) Multiparameter Instrument (Figure 19). Before water quality measurements were taken, the instrument was calibrated for temperature (˚C), pressure (mmHg), dissolved oxygen (DO) (%), DO (mg), conductivity (µS/cm), pH, and total dissolved solids (TDS)

(mg/L) using the methods outlined by the manufacturer (YSI Incorporated, 2009). Water quality parameters were collected at depths of 0 m (surface), 1m, 2m, and 2.3m (bottom) of the water column.

3.2 Phase Two: Differentiation of Sediment Types

3.2.1 C/N Isotope Comparative Analysis

The two sediment types in the BHSL have significantly different concentrations of organic carbon (i.e. organic matter) (Alimohammadi et al., 2019; Song, 2020). Song (2020) found the organic carbon in the GEIS to average 1.5% while Alimohammadi et al. (2020) found the BEIS contains 25-31% organic carbon. Davidson (2018) and Holmes (2018) identified the likely origin of organic matter within the BEIS and GEIS in the BHSL. However, these sediments were not directly compared to one another, and as such, the data has been amalgamated in this thesis to compare these two sediments. The same classification scheme has been used to classify the provenance of organics in each sediment type (Table 4).

The provenance of the organics within each sediment type have been further compared in the results section of this thesis. As outlined in the literature review, sediments are classified as having organics which are derived from marine, terrestrial, or a freshwater aquatic source. Whether or not these provenances are anthropogenically influenced or natural is not defined, however, in the case of the BEIS, it is known to be anthropogenically influenced (Alimohammadi et al., 2019; Davidson, 2018; Hoffman et al., 2019; Holmes, 2018; Song, 2020; Spooner and Dunnington, 2016; Tackley, 2019; Walker et al., 2016). Organics derived from a freshwater aquatic source have a total C/N and $\delta^{13}C$ range of 11 to 17 and -24.9% to -32.5% respectively. Organics derived from a marine source have a

total C/N and $\delta^{13}C$ range of 4 to 42 and >-23% respectively. Organics derived from a terrestrial source have a total C/N and $\delta^{13}C$ range of 5 to 11 and 17 to 58 and -24.9%- -32.5% respectively (Davidson, 2018; Galimov, 2012; Holmes, 2018; Mackie et al., 2005; Meyers and Lallier-Vergès, 1999).

3.3 Phase Three: Development of Interpretation Method

3.3.1 Laboratory

3.3.1.1 Preliminary Testing

The UVOST used in this study operated with both a fluorescence detector as well as a conductivity attachment. The UVOST laser required a 30-minute warm-up period prior to sample analysis so that a consistent beam strength could be obtained. The tool was calibrated using Dakota Technologies provided reference emitter (RE) and the launch adjust knob was adjusted so that the total area under the fluorescence curve was within the accepted parameter of 10000 +/- 1000. Background levels were calibrated to be within the accepted parameter of < 5 mV. After initial calibration, the tool was calibrated every 30 minutes (post initialization).

Ten (10) BEIS and 10 GEIS samples were used from the previously obtained sediment buckets. Samples were collected in standard aluminum weigh boats and collection implements were rinsed with deionization (DI) water prior to the collection of each new sample. Each of the 10 samples were subsampled three times for testing with the UVOST; 2 of the subsamples being used to test for fluorescence, and 1 being used to test for conductivity. Fluorescence samples were applied to the sapphire window of the probe head using a scoopula. The sub-samples were applied at a 1 cm thickness (above the sapphire window interface) so that UV light would not penetrate through the sample and provide

false readings. Figure 21 shows the UVOST device with a sample prepared for fluorescence testing on the instrument. Sediment was also applied to the conductivity sensor ensuring that it touched both the conductivity interface and the probe body (thus completing the dipole connection). This process was followed for all samples of the BEIS and GEIS, for a total of 20 fluorescence, and 10 conductivity data points being collected for each sediment type. The UVOST was rinsed with DI water after each sub-sample test was conducted. After the sample data was collected, the data was averaged, and fluorescence contributions from the sediment were extracted from the dataset for further analysis (in the form of a wavelength readout to the right of the dataset). Data obtained from this extraction include the peak height of the signal received (y-axis and in milli Volts (mV)) and the time resolution of the data (x-axis and in nanoseconds (ns)). The observed peaks were then

normalized to the blue wavelength to provide ratios for comparison between the sediment types.

Figure 21: Preliminary UVOST trials on a BEIS sample. The sample is placed atop the UVOST probes sapphire window, from which, UV light is emitted.

3.3.1.2 Mock Core

A mock core containing both the BEIS and GEIS was fabricated at SCG Industries Ltd (Figure 22). The core was designed to emulate the contact found between the two sediment types which exists at the BHSL. The holding vessel for the core was constructed out of a piece of 1m long, 150mm diameter PVC pipe, which was capped and sealed on one end. The artificial core was filled with 405 mm of GEIS and then was overlain by 355 mm of BEIS. The top of the core was left open to atmospheric influence. The GEIS was packed into the core to create a solid interface between the two sediment types, as to not allow for seepage of the overlying sediment. It was noted that because of packing and

condensing of the GEIS, the conductivity of the sediment would be different than that of the in-situ GEIS. The BEIS was mixed vigorously to ensure homogeneity before being poured atop the GEIS.

To test the mock core, an extension rod was added to the probe, to ensure that the maximum depth of the core could be reached. To measure the depth of the probe penetrating the sediment within the core, a potentiometer was attached to an extendable rod, and connected to the UVOST. The probe was then slowly inserted into the sediment, so that the sapphire window was just above BEIS-air interface, because of this, the conductivity results for the probe are offset by 60 mm for the mock core trial.

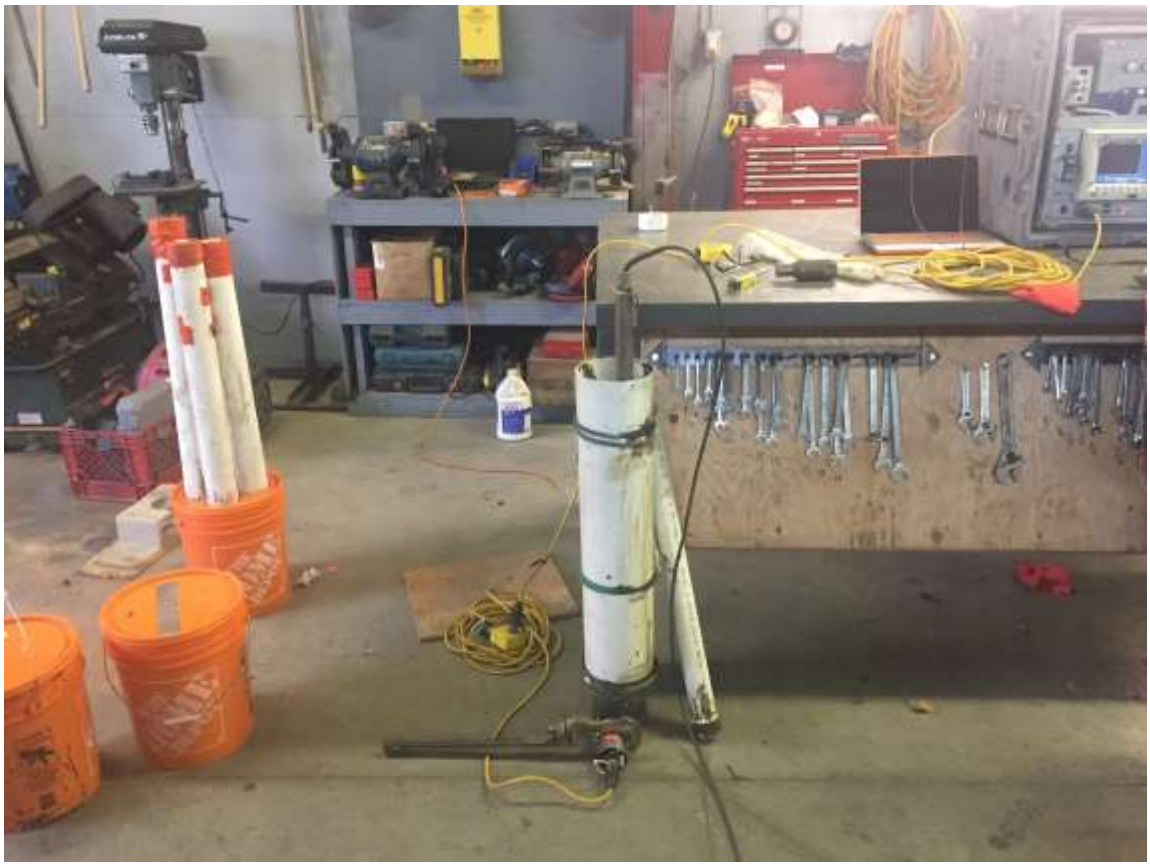

Figure 22: Boat Harbour BEIS and GEIS mock core trial.

The mock core trials were run three times, with the UVOST being washed down with DI water prior to each trial to avoid cross-contamination. Both the conductivity, and fluorescence, were analyzed through the BEIS and GEIS using the UVOST.

3.3.2 Pilot Study

3.3.2.1 Development of a Field Interpretation Method

A pilot study was conducted at the BHSL prior to phase four to develop an interpretation method of the UVOST data. The interpretation methods for the UVOST data logs are presented in Chapter 4 Results and Discussion of this thesis. The following methods outline how the UVOST was deployed and how data was collected from the BHSL in this phase. In total, nine UVOST data logs were collected throughout the stabilization basin. Due to weather conditions, the following UVOST sample locations experienced significant drifting; BH18-LIF-05, BH18-LIF-06, BH18-LIF-07 (Figure 23). As these logs showed anomalous readings, these logs were disregarded when interpreting sediment thickness, however, they did provide data which was used to aid in the delineation of layers. The remainder of the logs were noted to have similar defining characteristics to one another and were used to develop an interpretation method.

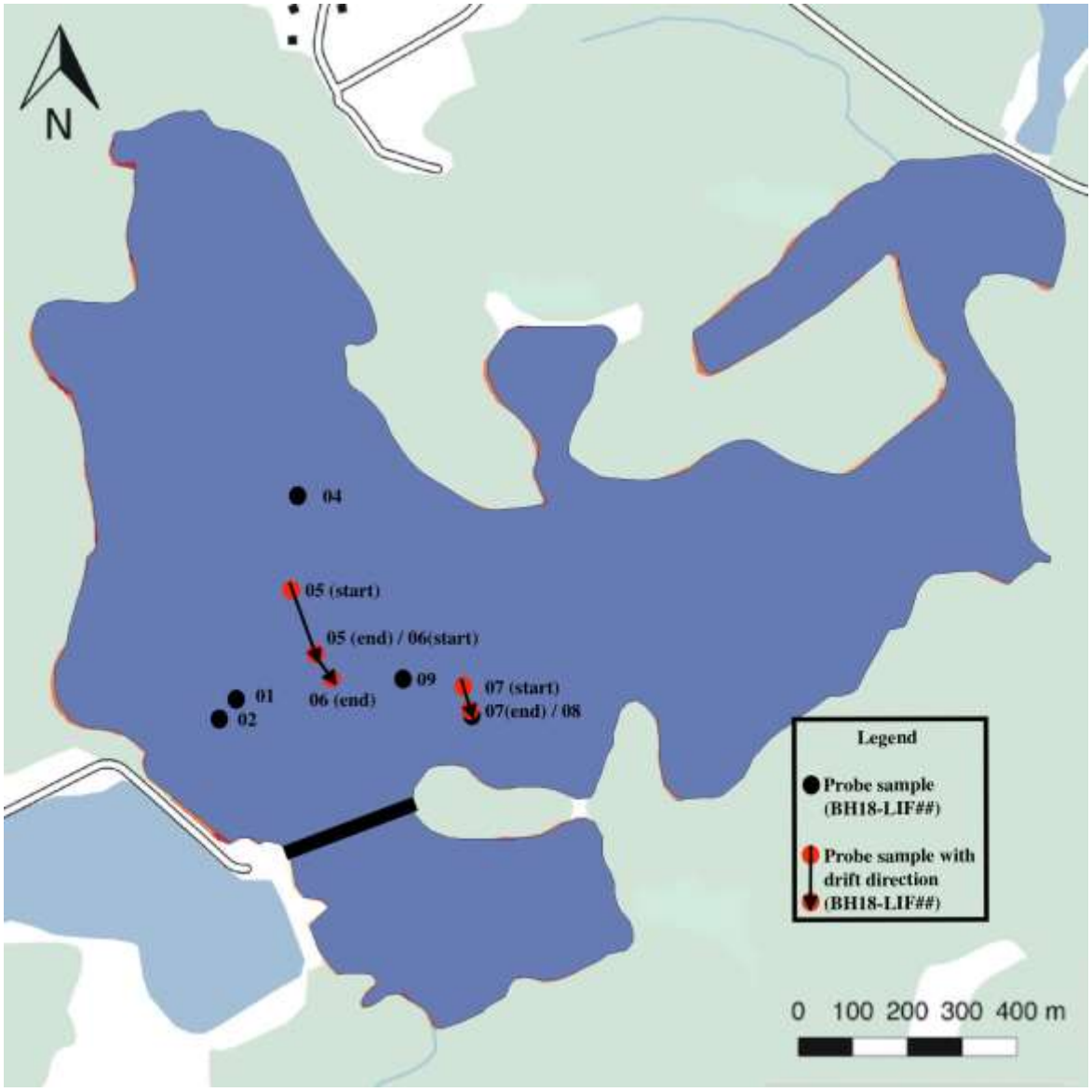

Figure 23: Boat Harbour pilot study UVOST sample location map.

3.3.2.2 UVOST Deployment

To collect UVOST data from Boat Harbour, an onsite barge was modified and used for the deployment of the UVOST. The original barge was constructed on top of a pontoon system of welded high-density polyethylene (HDPE) pipe (Song, 2020). Wooden decking was affixed to the surface of the pontoons and at one end of the system, a 300mm diameter hole was cut for sampling subsurface sediments (Song, 2020). The original barge measured 2.03m wide by 4.40m long and had a capacity of three people. During the phase 3

assessment, modifications to the barge were required to affix and safely operate the UVOST on the water. Modifications made to the barge included the addition of four 100lb floating docks (one to each corner) to increase buoyancy, as well as the installation of a safety railing around the barge (Figure 24).

A modified UVOST deployment station (designed and fabricated by SCG Industries Limited for this project) was attached to the center of the modified barge over the pre-cut sampling hole. The UVOST computational system was fastened to the UVOST aquatic deployment station and the probe was attached to a winch and pulley system above the sampling hole. The UVOST optical cable was fed through a series of extension rods and attached to the UVOST for in preparation of deployment. Prior to collecting data using the UVOST, the modified barge was towed to each sample location (Figure 23) using a small zodiac-type boat with a 2 hp watercraft motor. Upon arrival at each sample site, the modified barge was anchored from 2 corners using the secondary boat to assist. The anchors were dropped at least 5m away from the modified barge to avoid the disturbance of the sediment directly adjacent to the UVOST.

Figure 24: Phase three: UVOST deployment.

3.3.2.3 UVOST Data Collection

Quality control and quality assurance measures as stated by Dakota Technologies and outlined in section 1.5.4 Data collection QA/QC procedures of this study were followed during the collection of UVOST data. Before each data collection process was initiated, accurate RE intensity was ensured by adjusting the launch adjust knob so that the total area under the curve displayed on the oscilloscope was equal to $10{,}000 \pm 1000$ pVs. Background levels were calibrated to be less than 5 mV using the reference emitter (RE) provided by Dakota Technologies prior to data collection. The UVOST probe deployed beneath the modified barge at a rate of 2 cm/s, as to avoid missed data points which result in the blurring of data. A potentiometer was affixed to the UVOST aquatic deployment

station and the probe head to measure the probes displacement distance to provide accurate depth readings.

Using a winch and pulley system the UVOST probe was driven into the underlying mediums at each sample site, and 1m extension rods were attached to the probe when needed. The aforementioned procedures were followed before data collection was initiated on the UVOST's computer. Data was collected beginning above the water on the barge, down through the water column, into the BEIS, and into the GEIS (Figure 25). The UVOST collected real-time data, and as such, data collection was finalized when the fourth layer (the GEIS) was distinguished within the UVOST data log.

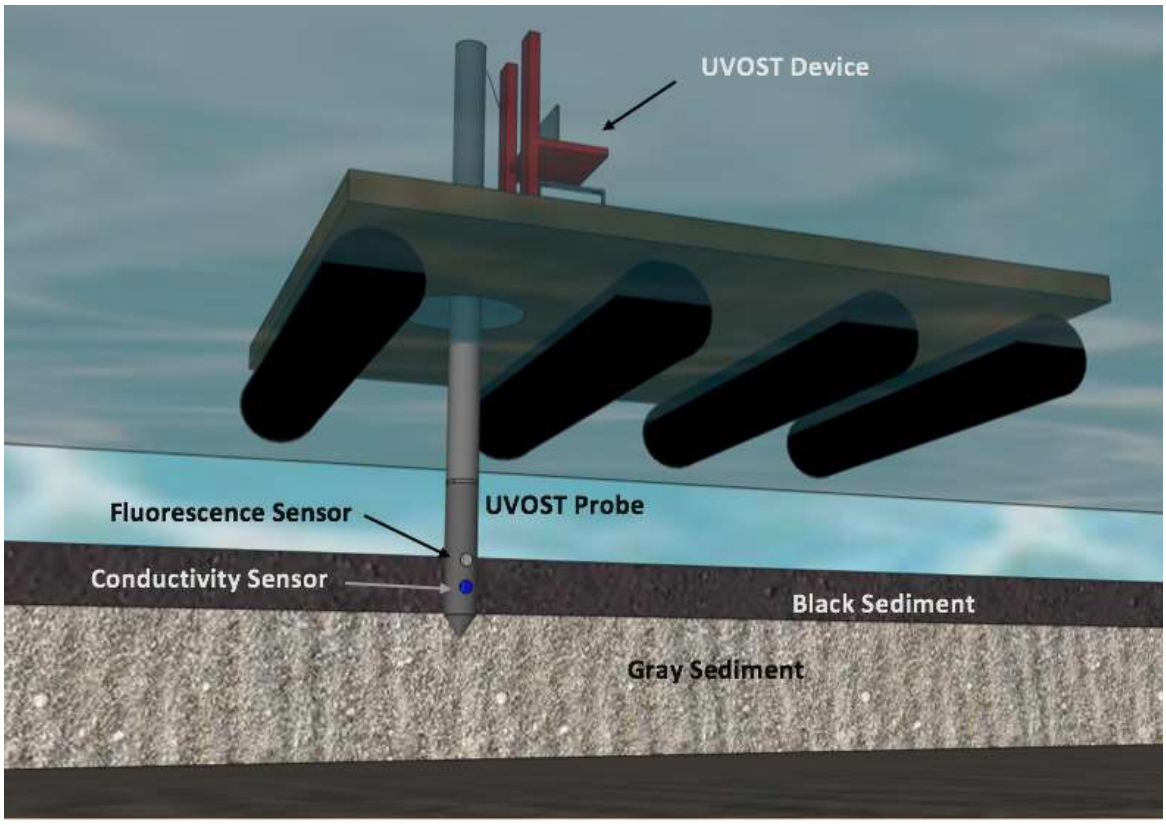

Figure 25: UVOST Sampling Schematic.

After the data was collected, the data from each medium was averaged, and fluorescence contributions of each medium was extracted from the dataset for further

analysis. Data obtained from this extraction include the peak height of the signal received (y-axis and in milli Volts (mV)) and the time resolution of the data (x-axis and in nanoseconds (ns)). The observed peaks were then normalized to the blue wavelength to provide ratios for comparison between the sediment types. In addition to this, the blue (350 nm), green (400 nm), orange (450 nm), and red (500 nm) waveforms (which have been normalized to the RE) were extracted from the data set. These waveforms were graphed using excel to allow for the visual assessment of the differential ratios which have been generated. The data used to create these waveforms is presented in Appendix C.

3.4 Phase Four: Field Trials

3.4.1 UVOST Deployment

Field trials at the BHSL were performed to collect sediment gravity cores and side-by side in-situ UVOST data from a new barge designed and constructed by SCG Industries Limited. (Figure 26). Wooden decking and rails were built, and the barge was constructed atop a series of floating dock segments, which were bolted to the underside of the barge's decking. The capacity of the new barge was up to 8 people, including the equipment for both coring and UVOST probing. The decking was constructed so that both core samples and UVOST samples could be taken as close as possible to one another. This included a 10 cm diameter sampling port for UVOST probing, as well as a 0.3 m x 0.3 m removable portion of the decking which was used for core sampling. This design made it possible for UVOST and core samples to be taken within 0.6 m from each other (Figure 27).

Figure 26: Field trails barge.

Figure 27: Field trails barge sampling sites for sediment gravity coring (left) and UVOST probing (right).

The UVOST deployment station was bolted to the barge over the pre-cut sampling hole. The UVOST's computational system was placed within the deployment station with the probe strapped securely above the sampling hole. In preparation of deployment, the systems optical cables were fed through the probe extension rods, and extension rods were stored on the deployment station. A winch and pulley system were used for both the deployment and retrieval of the probing system. The barge was towed to seven different sampling locations (Figure 28) using an aluminum boat with a 20 hp motor. To anchor the barge, anchoring spikes were deployed on two corners of the barge, this made it possible to pivot the barge and collect data points close to one another.

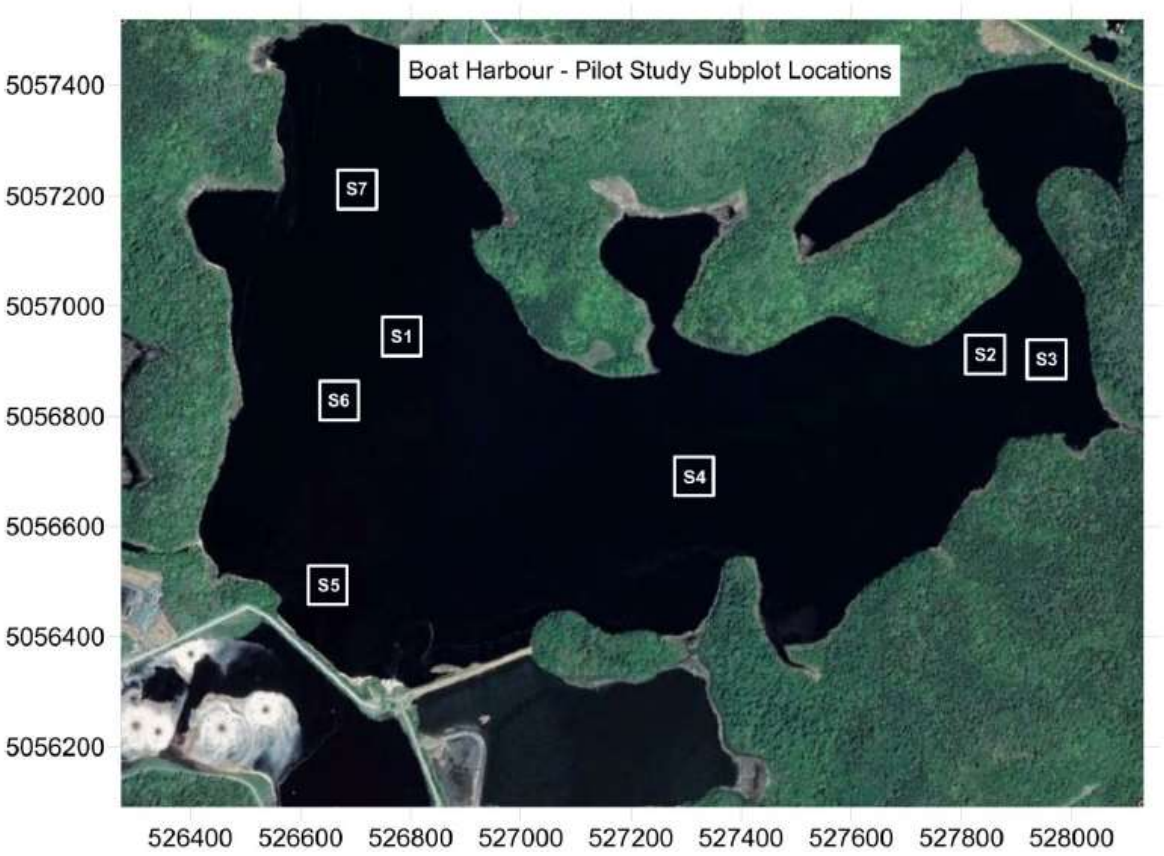

Figure 28: Field trial sampling locations (S1-S7) plotted in UTM Zone 20 (from SCG Industries Limited, 2019).

3.4.2 UVOST Data Collection

Quality control and quality assurance measures, as stated by Dakota Technologies and outlined in section 1.5.4 Data collection QA/QC procedures, were applied during field trials. These measures included the adjustment of RE intensity so that the area under the curve displayed on the oscilloscope was equal to $10{,}000 \pm 1000$ pVs, and background calibration (< 5mV) using the reference emitter prior to each probes data collection. During deployment, the integrated winch and pulley system allowed for a controlled deployment speed of <1 cm/s for high resolution data retrieval. To measure depth readings during deployment, a potentiometer was affixed to the UVOST aquatic deployment station in the same position as phase 3. To lower the probe down through the water column, 1 m extension rods were attached to the probe head. Data collection commenced above the water, which allowed for a continuous collection of multiple mediums (i.e., air, water, BEIS, GEIS). In total, 100 UVOST logs were collected during this phase of the assessment. The method developed to interpret the UVOST data is presented in section 4.3 and section 4.4 of this thesis.

After the samples were taken, the data was averaged, and fluorescence contributions from the sediment were extracted from the dataset for further analysis. Data obtained from this extraction include the peak height of the signal received (y-axis and in milli Volts (mV)) and the time resolution of the data (x-axis and in nanoseconds (ns)). The observed peaks were then normalized to the blue wavelength to provide ratios for comparison between the sediment types. The blue wavelength was selected for the normalization as it bore the lowest value of all four wavelengths which would make the ratios greater than 1.

3.4.3 Core Collection and Extrusion

Sediment cores were collected to provide a composite sample for the comparison the interpreted BEIS thicknesses produced by the UVOST logs (Appendix B). Sediment cores were collected using a Glew gravity coring device (Glew, 1989). Collection and sealing protocols used by Spooner and Dunnington (2016), Holmes (2018), and Davidson (2018) were followed for phase three of this assessment. Throughout the BHSL, a total of 100 sediment gravity cores were collected. Sediment cores were retrieved from the gravity coring sampling port on the modified barge (Figure 27) so that core samples could be taken as close as possible to the UVOST probe holes. Upon collection of each sediment gravity core, cores were immediately extruded on the barge to determine the thickness of the BEIS for comparison with the UVOST data. The location of sampling sites which contain the collected clusters can be seen in Figure 28 and samples (as well as their location) are outlined in Appendix B.'Cluster sample I.D.' denotes the numerical categorization of a sample within a cluster, starting at 1 (the first sample taken at the given cluster (Appendix B, Table 25, S1-S7). This numerical categorization allows for ease of comparison when assessing multiple collection methods which were taken from the same location. Sediment cores collected in each cluster are further detailed in Appendix B. Sediment gravity core were extruded using the Glew portable extruding device (Figure 29). The sediment was carefully extruded so that the contact between the BEIS and GEIS (Figure 30) could be accurately observed for a comparison to UVOST BEIS thickness results. In total, 100 sediment cores were extruded throughout Boat Harbour.

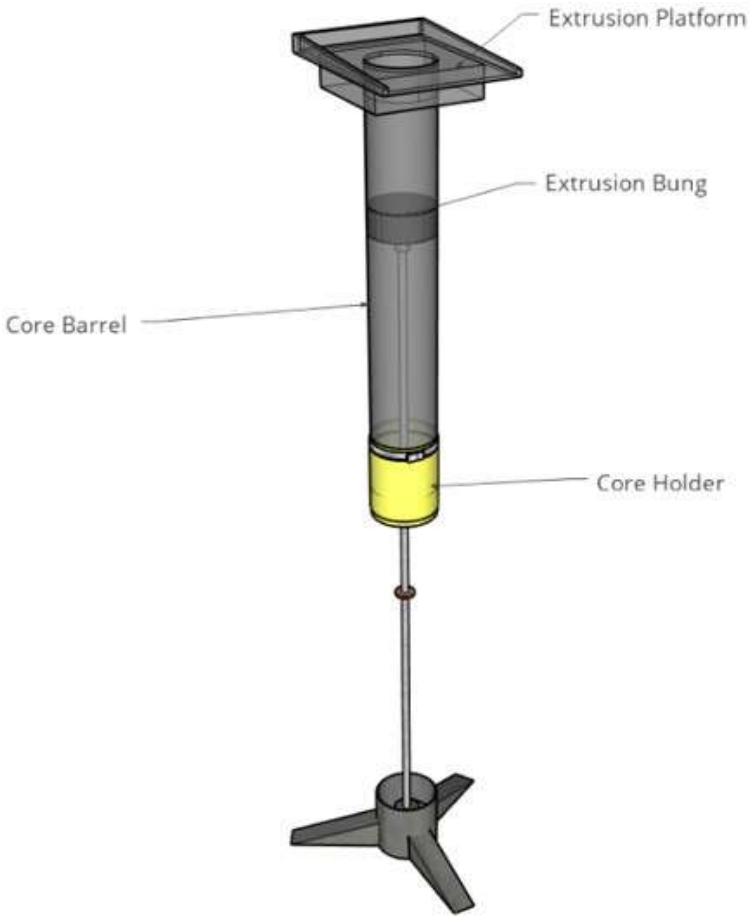

Figure 29: Rendering of the Glew portable extruding device.

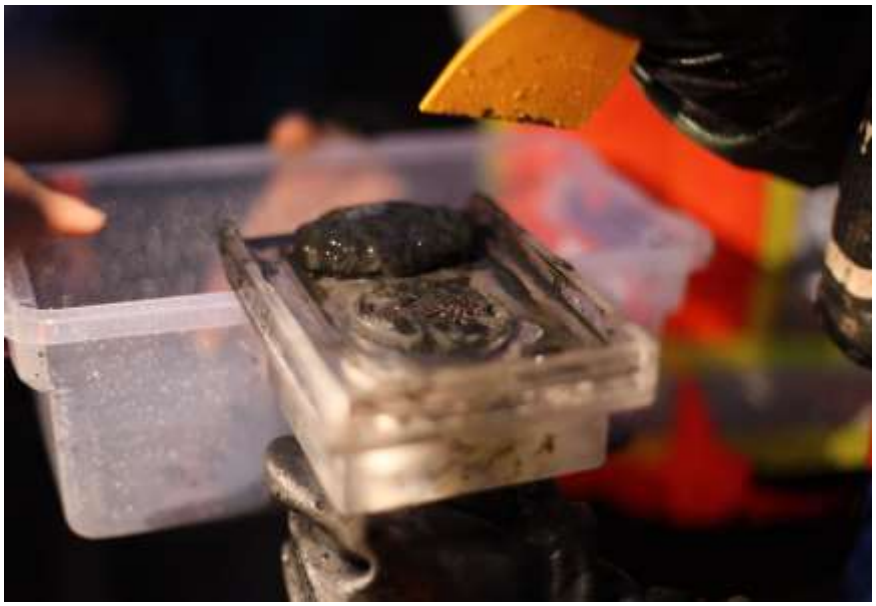

Figure 30: Phase three: sediment extrusion.

3.4.4 UVOST-Sediment Core Thickness Comparison

To compare BEIS thickness measurements made by the UVOST to the sediment gravity core samples, a number of statistical procedures were selected to characterize how closely the datasets compared to one another. These analyses include; The analysis of differences between paired measurements (UVOST-UVOST, core-core, UVOST-core); the plotting of data as bar graphs for samples within each cluster; a linear regression of the complete dataset to deduce the correlation between methods used; and a paired two-sample t-test for means to determine whether or not there are significant differences in datasets. In addition to this, duplicate samples were collected and plotted to visualize local stratigraphic variation that was observed during sampling at the site.

3.4.4.1 Variation in Observed Differences of Collection Methods

To assess variation of the sampling techniques (i.e. UVOST-UVOST, core-core, and UVOST-core) duplicate samples were collected, and the differences of these paired measurements was calculated. This calculation was also conducted on UVOST-core measurements at each cluster site (Figure 27, S1-S7) and is presented in Appendix B. Duplicate of both core and UVOST samples have been paired using an alphanumerical identification system, alongside the clusters from which they were collected (Table 8). Core samples which have been denoted with the same alphabetical classification indicate a duplicate sample, with the secondary classification of “1” and “2” indicating the order in which they were collected at each sampling site. UVOST samples with an identical identifier were collected in unison with the appropriately classified core sample. Duplicates were taken within 1ft of each other for this analysis. In total, 13 sets of both UVOST and sediment gravity core duplicates were taken. To assess the variation of sampling techniques, the differences between UVOST-UVOST, core-core, and UVOST-core results

have been plotted against mean measurements. To calculate the difference between the two samples, the secondary sample (denoted by a 2) was subtracted from the initial sample (denoted by a 1) for each duplicate pair (i.e. UVOST-UVOST and core-core) as well as UVOST-core samples. To calculate the mean measurement of the sample, the paired samples were added and divided by two. The average differences between UVOST-UVOST, core-core, and UVOST-core measurements were calculated and graphed in excel and are presented in the results section.

Table 8: Duplicate sample pairings.

Cluster	Core Pairing	Core sample	UVOST pairing	UVOST sample
5	A1	BHUV19-0052	A1	19LIF52
	A2	BHUV19-0053	A2	19LIF53
	B1	BHUV19-0058	B1	19LIF58
	B2	BHUV19-0059	B2	19LIF59
	C1	BHUV19-0061	C1	19LIF61
	C2	BHUV19-0062	C2	19LIF62
6	D1	BHUV19-0064	D1	19LIF64
	D2	BHUV19-0072	D2	19LIF72
	E1	BHUV19-0073	E1	19LIF73
	E2	BHUV19-0075	E2	19LIF75
	F1	BHUV19-0076	F1	19LIF76
	F2	BHUV19-0078	F2	19LIF78
	G1	BHUV19-0079	G1	19LIF79
	G2	BHUV19-0081	G2	19LIF81
7	H1	BHUV19-0083	H1	19LIF83
	H2	BHUV19-0085	H2	19LIF85
	I1	BHUV19-0087	I1	19LIF87
	I2	BHUV19-0089	I2	19LIF89
	J1	BHUV19-0091	J1	19LIF91
	J2	BHUV19-0094	J2	19LIF94
	K1	BHUV19-0095	K1	19LIF95
	K2	BHUV19-0096	K2	19LIF96
	L1	BHUV19-0097	L1	19LIF97
	L2	BHUV19-0098	L2	19LIF98
	M1	BHUV19-0099	M1	19LIF99
	M2	BHUV19-0100	M2	19LIF100

3.4.4.2 Sediment Thickness Bar Graphs

To demonstrate the similarities of results collected, samples have been divided into their clusters and plotted as a UVOST vs. core sediment thickness bar graph. Individual samples have been plotted on the X-axis, with thicknesses being plotted on the Y-axis so that the variation within samples of each cluster can be visually compared. To visually assess the variability of the dataset, standard deviation ((+/-) 1 standard deviation from the mean) error bars were plotted on each graph of cluster samples. All data was processed within excel, with the standard deviation being calculated initially, and then plotted atop thickness data in each cluster. Sediment gravity core thickness results were subtracted from paired UVOST thickness result to determine the average amount by which UVOST results varied from sediment gravity core thicknesses at each cluster site (S1-S7). In total, seven bar graphs are presented in the results section.

3.4.4.3 t-test (Paired Two Sample for Means)

To statistically determine the significance of variation within the data set, a t-test (paired two sample for means) was conducted on each cluster. This t-test (paired two sample for means) was selected to test whether the mean difference within each of the datasets was equal or unequal. For each t-test which was conducted, a 95% confidence interval was applied to the analysis. The null hypothesis (Eq. 3) for each t-test is that the mean difference between the paired observations of the UVOST sediment thickness dataset (M1) and sediment gravity core thickness dataset (M2) is zero (0). If the null hypothesis is accepted, the means of the dataset are deemed to be statistically equal.

$$H_o: M1 - M2 = 0 \qquad [3]$$

The alternate hypothesis (Eq. 4) for each t-test is that the mean difference between the paired observations of the UVOST sediment thickness dataset (M1) and sediment

gravity core thickness dataset (M2) does not equal zero (0). If the null hypothesis is rejected, and the alternate hypothesis accepted, the means of the dataset are deemed to be statistically unequal

$$H_a: M1 - M2 \neq 0 \quad [4]$$

To test these hypothesis', the t-stat result generated from excel must be less then t Critical two-tail, but greater than negative (-) t Critical two-tail. If this criterion holds true, then we accept the null hypothesis that the means of the dataset are equal. Alternatively, if this criterion is not met, we reject the null hypothesis and accept the alternate hypothesis which indicates that the means of the datasets are not equal.

3.4.4.4 Regression Analysis

To examine the linear relationship between the two measurements, that in theory should be the same if the hypothesis is correct, a linear regression of the thickness data collected from UVOST and sediment gravity cores was conducted. UVOST sediment thickness (cm) was plotted against core sediment thickness (cm) for the entire dataset. A regression analysis was also performed using Excel with a 99% confidence interval.

Chapter 4 Results and Discussion

4.1 Phase One: Water Quality

4.1.1 Water Quality

Water quality data taken from the bulk sediment collection site (Figure 19) indicates that the water has a low DO (%) and DO (mg/L), which decreases with depth (Table 9). Parameters which decrease slightly with depth include temperature, conductivity, and pH. Total dissolved solids (TDS) were consistent throughout the water column. Of particular interest for this study are conductivity results. Results indicate that the conductivity throughout the water column does not vary greatly. The consistent conductivity of BHSL water may aid in the delineation the water column from the BEIS when conducting UVOST testing.

Table 9: Water quality parameters collected from the bulk sediment collection site (Figure 19), Boat Harbour, Nova Scotia.

Boat Harbour Bulk Sample water characteristics				
Depth (m)	0.0 (surface)	1.0	2.0	2.3 (bottom)
Temperature (˚C)	18.5	17.7	17.1	17.1
DO (%)	8.8	2.3	-2.5	-2.8
DO (mg/L)	0.8	0.3	0.0	0.0
Conductivity (µS/cm)	1379.0	1360.0	1340.0	1342.0
pH	8.0	8.0	8.0	8.0
TDS (mg/L)	1027.0	1027.0	1027	1033.5

4.2 Phase Two: Organic Matter Differentiation Within the BEIS and GEIS

4.2.1 C/N Isotope Comparative Analysis

Data compiled from Davidson (2018) and Holmes (2018) was re-examined in this research to depict differences in the origin of organics within both the BEIS and GEIS in

the BHSL. The BEIS organics appear to be distinctly of terrestrial origin and fall within the total C/N and $\delta^{13}C$ range 17-58 and -32.5% respectively (Figure 31). There are a few points which suggest that the organics are freshwater derived but fall very close to the dividing line of these two origins. These points fall within a total C/N and $\delta^{13}C$ range of 11-17 and -24.9% to -32.5% respectively. Given that the BHSL is fed by a series of freshwater systems, it should be expected that there would be some mixing of freshwater sources with primarily terrestrial sources (i. e. effluent). The origin of the GEIS organics are exclusively of marine origin. The GEIS organics have total C/N and $\delta^{13}C$ values which range from 4-42 and >-23% respectively. These results on both total C/N and $\delta^{13}C$ indicate that the origin of organics within each of the sediment types of interest, the BEIS and GEIS, differ and are visually distinct when plotted. This information, when combined with the relative differences in organic matter content of the two sediment types, suggests that there is a potential for the UVOST to detect these variations in the form of a fluorescence signal (%RE). The premise that these variations may allow for the delineation of these two layers led to the initial laboratory and pilot study completed in phase three of this thesis.

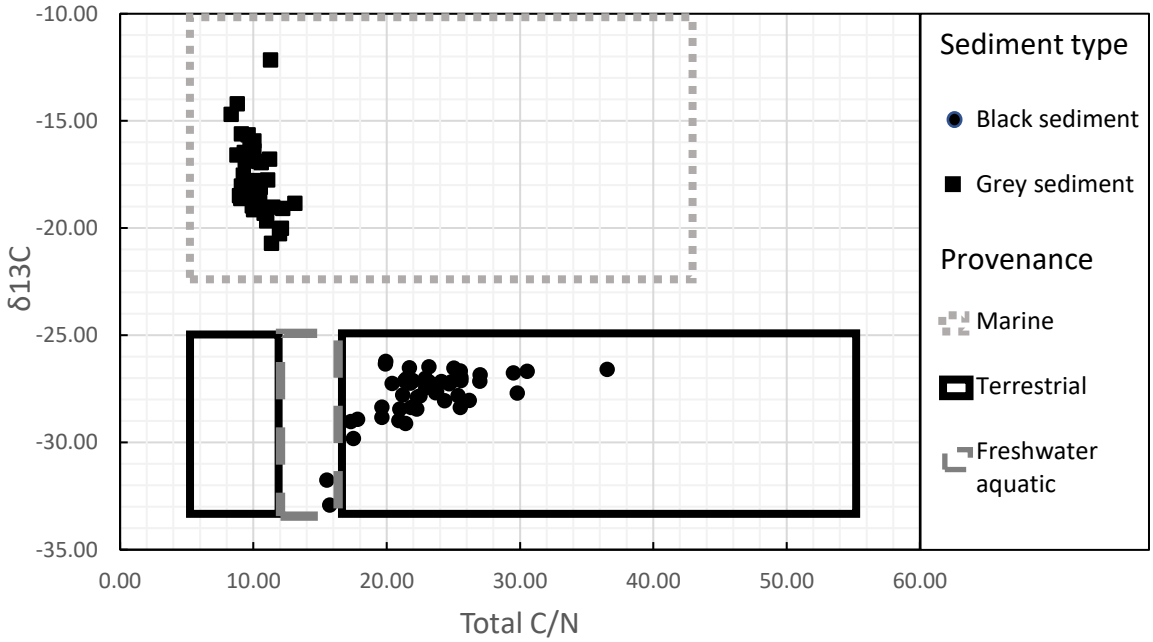

Figure 31: Origin of organics total C/N and δ13C plot.

4.3 Phase Three: Initial Trials and Development of Interpretation Method

4.3.1 Laboratory Study

4.3.1.1 Development of an Interpretation Method

UVOST lab trial results for the fluorescence and conductivity of the BEIS are presented side by side for comparison (Figure 32). The fluorescence data was averaged and indicates fluorescence contributions from the blue (350 nm) green (400 nm), orange (450 nm), and red (500 nm) ultraviolet wavelengths in the order of 1.6 mV, 4 mV, 5 mV, and 2 mV respectively. For further comparative analysis, these wavelengths have been normalized to the blue wavelength to generate some base ratios. The BEIS wavelengths show the following approximate ratios; green:blue = 2:1, orange:blue = 2.5:1 and red:blue 1.25:1. The blue, green, and orange wavelengths were noted to have slight tails, which indicate an increased fluorescence decay time. This increased decay time can be observed

as the elongated peaks and tails which trail from the right side of each wavelength. On average, the observed percentage of fluorescence above the reference emitter for the BEIS ranged from 1.0-1.2 %RE and averaged 1.1%RE. The conductivity of the BEIS averaged 25 mS/m.

UVOST lab trial results for the fluorescence and conductivity of the GEIS are presented side by side for comparison (Figure 33).The fluorescence data was averaged and indicates fluorescence contributions from the blue (350 nm) green (400 nm), orange (450 nm), and red (500 nm) ultraviolet wavelengths in the order of 1.2 mV, 3.6 mV, 6 mV, and 2.8 mV respectively. For further comparative analysis, these wavelengths have been normalized to the blue wavelength to generate some base ratios and allow comparison to the base ratios generated for the BEIS. The GEIS wavelengths show the following approximate ratios; green:blue = 3:1, orange:blue = 5:1 and red:blue 2.5:1. The blue, green, and orange wavelengths were noted to have slight tails, with an increased decay time of the blue wavelength. The decay time of the GEIS blue wavelength, however, was less than the BEISs blue wavelength. On average, the observed percentage of fluorescence above the reference emitter for the GEIS ranged from 0.8-1.0 %RE and averaged 1.0% RE. The conductivity of the GEIS averaged 100 mS/m.

Initial tests conducted on individual samples of the BEIS and GEIS suggest that variation in %RE, conductivity, and wavelength ratios may be able to aid in the assessment of sediment type. On average, the BEIS showed a higher %RE then the GEIS in the individual sample tests (i.e. an indication of difference in amount and type of organic matter). Conductivity was noted to be significantly higher (4:1) in the GEIS when compared to the conductivity of the BEIS, which is in agreement to the salinity results presented by Song (2020). When assessing the differences in wavelength ratios between

the two sediment types; green: blue; orange: blue; and red: blue comparative wavelength ratios may be able to assist in predicting the sediment type from which the UVOST is collecting data. Wavelength ratios from the GEIS for the green: blue; orange: blue; and red: blue wavelengths show a trend of being 1.5x, 2x, and 2x larger than that of the BEIS, respectively. It must be noted, however, that these trials were conducted in an oxidized environment, and as oxygen is a known fluorescence quencher, these results may have been impacted by this signal quenching effect. Results, however, were promising at the preliminary stages of this thesis, and further testing was conducted on mock core to examine these relationships.

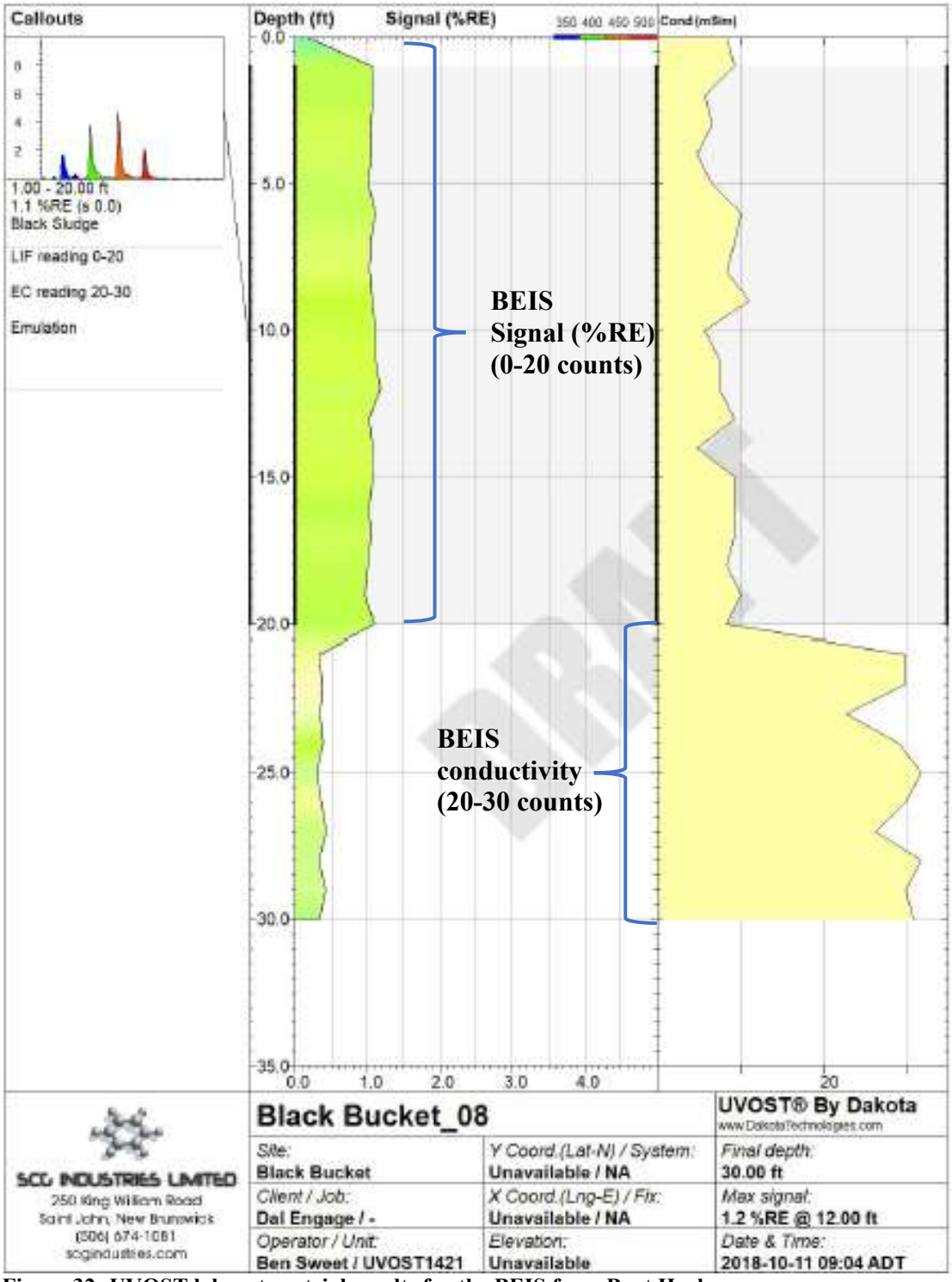

Figure 32: UVOST laboratory trial results for the BEIS from Boat Harbour.

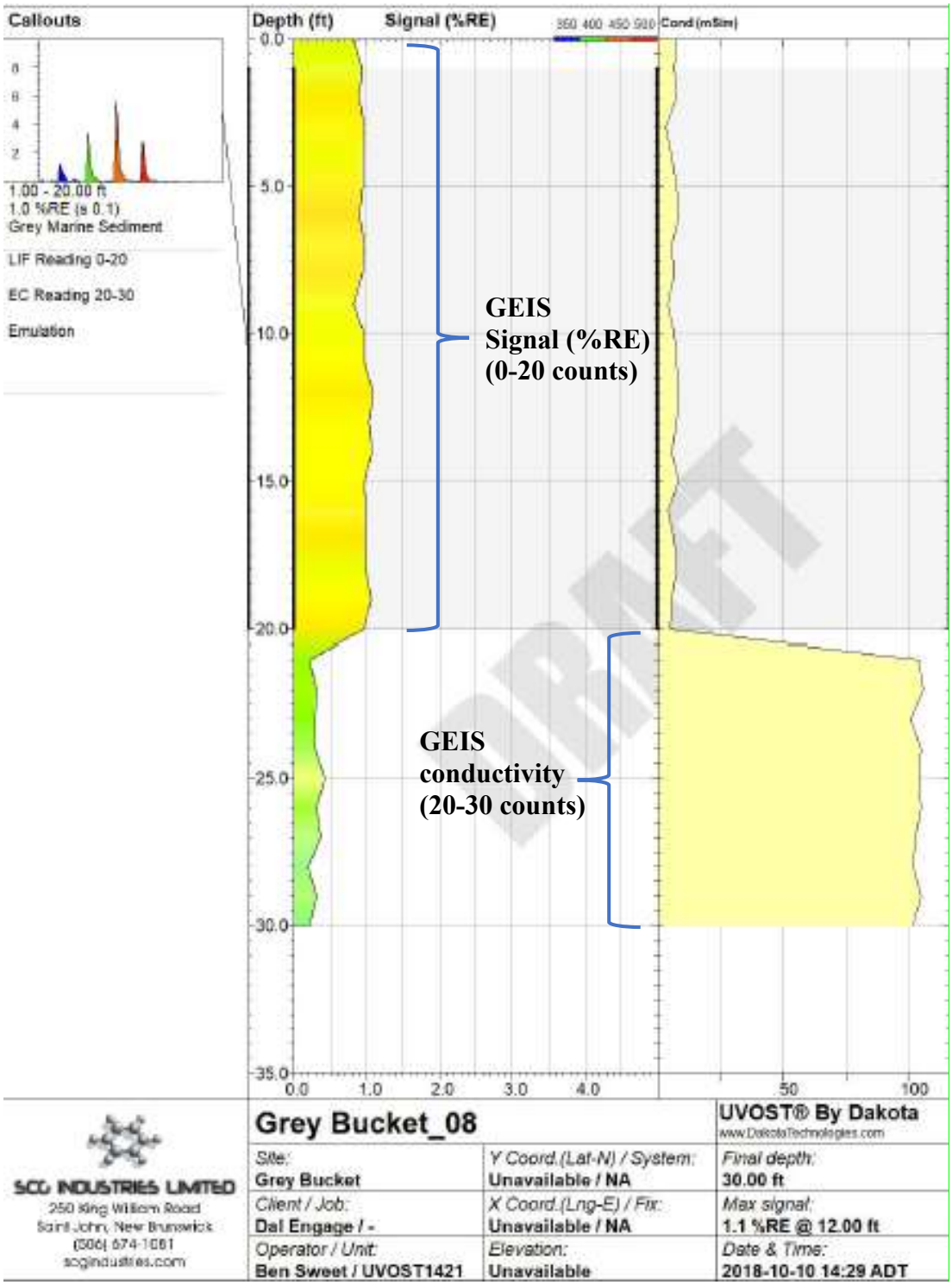

Figure 33: UVOST laboratoy trial results for the GEIS from Boat Harbour.

Initial test results for the fluorescence and conductivity of the mock core are presented side by side for comparison (Figure 34). After insertion, the BEIS was measured from a depth of 0-1.2 ft. The fluorescence data was averaged and indicates fluorescence

contributions from the blue (350 nm) green (400 nm), orange (450 nm), and red (500 nm) ultraviolet wavelengths in the order of 1.6 mV, 4 mV, 5.6 mV, and 2.8 mV respectively. For further comparative analysis, these wavelengths have been normalized to the blue wavelength (similar to the previous work) to generate some base wavelength ratios. The BEIS wavelengths show the following approximate ratios: green: blue = 2.5:1; orange: blue = 3.5:1; and red: blue = 1.75:1. The blue, green, and orange wavelengths were noted to have slight tails, which indicate an increased fluorescence decay time. This increased decay time can be observed as the elongated peaks and tails which trail from the right side of each wavelength. The observed percentage of fluorescence above the reference emitter for the BEIS ranged from 1.0-1.4 %RE and averaged 1.1% RE. The conductivity of the BEIS was greater than the previous test and averaged 200 mS/m. This increase in conductivity is likely the result of compaction of the sediment during the creation of the mock core.

The GEIS was measured from a depth of 1.2-1.5 ft. The fluorescence data was averaged and indicates fluorescence contributions from the blue (350 nm) green (400 nm), orange (450 nm), and red (500 nm) ultraviolet wavelengths in the order of 1.2 mV, 3.2 mV, 5.6 mV, and 2.4 mV respectively. For further comparative analysis, these wavelengths have been normalized to the blue wavelength to generate some base ratios. The GEIS wavelengths show the following approximate ratios; green: blue = 2.5:1, orange: blue = 4.5:1 and red: blue 2:1. No wavelengths were noted to have tails which indicate an increased fluorescence decay time. The observed percentage of fluorescence above the reference emitter for the GEIS ranged from 0.8-1.1 %RE and averaged 0.8% RE. The conductivity of the GEIS was greater than the previous test and averaged 800 mS/m. This increase in conductivity could be the result of compaction of the sediment during the creation of the mock core.

Initial tests conducted on the mock core of BEIS and GEIS provided further evidence that variations in %RE, conductivity, and wavelength ratios may be able to aid in the assessment of sediment type. On average, the BEIS showed a higher %RE then the GEIS. Conductivity was noted to be significantly higher (4:1) in the GEIS when compared to the conductivity of the BEIS. When assessing the wavelengths themselves, the orange: blue and red: blue comparative wavelength ratios are different in the two sediment types and may be able to assist in predicting from which sediment the UVOST is collecting data. Ratios calculated from the GEIS for the orange: blue and red: blue wavelengths were shown to be 1.29 times and 1.14 times larger than that of the BEIS, respectively. There was no difference observed for the green: blue ratio. These ratios show less variation then determined in the individual sample trials. However, variation is still present and may yet aid in the delineation of sediment types as a method of quality control, alongside %RE and conductivity measurements of the sediments.

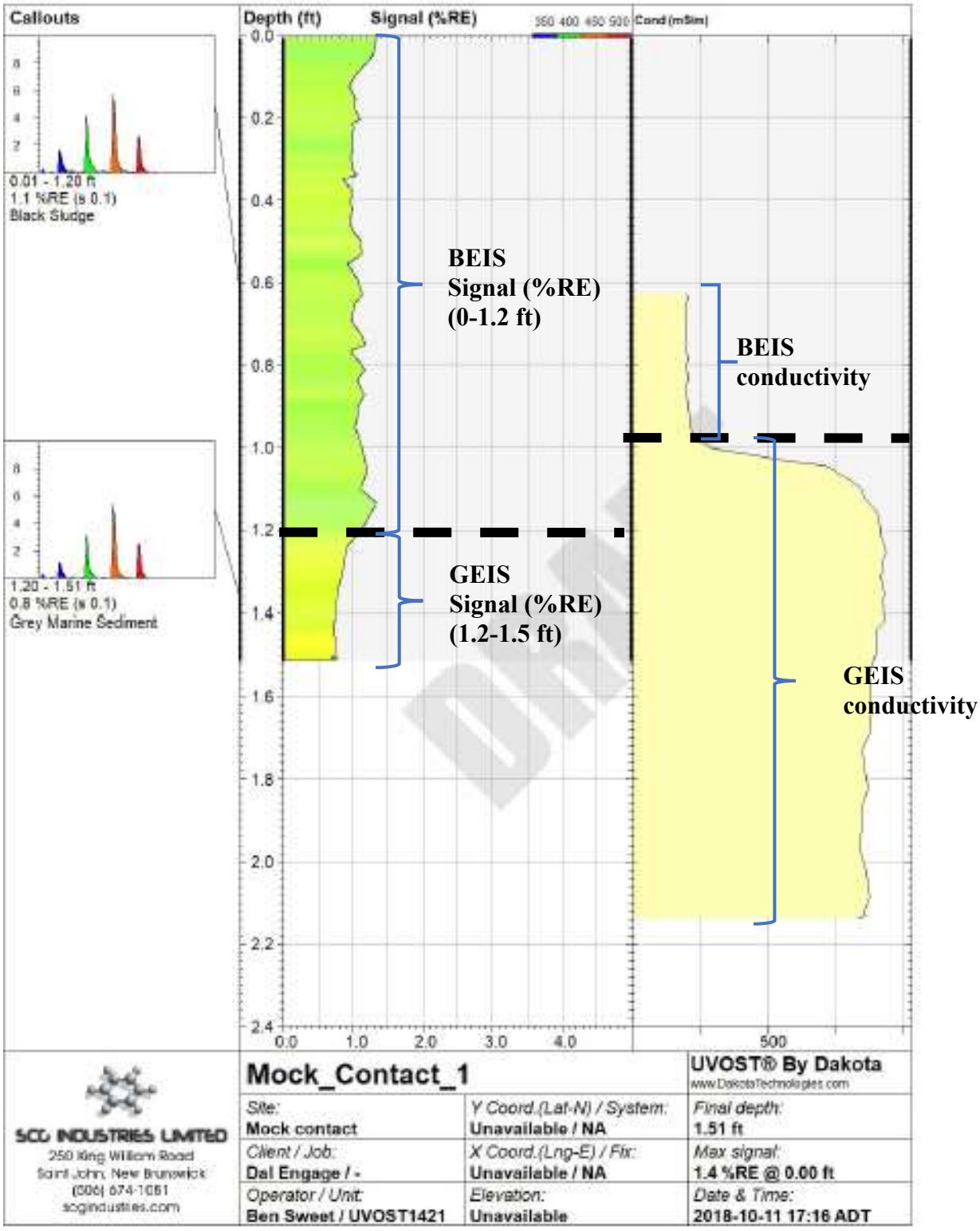

Figure 34: UVOST laboratoy trial results for the mock core consisting of both BEIS (0-1.2ft) and grey (1.2-1.5ft) sediment from Boat Harbour.

Observation of the differences in %RE values and relative peak heights of the wavelength signatures of the two sediments provided the impetus to explore a feature available in the UVOST data processing software whereby a given sediment layer's fluorescence signature can be internally stored and subtracted from another sediment layer's fluorescence signature. The fluorescence signal of the GEIS was subtracted from that of the BEIS, (shown in Figure 34 above), a unique signature was produced in which the fluorescence wavelength contributors of the BEIS can be seen more clearly (Figure 35). The fluorescence data from Figure 35 was averaged and indicates fluorescence contributions from the blue (350 nm) green (400 nm), orange (450 nm), and red (500 nm) ultraviolet wavelengths in the order of 0.4 mV, 1.2 mV, 0.4 mV, and 0.2 mV respectively. The observed percentage of fluorescence above the reference emitter for the BEIS ranged from 0.2-0.4 %RE and averaged 0.3% RE. This method provides a complementary assessment which can be applied when discerning sediment layers.

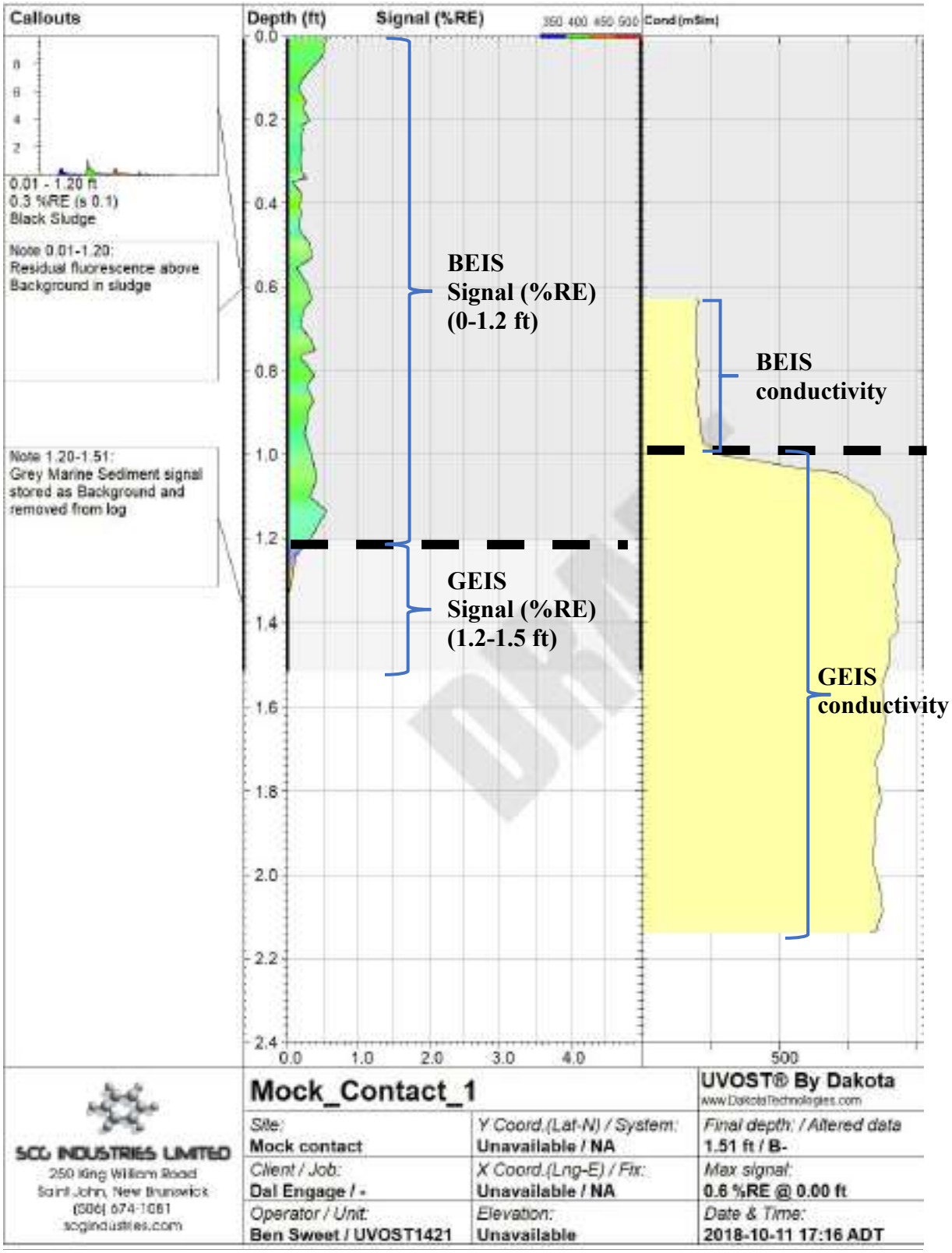

Figure 35: UVOST laboratoy trial results for mock core, consisting of both BEIS (0-1.2 ft) and GEIS from Boat Harbour, with the %RE signal of the GEIS subtracted from the BEIS.

4.3.1.2 General Observations from Phase Three Laboratory Trials

Throughout the laboratory trials both the BEIS and GEIS showed unique %RE and conductivity readings in the UVOST logs and wavelength ratios. For the purpose of developing an interpretation method to detect differences in sediment types, the following observations were made:

1) %RE varied for both the BEIS and GEIS individually and when tested in the mock core. On average, the BEIS displayed a higher %RE when compared to the GEIS during both individual sample trials, and mock core trials. For further sampling, the difference in %RE of the sediment types made it possible to subtract the GEIS %RE reading from the BEIS %RE reading and easily discern the two sediment types in a laboratory setting.
2) Conductivity varied greatly for both the BEIS and GEIS individually and when tested in the mock core. On average, the GEIS had significantly higher conductivity values when compared to the BEIS. The variation in conductivity is likely caused by variation in the salinity of pore water within the sediment types as noted by previous work (Song, 2020).
3) Although the type of organic compound cannot be identified using this method, there are variations which suggest differences in the organic compositions of each sediment. The callouts show a larger fluorescence decay time in the BEIS as compared to the GEIS (Figure 34). The decay time is displayed in the callouts as the tail extending from each of the wavelength peaks (blue, green, orange, red).
4) Comparative analysis of wavelength ratios between the two sediment types showed a trend of the GEIS have a larger variation of these ratios (green: blue, orange: blue,

and red: blue) than that of the BEIS. The variation in ratios was noted to be greater in the individual sample trials then that of the mock core.

4.3.1.3 Summary of Method Development During Laboratory Trials

Preliminary laboratory trial results informed further pilot and field analysis and aided in the development of a method of interpretation for various sediment types. The parameters of %RE, conductivity, and wavelength ratios have the potential to delineate these layers, as shown in the laboratory trials. The BEIS consistently bore a higher %RE then that of the GEIS. The GEIS consistently bore a higher conductivity than that of the BEIS. The variations of wavelength ratios were greater in GEIS then that of the BEIS, however, the variation lessened during the mock core trials. The validity of using the last technique (wavelength ratios) to discern layers was not proven effective during of the laboratory trials, and as such, individual wavelengths are more closely examined in the following pilot study. The culmination of these 3 techniques provide the basis for the interpretation of sediment types and are refined in the pilot study section of this thesis. It is important to note that the final method mentioned of subtracting one sediment %RE from another sediment to assess the difference may not always be effective. In the case of this studies sediment types, there is only a slight variation in %RE between the two sediment types (0.3%). If the %RE of the two samples prove to be similar during field trials, the previously discussed methods may be more suitable for discerning sediment layers.

The interpretation of the laboratory trial results informs the development of the field method . This data, however, may have been impacted by the fluorescence quenching effect of oxygen. Although this is possible, the general trends which have been observed may prove useful for further testing. The following section on the pilot study component of this

methods development was conducted in an anoxic environment (the BHSL) as shown in section 4.1.1 **Water quality** of this study. The parameters of %RE, conductivity, wavelength ratios, and an additional analysis on individual wavelength readings are further assessed as a method of delineating sediment type in the proceeding pilot study.

4.3.2 Pilot Study

To further develop an interpretation method, building on the information gained in the laboratory, pilot study sample Boat Harbour18-LIF**01 (BH18-LIF01)** was selected for further analysis (Figure 36). This sample was selected as it was taken under ideal field conditions and shows clearly definable boundaries between various layers. Both the fluorescence and conductivity results have been presented side by side for comparison (the data for which can be found in Appendix C). In UVOST log BH18-LIF01, there are 4 unique units which were identified by the UVOST device and can defined by internal variations in %RE, conductivity, and wavelength ratios. These units have been interpreted as (from top to bottom) air, water, BEIS, and GEIS. Post analysis of UVOST log BH18-LIF01, the blue, green, orange, and red wavelengths have been graphed to show their relation to %RE and how they in turn can be used to identify various mediums as well.

4.3.2.1 UVOST Field-log Interpretation

UVOST field logs were interpreted to have 4 mediums which include, air, water, BEIS, and GEIS (Figure 36). The UVOST began producing fluorescence data prior to entering the water, which can be considered background fluorescence, and has been interpreted as an air medium. Fluorescence data for air (background) was collected in depths ranging from 0 m to 0.30m, which corresponds to the distance from the barges probe entry point, to the water's surface at sample site BH18-LIF01 (Figure 23). The fluorescence data was averaged and indicates fluorescence contributions from the blue (350 nm) green

(400 nm), orange (450 nm), and red (500 nm) ultraviolet wavelengths in the order of 0.8 mV, 1 mV, 0.8 mV, and 0.2 mV respectively. Ideally, these readings would all be 0 mV, however, interference from external light sources (i.e. sunlight), have likely caused an increased reading in the air medium.

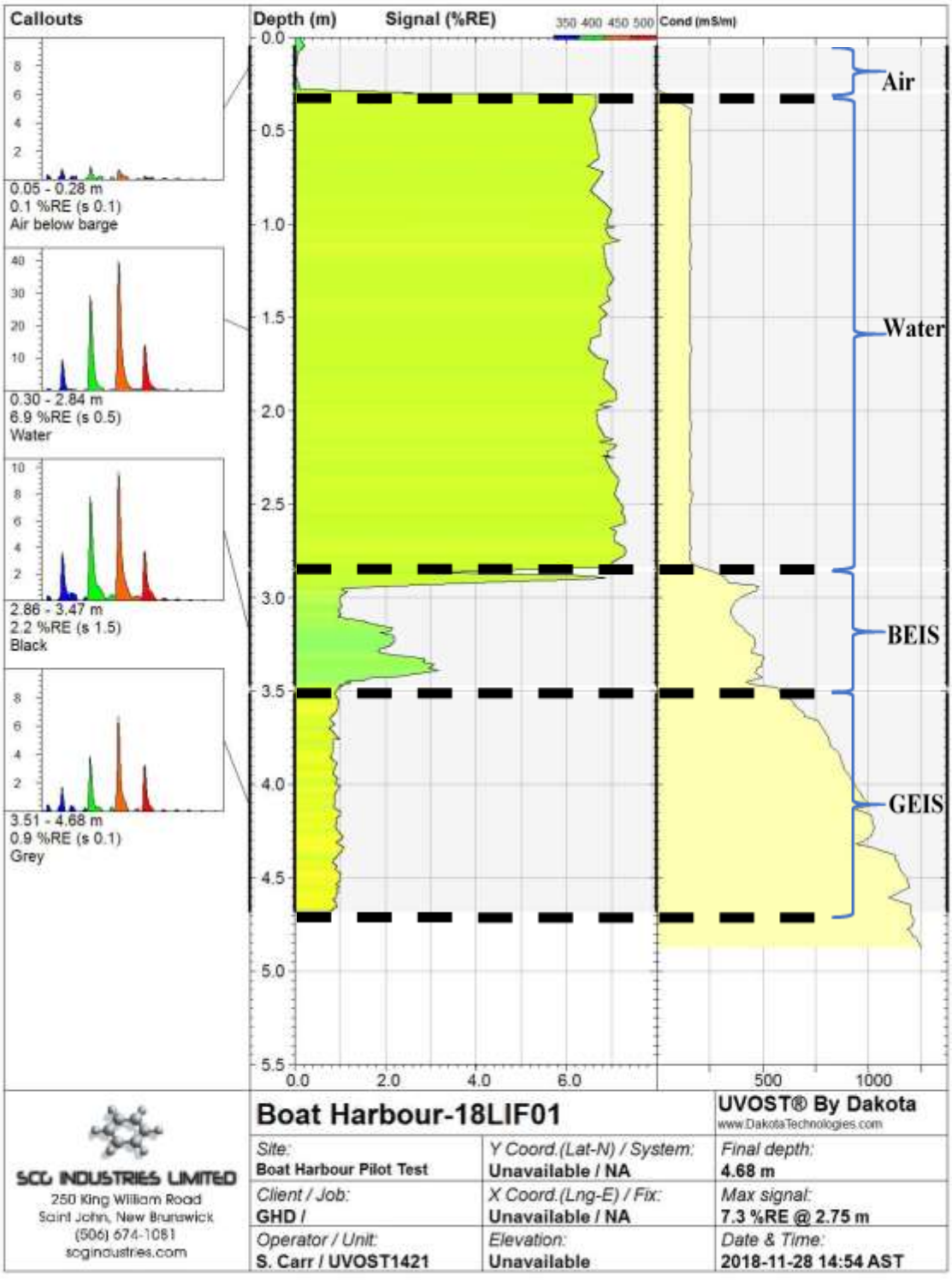

Figure 36: UVOST data log "Boat Harbour-18LIF01".

As background levels (which are taken in the air medium) are collected as close to 0 %RE as possible, and thus are known to be essentially 0 %RE, no further wavelength ratios have been analyzed for this medium. The air mediums %RE ranged from 0-0.2 %RE and averaged 0.1% RE. The air mediums conductivity was noted to be 0 mS/m.

Fluorescence data for water was collected in depths ranging from 0.3m to 2.84 m, a water depth of 2.54 was indicated for site BH18-LIF01 (Figure 23). The fluorescence data was averaged and indicates fluorescence contributions from the blue (350 nm) green (400 nm), orange (450 nm), and red (500 nm) ultraviolet wavelengths in the order of 10 mV, 29 mV, 40 mV, and 15 mV respectively. For further comparative analysis, these wavelengths have been normalized to the blue wavelength to generate some base ratios. The water medium's wavelengths show the following approximate ratios; green: blue = 3:1, orange: blue = 4:1 and red: blue 1.5:1. Additionally, as shown in the callouts to the left of Figure 36, none of the wavelengths were noted to have tails (protrusions to the right of a wavelengths maximum peak which indicate an increased fluorescence decay time). The water mediums %RE ranged from 6.4-7.3 %RE and averaged 6.9% RE. This unit was characterized as having the highest %RE return when compared to the other 3 mediums. Compared to the underlying sediment, the water medium had a relatively low average conductivity of 159 mS/m. The conductivity within the water column showed a uniform trend which is comparable to results collected using the YSI multiparameter probe.

Fluorescence data for the BEIS was collected in depths ranging from 2.84m to 3.47m, a BEIS thickness of 0.63 was indicated for site BH18-LIF01 (Figure 23). The fluorescence data was averaged and indicates fluorescence contributions from the blue (350 nm) green (400 nm), orange (450 nm), and red (500 nm) ultraviolet wavelengths in the

order of 3.6 mV, 8 mV, 9.8 mV, and 3.6 mV respectively. For further comparative analysis, these wavelengths have been normalized to the blue wavelength to generate some base ratios. The BEIS wavelengths show the following approximate ratios; green: blue = 2.5:1, orange: blue = 2.75:1 and red: blue 1:1. The blue, green, and orange and red wavelengths were noted to have tails, which indicate an increased fluorescence decay time. This increased decay time can be observed as the elongated peaks and tails which trail from the right side of each wavelength. These peaks and tails are the largest which have been observed in any medium. The BEIS's %RE ranged from 1.1-3 %RE and averaged 2.2 %RE. This unit's 2.2 %RE value was characterized as being less than the %RE of the BHSL's water, but greater than the %RE of the underlying GEIS. The sample displayed a range of conductivities from 207 mS/m to 470 mS/m with an average conductivity of 413 mS/m. Both conductivity and %RE were noted to increase with depth throughout the BEIS.

Fluorescence data for the GEIS was collected in depths ranging from 3.47m to 4.68m, as no further facies were observed, the thickness of this unit cannot be determined at the sample site. The fluorescence data was averaged and indicates fluorescence contributions from the blue (350 nm) green (400 nm), orange (450 nm), and red (500 nm) ultraviolet wavelengths in the order of 1.6 mV, 4 mV, 6.8 mV, and 3.2 mV respectively. For further comparative analysis, these wavelengths have been normalized to the blue wavelength to generate some base ratios. The GEIS wavelengths show the following approximate relations; green: blue = 2.5:1, orange: blue = 5.5:1 and red: blue 2:1. The blue, green, orange and red wavelengths were noted to have slight tails, which indicate an increased fluorescence decay time. These tails, however, did not have as large of an area beneath the curve as those in the BEIS. This is an indication of both shorter decay times and fluorescence intensities of the fluorophores present in the GEIS. The GEIS's %RE

ranged from 0.8-1.1 %RE and averaged 0.9 %RE. The GEIS's conductivity ranged from 569 mS/m to 1248 mS/m and averaged 973 mS/m. The GEIS layer showed a trend of increasing conductivity with depth, however, its %RE stayed relatively the same throughout the sampled depth.

4.3.2.2 Independent Waveforms

To further examine how the ratios between various wavelengths in the mediums of interest (ie: BEIS and GEIS) interact, each normalized wavelength (blue, green, orange, and red) was extracted from the data log (BH18-LIF01) and graphed with depth (Figure 37). Together, these waveforms add to become the total %RE graph (Figure 36). Independently however, they provide insight into the relationships of these wavelengths between the water, BEIS, and GEIS when using ratios to infer differences.

Significant variation between the blue, green, orange, and red wavelengths were noted in the water medium, and are reflected in its comparative ratios. When compared to the BEIS, the water shows the variation in the green:blue and orange:blue ratios differ greatly. When compared to the GEIS, the green: blue and orange: blue ratios are likely to be much closer in comparison. As well, the red: blue ratio for the water medium is expected to be larger than the BEISs red: blue ratio.

The annotated BEIS shows the green and orange wavelengths have similar variation from the blue wavelength (Figure 37). This contrasts the GEIS where the orange wavelength shows a much greater difference then that of the green wavelength. The red wavelength shows a relationship with the blue wavelength that is very similar in both the BEIS and GEIS. This relationship, however, shows a larger degree of variation from the blue wavelength in the GEIS when compared to the BEIS. Using this methodology, one can distinguish between the various sediment types with a ratio-based approach. The ratio

relationships of several logs gathered during the pilot study are presented below (Table 10 to 14).

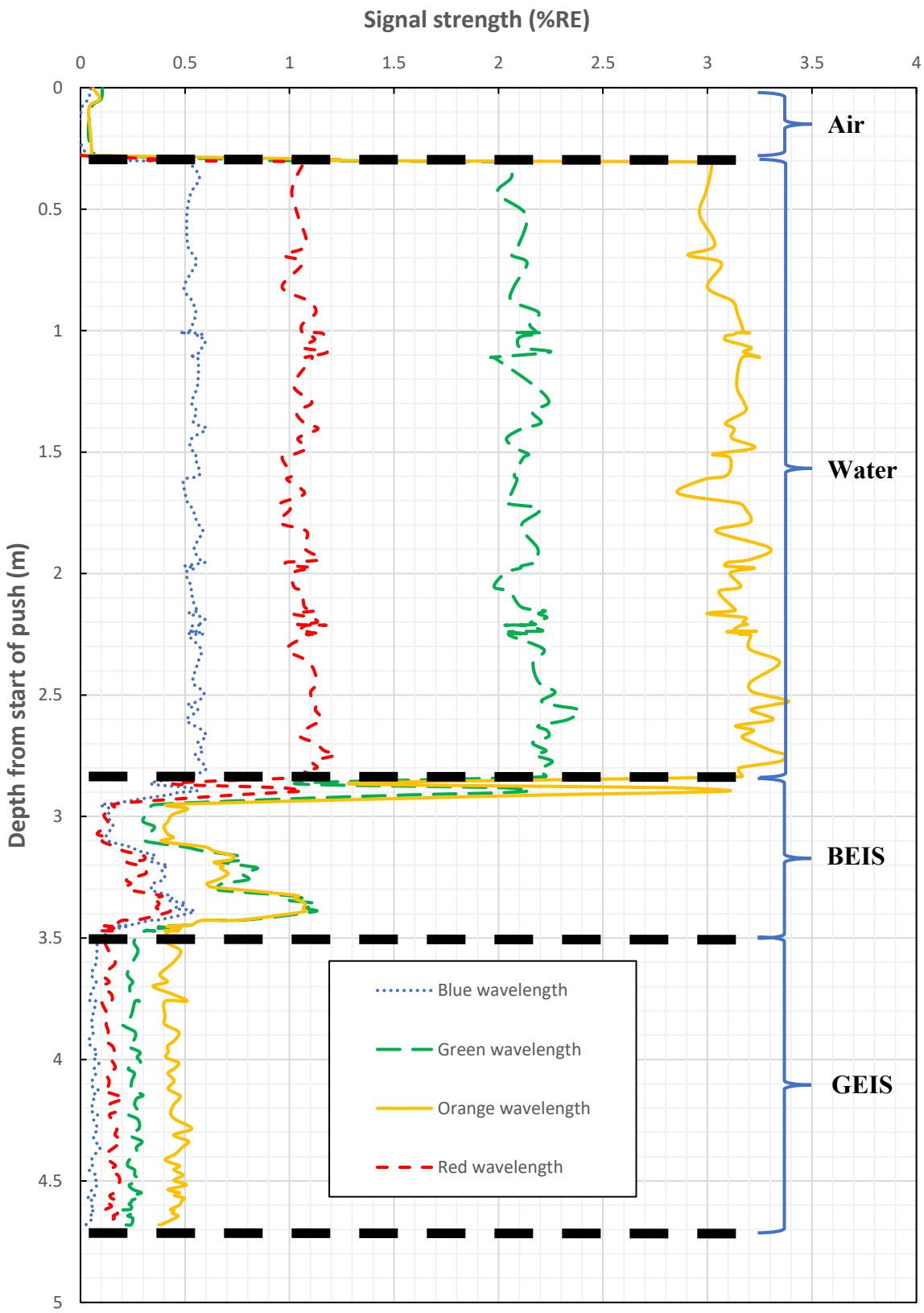

Figure 37: Independent waveform plot of blue, green, orange, and red waveforms after RE normalization.

When examining the green:blue, orange:blue, and red:blue comparative ratios, results indicate that there is much more variation from the blue wavelength in the GEIS when compared to the BEIS. The green:blue comparison suggests that the variation of this ratio in the BEIS is equal to that of the GEIS. Both the orange:blue and red:blue ratios were consistently higher in the GEIS, when compared to the BEIS in all five data logs. The orange:blue comparison, however, showed the greatest variation of all the ratios, and as such, is likely the optimal indicator of the transition from BEIS to GEIS.

Table 10: BH18-LIF01 ratio relationship.

BH18-LIF01					
Comparative ratio	**Medium**			**Ratio relationship**	
	Water	**BEIS**	**GEIS**	**Water-BEIS**	**BEIS - GEIS**
Green: blue	3:1	2.5: 1	2.5:1	Water > BEIS	GEIS = BEIS
Orange: blue	4:1	2.75:1	5.5:1	Water > BEIS	GEIS > BEIS
Red: blue	1.5:1	1.1:1	2:1	Water > BEIS	GEIS > BEIS

Table 11: BH18-LIF02 ratio relationship.

BH18-LIF02					
Comparative ratio	**Medium**			**Ratio relationship**	
	Water	**BEIS**	**GEIS**	**Water-BEIS**	**BEIS - GEIS**
Green: blue	3:1	2: 1	3:1	Water > BEIS	GEIS > BEIS
Orange: blue	4.1:1	3:1	6:1	Water > BEIS	GEIS > BEIS
Red: blue	1.5:1	1.1:1	3:1	Water > BEIS	GEIS > BEIS

Table 12: BH18-LIF05 ratio relationship.

BH18-LIF05					
Comparative ratio	**Medium**			**Ratio relationship**	
	Water	**BEIS**	**GEIS**	**Water-BEIS**	**BEIS - GEIS**
Green: blue	3:1	2.2: 1	2.7:1	Water > BEIS	GEIS > BEIS
Orange: blue	4.4:1	2.8:1	4.3:1	Water > BEIS	GEIS > BEIS
Red: blue	1.5:1	1.1:1	2.25:1	Water > BEIS	GEIS > BEIS

Table 13: BH18-LIF07 ratio relationship.

BH18-LIF07					
Comparative ratio	**Medium**			**Ratio relationship**	
	Water	**BEIS**	**GEIS**	**Water-BEIS**	**BEIS - GEIS**
Green: blue	3.6:1	2.5: 1	3.75:1	Water > BEIS	GEIS > BEIS
Orange: blue	4.9:1	3.5:1	6:1	Water > BEIS	GEIS > BEIS
Red: blue	1.7:1	1.5:1	3:1	Water > BEIS	GEIS > BEIS

Table 14: BH18-LIF08 ratio relationship.

BH18-LIF08					
Comparative ratio	**Medium**			**Ratio relationship**	
	Water	**BEIS**	**GEIS**	**Water-BEIS**	**BEIS - GEIS**
Green: blue	3.6:1	2.25: 1	2.5:1	Water > BEIS	GEIS > BEIS
Orange: blue	4.9:1	3.25:1	4.75:1	Water > BEIS	GEIS > BEIS
Red: blue	1.7:1	1.5:1	2:1	Water > BEIS	GEIS > BEIS

4.3.2.3 General Observations

Throughout the pilot study there were general trends with each unit that were observed and aided in the development of a field interpretation method. For the purpose of developing this interpretation method, the following information was noted to be an ideal indicator of a unit's extent at the site.

1) Both the %RE and conductivity readings for the air unit were noted to be approximately '0' consistently. The %RE measurements being taken during this period were of background values which the device is set to as a baseline prior to each reading. Conductivity is also expected to be approximately 0 as there is no connection between the dipoles of the conductivity attachment on the probe.

2) When examining water in the logs, consistent readings of both the %RE and conductivity were observed. This likely indicates that the fluorophores and salinity profile of the water do not vary significantly with depth. This assumption of the salinity profile can be verified with the previously collected YSI data in section

4.1.1 water quality (Table 9). Both conductivity and TDS throughout the water column remained relatively consistent.

3) The thickness of the BEIS was defined by two unique transitionary interfaces. As the probe was pushed through the water and into the BEIS %RE decreased rapidly. The top of the BEIS was interpreted as the initial inflection point of this interface. After passing through the top of the BEIS, a 'low point' of %RE would be reached, and gradually increase with depth. Conductivity increased with depth throughout the BEIS as well and was noted as potential indicator of the transition from water to BEIS. This increase in %RE is likely caused by the consolidation of the BEIS, and in turn, the concentration of organic molecules within the sediment. The transition between the BEIS to GEIS was marked by a sharp decrease in %RE, as well as an increase in conductivity.

4) The GEIS was easily discernable from the BEIS as its %RE remained consistent throughout its measurement. Some abnormalities were observed occasionally where large spikes in %RE would occur. Sediment gravity cores were taken at these sites and it was noted that shells within the GEIS were likely creating a false positive reading. In these cases, these signals were easy to identify as false readings as the %RE spikes where quite significant. Conductivity throughout the GEIS increased steadily with depth and was often a useful indicator of the transition from BEIS to GEIS.

5) The wavelength ratios show a trend of having greater variation in the water medium, over that of the BEIS, as well as in the GEIS when compared to the BEIS. For both the water/BEIS, and BEIS/GEIS comparison, the orange:blue ratio showed the greatest level of variation and can be used to delineate the layers from one another

respectively. The green:blue and red:blue comparative ratios also showed a trend of the water having greater variation than the BEIS, and the GEIS having greater variation then that of the BEIS. Further examining the independent waveforms, the green and orange wavelengths showed a very similar reading in the BEIS (Figure 37). In contrast, the GEIS's orange and green waveforms were clearly distinct from one another, with the orange being greater in intensity then the green wavelength. By examining independent waveforms and calculating waveform ratios, it is possible to automate the process of delineating the mediums present at the site. The application of a program which has the capability to sort these ratios and directly compare differences between independent waveforms in each medium could expediate the process of defining a mediums extent.

4.3.2.4 Summary of Method Development During Pilot Study

Results from the preliminary laboratory trial were used to inform the development of the interpretation method during the pilot phase of this analysis. The parameters of %RE, conductivity, and wavelength ratios were further tested for the capability of delineating the mediums present onsite (air, water, BEIS, GEIS).

The air medium bore no significant %RE, conductivity, or wavelength ratios, and as such, was easily discernable in the field logs as having effectively '0' in all three parameters. The transition between the air medium and water medium began when all parameters (%RE, conductivity, or wavelength ratios) increased rapidly to a consistent reading. These results affirm the method of delineating the air medium from the water medium, which was applied onsite during the pilot study, and was applied during the field trials portion of this thesis.

The water medium had the highest %RE of all mediums, which was consistent throughout its entirety. The transition from water to BEIS using %RE was determined to be the inflection point at which the waters consistent %RE dropped to definitive low point. This zone of high-low %RE is the transition zone where the BEISs water content is effectively that of water itself. Conductivity measurements were often less than that of the BEIS, however, they did fluctuate at different testing locations. Fluctuations in conductivity within the BHSL are thought to be related to the proximity of the sample site to the BSHL's effluent inlet, differential settling of the effluent throughout the basin, and the dilution of effluent by external water sources (i.e. small brooks which feed into the BHSL). When using conductivity to delineate the water medium from the BEIS, the transition from a consistent conductivity to one which fluctuated, either positively or negatively, marked the transition from water to BEIS. When using differential ratios, the water consistently showed greater variation in all wavelengths when compared the BEIS. Results suggest that the green:blue and red:blue ratios can be used to delineate this transition, however, the orange:blue wavelength ratio exhibits the greatest variation, and therefore may prove to be the most effective indicator of this transition. These results aided in the validation of this method of delineating the water medium from the BEIS, which was applied onsite during the pilot study, and have been applied during the field trials portion of this thesis.

When examining the differences between the BEIS and GEIS within the BHSL, the parameters of %RE, conductivity, and wavelength ratios were all utilized. The %RE of the BEIS was noted to be consistently higher than that of the GEIS. The BEIS tended to show a trend of increasing %RE with depth, and the point at which %RE decreased rapidly, was determined to be the BEIS to GEIS transition zone. The conductivity of the GEIS was consistently greater than that of the BEIS. The transition between the two sediments

occurred consistently when conductivity increased rapidly. The depth at which there was a notable increase in conductivity was interpreted as the point of transition between the BEIS and GEIS. When using differential ratios, the GEIS consistently exhibited greater variation in all wavelengths compared to the BEIS. Using differential ratios, the BEIS was determined to have transitioned to the GEIS when the variation between the orange:blue wavelengths began to increase. These results coincide with those determined in the laboratory trials of this thesis. These results conclude the method of delineating the GEIS from the BEIS, which was applied onsite during the pilot study, and was applied during the field trials portion of this thesis.

Results gathered from both the laboratory trials and pilot study suggest that the use of %RE, conductivity, and wavelength ratios are an effective means of delineating a variety of mediums. Their accuracy, however, required further field validation. The field trial portion of this thesis used the methods defined within this section to delineate the sediment stratigraphy of multiple sites (100) within the BHSL. To assess the accuracy of this method, sediment gravity cores were collected and extruded at each sampling site (100), which provided a comparison for the two methods. As sediment gravity coring and core extrusion are physical methods of sediment collection and analysis, both act as a control for the accuracy of the UVOST's measurements using the discussed methods to determine the BEIS's thickness.

4.4 Phase Four: Field Trials

4.4.1 UVOST and Sediment Gravity Core Sample Locations

In total, 100 UVOST and sediment gravity core samples were obtained during the UVOST field trials (Figure 38). Samples were collected from 7 clusters with the following

number of samples being collected and analyzed from clusters 1-7 respectively; 8, 10, 9, 15, 17, 18, 19. The methods which were observed during the laboratory trials were refined during the pilot study and have been used to interpret UVOST logs collected during the field trials. All sediment thickness results for the 100 collected UVOST logs and sediment gravity cores are presented in Appendix B. Given that many of the sample locations are close together, sample locations have been grouped into clusters which are represented by a single black (Figure 38).

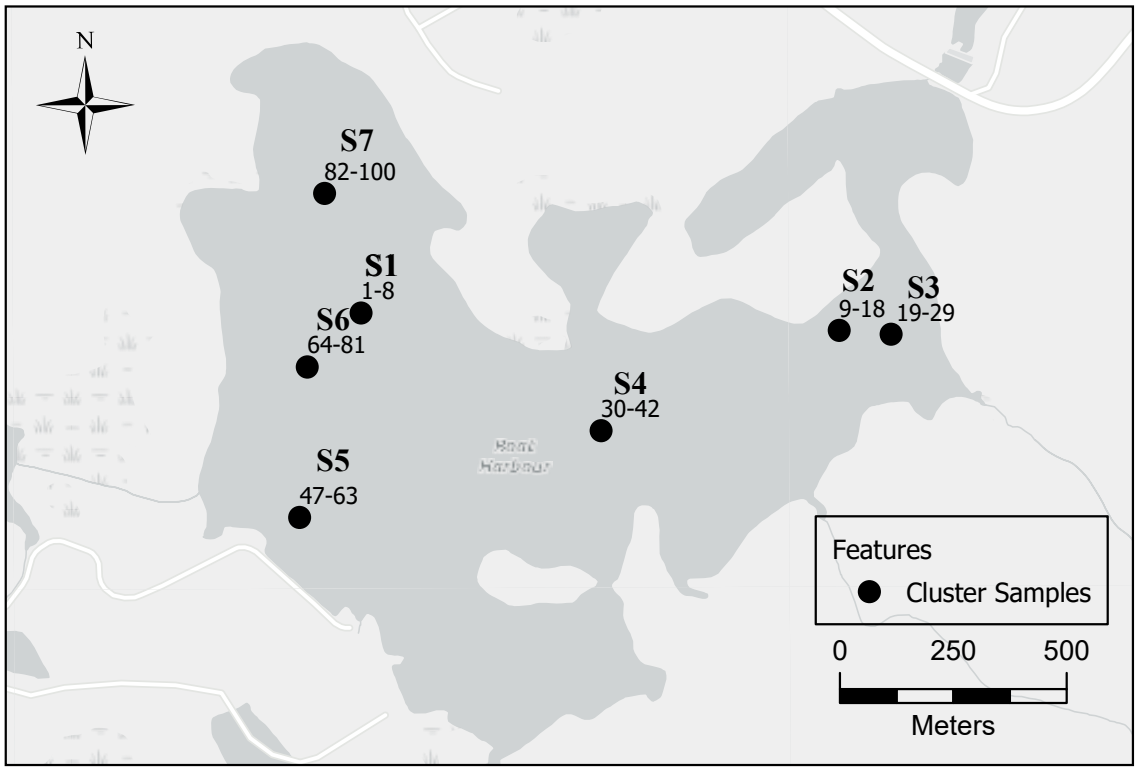

Figure 38: Cluster sample locations.

4.4.1.1 Excluded Data

Results for UVOST logs 19LIF22 and 19LIF23 were disregarded from the dataset as they were used to examine the effect of adjusting the UVOST's wave frequency from 64 hertz to 100 hertz. This was done as an attempt to obtain higher resolution data, however, this change resulted in the over-estimation of UVOST sediment thicknesses by up to 2x

that of sediment gravity core thicknesses. Results for UVOST logs 19LIF44 and 19LIF45 were disregarded from this analysis as the BEIS was too thick for the sediment gravity core to obtain a measurement. The sediment gravity core tubes used on site were capable of collecting 72cm of BEIS, however, it is likely that sediment was lost through the top of the core, as the sediment gravity core tube was completely filled with BEIS. Results for 19LIF46 are not shown in the cluster map, as the sample was collected outside of one of the pre-determined clusters.

4.4.2 UVOST-sediment Gravity Core Comparison

4.4.2.1 Variation in Observed Differences of Collection Methods

Results on the differences of sample measurements versus sample means from Table 15 and Appendix B are presented in Figure 39 and Figure 40 respectively. There is variability present in both UVOST-UVOST and core-core duplicate measurements (Figure 39). Variability is also present in paired UVOST-core measurements (Figure 40).

Table 15: UVOST-UVOST and core-core duplicate sample averages and differences.

Core sample	UVOST sample	Average core thickness (cm)	Average UVOST thickness (cm)	Calculated difference in core duplicates (cm)	Calculated difference in UVOST duplicates (cm)
BHUV19-0095 BHUV19-0100	19LIF95 19LIF100	37	43.5	2	9
BHUV19-0083 BHUV19-0094	19LIF83 19LIF94	44.15	47.5	1.1	13
BHUV19-0085 BHUV19-0096	19LIF85 19LIF96	42.95	42.5	11.1	11
BHUV19-0087 BHUV19-0097	19LIF87 19LIF97	43.25	43.5	1.7	7
BHUV19-0089 BHUV19-0098	19LIF89 19LIF98	42.5	44.5	1	1
BHUV19-0091 BHUV19-0099	19LIF91 19LIF99	40.15	37.5	0.3	13
BHUV19-0064 BHUV19-0081	19LIF64 19LIF81	36.2	33.5	-5.2	-3

Core sample	UVOST sample	Average core thickness (cm)	Average UVOST thickness (cm)	Calculated difference in core duplicates (cm)	Calculated difference in UVOST duplicates (cm)
BHUV19-0072	19LIF72				
BHUV19-0073	19LIF73	37.35	36	0.7	-2
BHUV19-0075	19LIF75				
BHUV19-0076	19LIF76	34.7	32	2.4	8
BHUV19-0078	19LIF78				
BHUV19-0079	19LIF79	35.4	34	-0.2	0
BHUV19-0061	19LIF61				
BHUV19-0062	19LIF62	35	32.5	2	3
BHUV19-0058	19LIF58				
BHUV19-0059	19LIF59	28.3	30.5	-3.4	1
BHUV19-0052	19LIF52				
BHUV19-0053	19LIF53	34	35.5	-2	-1

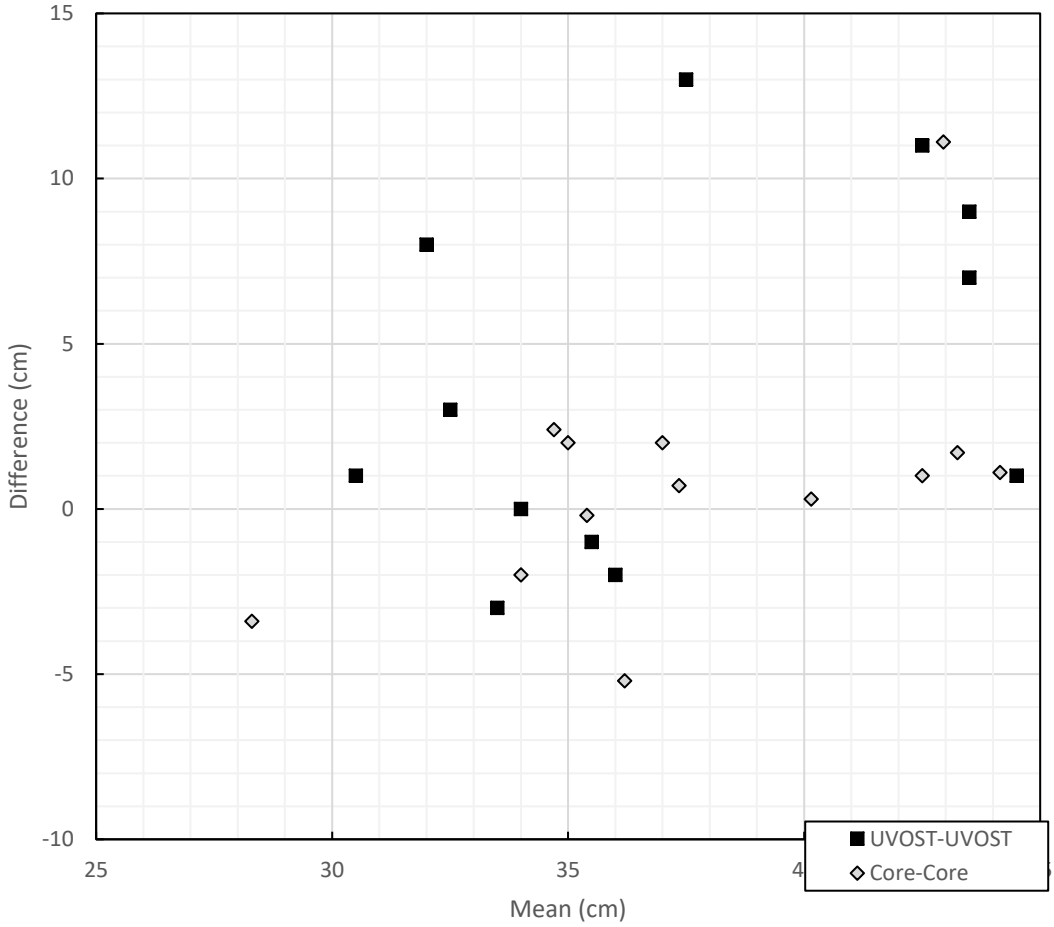

Figure 39: Variability of duplicate UVOST-UVOST and core-core samples.

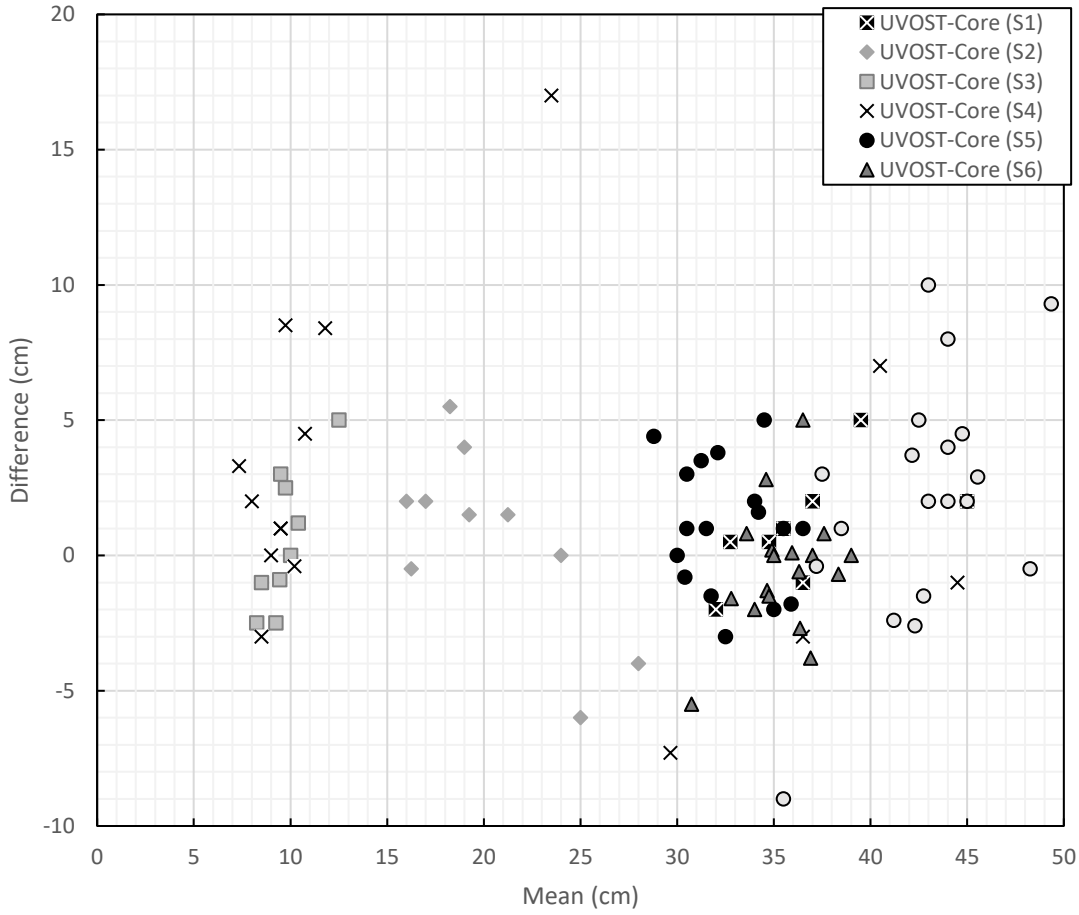

Figure 40: Variability of duplicate UVOST-core samples.

These results suggest that variation exists between individual methods. As well, stratigraphic, and spatial variation on a local scale may influence the observed differences noted between duplicate samples. The variation and relationship between UVOST-core samples, however, must be further assessed. These samples have been assessed using bar graphs and further statistical analysis in the form of t-tests (paired two sample for means) for each cluster that was collected.

4.4.2.2 Sediment Thicknesses Obtained at Each Cluster: Bar Graphs and t-test (Paired Two Sample for Means)

To visually demonstrate the variation in sediment thickness, results collected at each cluster site (Figure 38, S1-S7) are presented below as a series of bar graphs, the data from which is detailed further in **Appendix B**. Error bars at each data-point represents the mean thickness at each cluster for each sample type (UVOST or sediment gravity core) +/- 1 standard deviation of the mean (Figure 41-47). These error bars are meant to show the variation of sediment thicknesses present at each cluster and are a reflection of the mean observed at that site. To further assess the variability of the dataset, a t-test (paired two sample for means) was conducted on each cluster of samples collected in the BHSL (Figure 38) and is presented after each bar graph.

As variation at each cluster has been previously noted, and each sample was taken within 1-2m of the next in each cluster, some variation on a local scale is to be expected. The sediment thickness data collected from each core and UVOST log are presented in Appendix B, with the cluster sample ID being listed beside each UVOST and core sample. The cluster sample ID (Appendix B) has been used to identify which UVOST and core samples correspond with each bar graph of an individual cluster.

Measured BEIS thicknesses for cluster 1 show a range of thickness readings from 32.5 cm to 44 cm (Figure 41). UVOST sediment readings were noted to range from 31 cm to 46 cm. The difference in UVOST measurements from sediment gravity cores results ranged from -2 cm (being 2 cm less then sediment gravity core results) to +5 cm (5 cm greater then sediment gravity core results), with an average difference of +1 cm (1 cm greater than sediment gravity core results) of variation for the sampling methods at cluster

1 (S1). Core sediment thickness samples 2-8 fell within (+/-) 1 standard deviation of the mean, while sample 1's measured thickness was greater than (+/-) 1 standard deviation of the mean. UVOST sediment thickness samples 2 and 4-8 fell within (+/-) 1 standard deviation of the mean, while sample 1 was greater than, and sample 3 was less then (+/-) 1 standard deviation of the mean. These results indicate that there was slight variation on a local scale of sediment thicknesses in the sampled area (S1). To determine the significance of the variation noted between sampling techniques (sediment gravity core vs UVOST), cluster one (S1) has been further assessed statistically using the t-test.

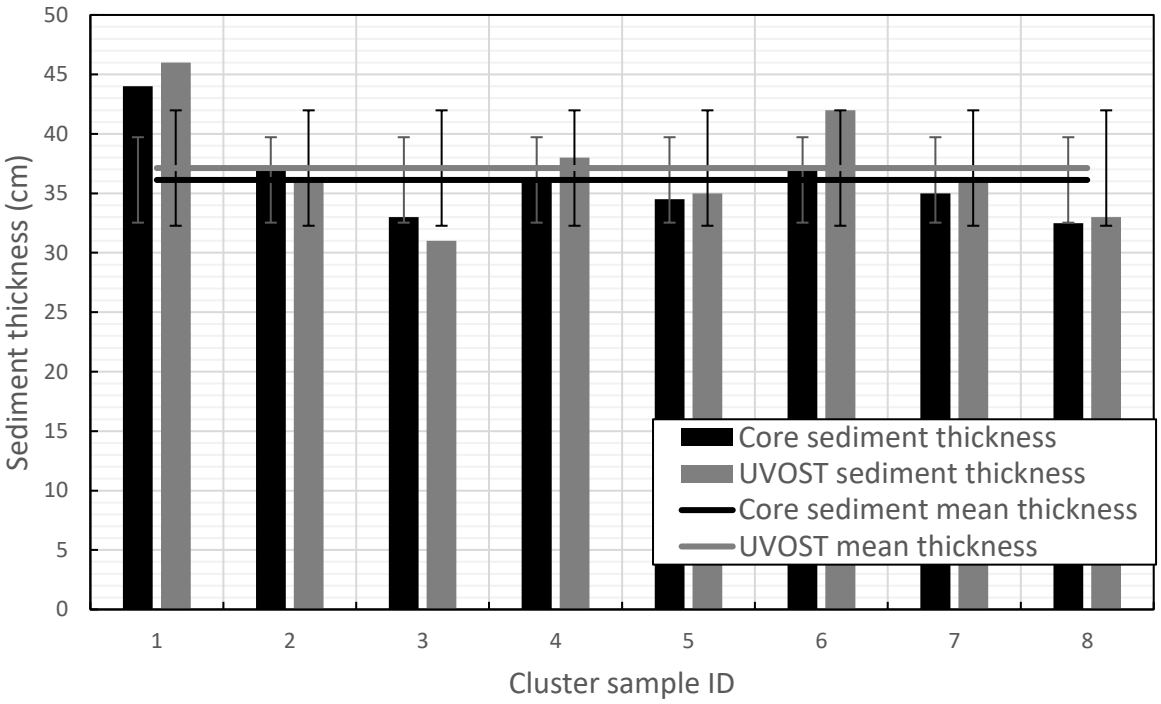

Figure 41: Cluster 1 samples bar graph comparison (error bars are mean +/- 1 standard deviation (n = 8) for both UVOST and core measured thicknesses).

Cluster 1 t-Test results indicate that as t Stat is less then t critical two tail, and greater than -t critical two tail, we accept the null hypothesis (Table 16). The mean difference

between the paired observations of sediment gravity core and UVOST sediment thicknesses are equal and are not significantly different at alpha = 0.05.

Table 16: Cluster 1 t-Test: paired two sample for means.

Cluster 1		
	Core sediment thickness (cm)	***UVOST sediment thickness (cm)***
Mean	36.13	37.13
Variance	12.91	23.55
Observations	8.00	8.00
Pearson Correlation	0.92	
Hypothesized Mean Difference	0.00	
df	7.00	
t Stat	-1.33	
P(T<=t) one-tail	0.11	
t Critical one-tail	1.89	
P(T<=t) two-tail	0.22	
t Critical two-tail	2.36	
P-value	0.22	
Result	**-1.33 < 2.36 and -1.33 > -2.36**	**Accept Ho**

Measured BEIS thicknesses in cluster 2 for samples 1 – 10 show a range of thickness readings from 15 cm to 30 cm (Figure 42). UVOST sediment readings were noted to range from 16 cm to 26 cm. The difference in UVOST measurements from sediment gravity core results ranged from -6 cm to +5.5 cm, with an average difference of +0.6 cm of variation for the sampling methods at cluster 2 (S2). Core sediment thickness samples 1-5, and 8-10 fell within (+/-) 1 standard deviation of the mean, while sample 6 and sample 7 measured thicknesses were greater than (+/-) 1 standard deviation of the mean. UVOST sediment thickness samples 1-4, 7, 8, and 10 displayed (+/-) 1 standard deviation of the mean, while sample 6 was greater than, and sample 5 and 9 were less than (+/-) 1 standard

deviation of the mean. These results indicate that there was a slight variation on a local scale of sediment thicknesses in S2. To determine the significance of the variation noted between sampling techniques (sediment gravity core vs UVOST), cluster two (S2) has been further assessed statistically using the t-test.

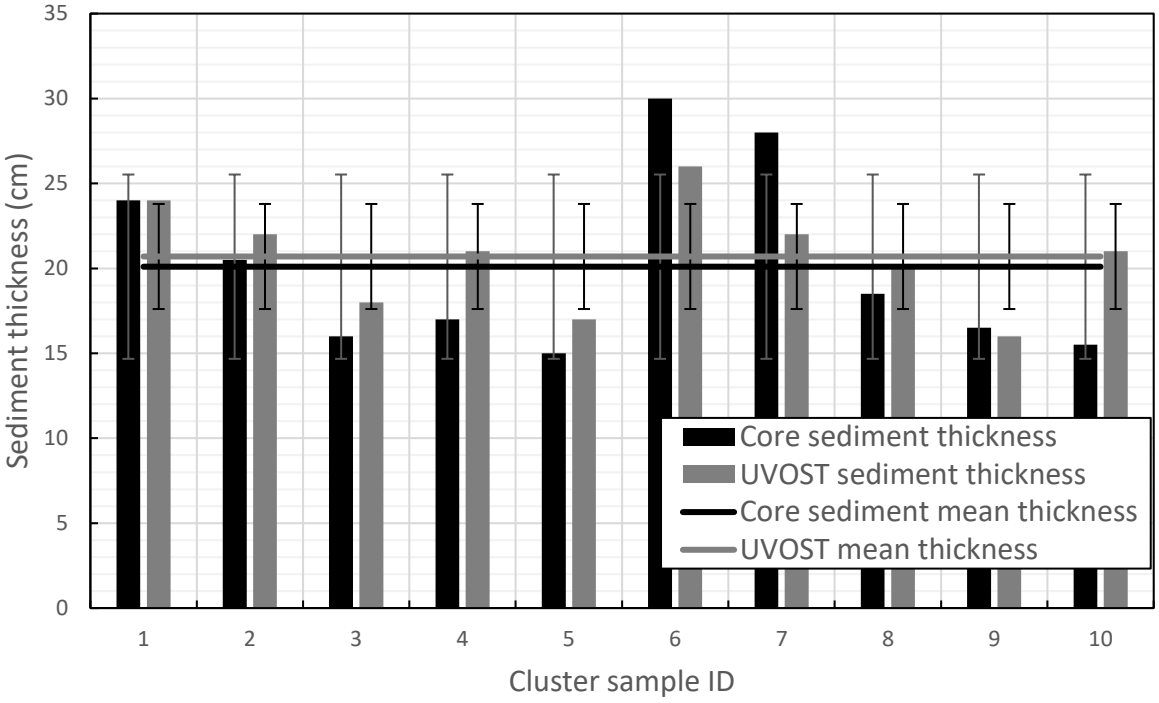

Figure 42: Cluster 2 samples bar graph comparison (error bars are mean +/- 1 standard deviation (n = 10) for both UVOST and core measured thicknesses).

Cluster 2 t-Test results indicate that as t Stat is less then t critical two tail, and greater than -t critical two tail, we accept the null hypothesis (Table 17). The mean difference between the paired observations of sediment gravity core and UVOST sediment thicknesses are equal and are not significantly different at alpha = 0.05.

Table 17: Cluster 2 t-Test: paired two sample for means.

Cluster 2		
	Core sediment thickness (cm)	***UVOST sediment thickness (cm)***
Mean	20.10	20.70
Variance	29.43	9.57

Cluster 2		
	Core sediment thickness (cm)	***UVOST sediment thickness (cm)***
Observations	10.00	10.00
Pearson Correlation	0.81	
Hypothesized Mean Difference	0.00	
df	9.00	
t Stat	-0.55	
P(T<=t) one-tail	0.30	
t Critical one-tail	1.83	
P(T<=t) two-tail	0.60	
t Critical two-tail	2.26	
P-value	0.6	
Result	**-0.55 < 2.26 and -0.55 > -2.26**	**Accept Ho**

Measured BEIS thicknesses for cluster 3 show a range of thickness readings from 8 cm to 10.5 cm (Figure 43). UVOST sediment readings were noted to range from 7 cm to 15 cm. The difference in UVOST measurements from sediment gravity core results ranged from -2.5 cm to +5 cm, with an average difference of +0.53 cm of variation for the sampling methods at cluster 3 (S3). Core sediment thickness samples 1, 2, 4, and 6-8 fell within (+/-) 1 standard deviation of the mean. Sample 5's measured thickness was greater than (+/-) 1 standard deviation of the mean and sample 3 and 9 measured thicknesses were less than (+/-) 1 standard deviation of the mean. UVOST sediment thickness samples 2-5, and 7-9 fell within (+/-) 1 standard deviation of the mean, while sample 1 was greater than, and sample 6 was less than (+/-) 1 standard deviation of the mean. These results indicate that there was slight variation on a local scale of sediment thicknesses in the sampled area (S3). To determine the significance of the variation noted between sampling techniques (sediment gravity core vs UVOST), cluster three (S3) has been further assessed statistically using the t-test.

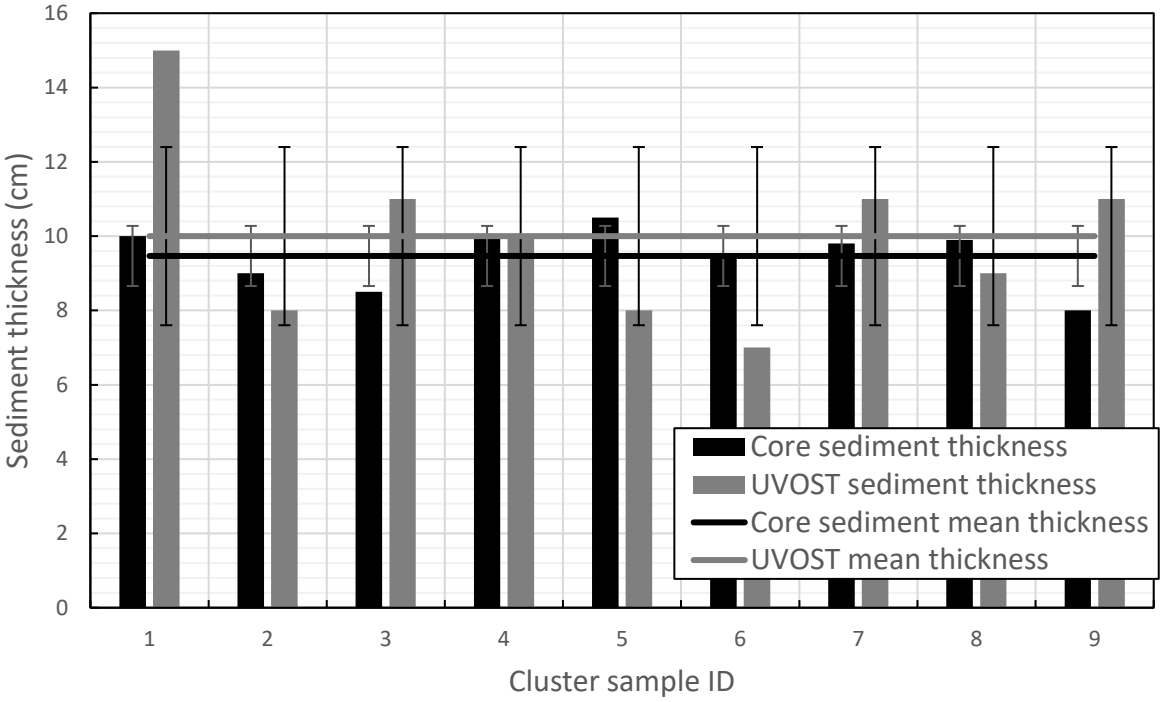

Figure 43: Cluster 3 samples bar graph comparison (error bars are mean +/- 1 standard deviation (n = 9) for both UVOST and core measured thicknesses).

Cluster 3 t-Test results indicate that as t Stat is less then t critical two tail, and greater than -t critical two tail, we accept the null hypothesis (Table 18). The mean difference between the paired observations of sediment gravity core and UVOST sediment thicknesses are equal and are not significantly different at alpha = 0.05.

Table 18: Cluster 3 t-Test: paired two sample for means.

Cluster 3		
	Core sediment thickness (cm)	***UVOST sediment thickness (cm)***
Mean	9.47	10.00
Variance	0.66	5.75
Observations	9.00	9.00
Pearson Correlation	-0.07	
Hypothesized Mean Difference	0.00	
df	8.00	

Cluster 3		
	Core sediment thickness (cm)	***UVOST sediment thickness (cm)***
t Stat	-0.62	
P(T<=t) one-tail	0.28	
t Critical one-tail	1.86	
P(T<=t) two-tail	0.55	
t Critical two-tail	2.31	
P-value	0.55	
Result	**-0.62 < 2.31 and -0.62 > -2.31**	**Accept Ho**

Measured BEIS thicknesses for cluster 4 show a range of thickness readings from 5.5 cm to 45 cm (Figure 44). UVOST sediment readings were noted to range from 7 cm to 44 cm. The difference in UVOST measurements from sediment gravity core results ranged from -7.3 cm to +17 cm, with an average difference of +2.53 cm of variation for the sampling methods at cluster 4 (S4). Core sediment thickness samples 1-3, 5-8, and 10-13 fell within (+/-) 1 standard deviation of the mean, while samples 4, 9, 14, and 15 were greater than (+/-) 1 standard deviation of the mean. UVOST sediment thickness samples 1-3 and 5-13 fell within (+/-) 1 standard deviation of the mean, while samples 4, 14, and 15 were greater than (+/-) 1 standard deviation of the mean. These results indicate that there was major variation on a local scale of sediment thicknesses in the sampled area (S4). When comparing the sampled site (S4) to the bathymetric model (Appendix A), this area was noted to be beside a natural channel in the BHSL which could account for the range of thicknesses observed at the site. To determine the significance of the variation noted between sampling techniques (sediment gravity core vs UVOST), cluster four (S4) have been further assessed statistically using the t-test.

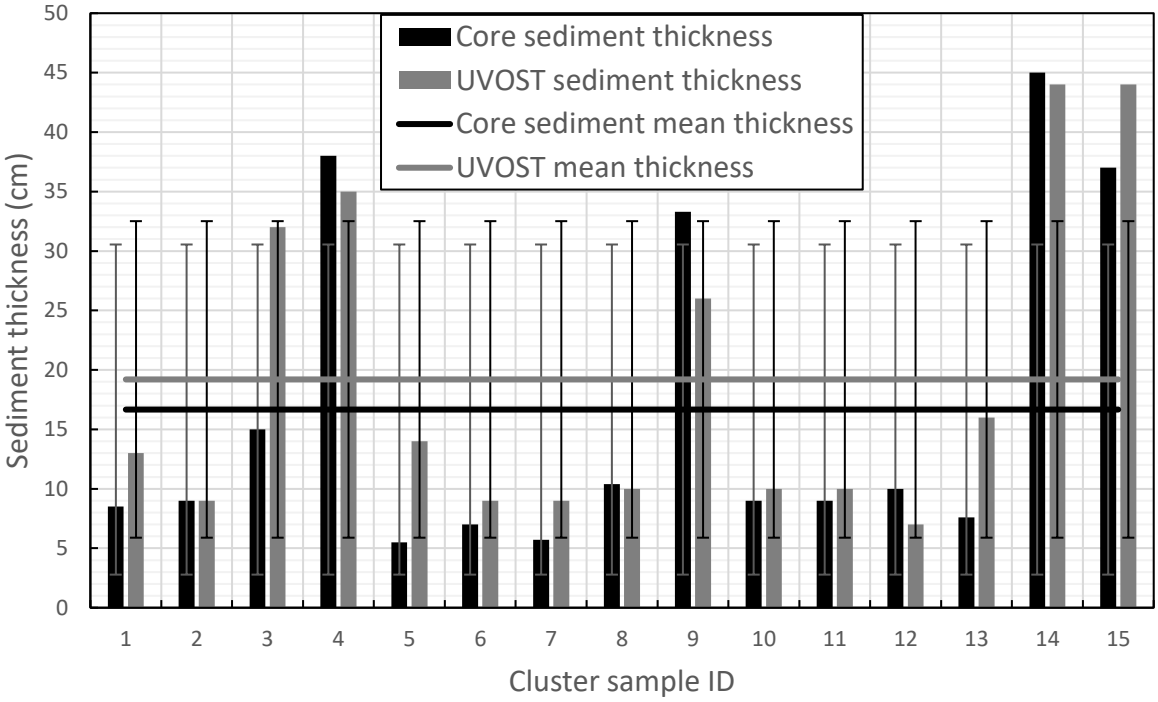

Figure 44: Cluster 4 samples bar graph comparison (error bars are mean +/- 1 standard deviation (n = 15) for both UVOST and core measured thicknesses).

Cluster 4 t-Test results indicate that as t Stat is less then t critical two tail, and greater than -t critical two tail, we accept the null hypothesis (Table 19). The mean difference between the paired observations of sediment gravity core and UVOST sediment thicknesses are equal and are not significantly different at alpha = 0.05.

Table 19: Cluster 4 t-Test: paired two sample for means.

Cluster 4		
	Core sediment thickness (cm)	***UVOST sediment thickness (cm)***
Mean	16.67	19.20
Variance	192.72	177.17
Observations	15.00	15.00
Pearson Correlation	0.91	
Hypothesized Mean Difference	0.00	

Cluster 4		
	Core sediment thickness (cm)	***UVOST sediment thickness (cm)***
df	14.00	
t Stat	-1.65	
P(T<=t) one-tail	0.06	
t Critical one-tail	1.76	
P(T<=t) two-tail	0.12	
t Critical two-tail	2.14	
P-value	0.12	
Result	**-1.65 < 2.14 and -1.65 > -2.14**	**Accept Ho**

Measured BEIS thicknesses for cluster 5 show a range of thickness readings from 26.6 cm to 36.8 cm (Figure 45). UVOST sediment readings were noted to range from 30 cm to 37 cm. The difference in UVOST measurements from sediment gravity core results ranged from -3 cm to +4.4 cm, with an average difference of +1.1 cm of variation for the sampling methods at cluster 5 (S5). Core sediment thickness samples 2-4, 6-11, 13, 14, and 16 fell within (+/-) 1 standard deviation of the mean, while samples 1, 5, and 15 were greater than (+/-) 1 standard deviation of the mean, and sample 12 was less than (+/-) 1 standard deviation of the mean. UVOST sediment thickness samples 4-6, 8-12, and 14-17 fell within (+/-) 1 standard deviation of the mean, while samples 1, 2, and 7 were greater than (+/-) 1 standard deviation of the mean, and samples 3 and 13 were less than (+/-) 1 standard deviation of the mean. These results indicate that there was slight variation on a local scale of sediment thicknesses in the sampled area (S5). To determine the significance of the variation noted between sampling techniques (sediment gravity core vs UVOST), cluster five (S5) have been further assessed statistically using the t-test.

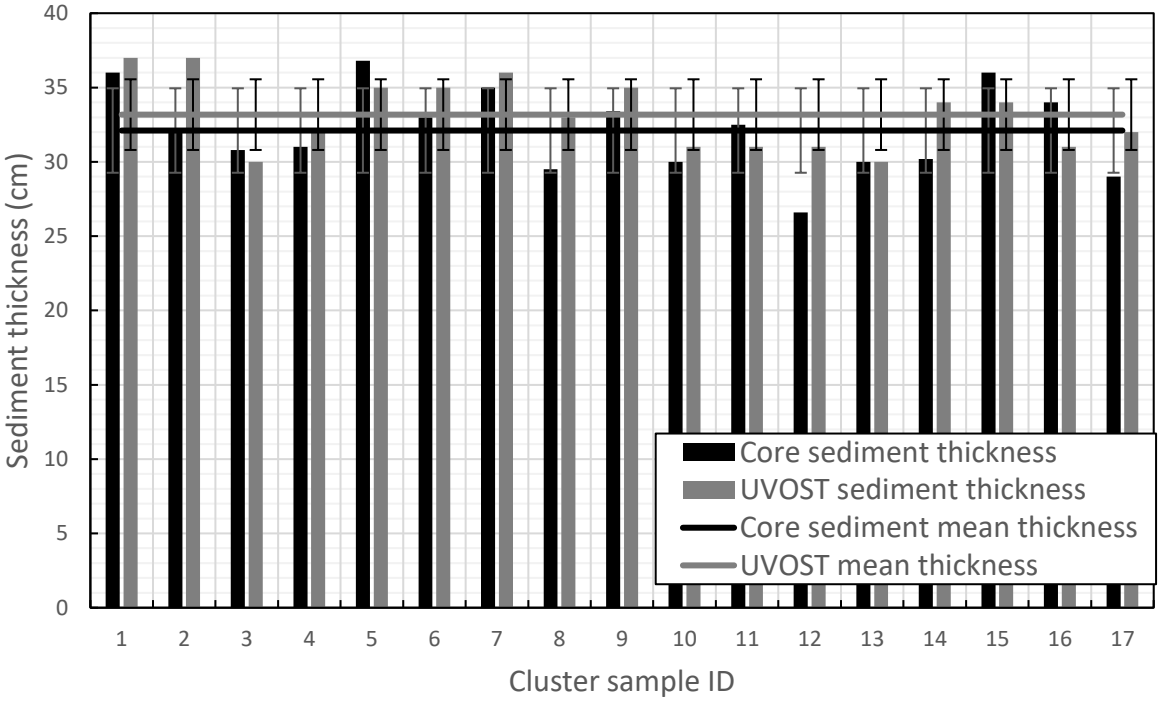

Figure 45: Cluster 5 samples bar graph comparison (error bars are mean +/- 1 standard deviation (n = 17) for both UVOST and core measured thicknesses).

Cluster 5 t-Test results indicate that as t Stat is less then t critical two tail, and greater than -t critical two tail, we accept the null hypothesis (Table 20). The mean difference between the paired observations of sediment gravity core and UVOST sediment thicknesses are equal and are not significantly different at alpha = 0.05.

Table 20: Cluster 5 t-Test: paired two sample for means.

Cluster 5		
	Core sediment thickness (cm)	***UVOST sediment thickness (cm)***
Mean	32.11	33.18
Variance	8.07	5.65
Observations	17.00	17.00
Pearson Correlation	0.60	
Hypothesized Mean Difference	0.00	
df	16.00	

Cluster 5		
	Core sediment thickness (cm)	***UVOST sediment thickness (cm)***
t Stat	-1.86	
P(T<=t) one-tail	0.04	
t Critical one-tail	1.75	
P(T<=t) two-tail	0.08	
t Critical two-tail	2.12	
P-value	0.08	
Result	**-1.86 < 2.12 and -1.86 > -2.12**	**Accept Ho**

Measured BEIS thicknesses for cluster 6 show a range of thickness readings from 33.2 cm to 39 cm (Figure 46). UVOST sediment readings were noted to range from 28 cm to 39 cm. The difference in UVOST measurements from sediment gravity core results ranged from -5.5 cm to +5 cm, with an average difference of -0.56 cm of variation for the sampling methods at cluster 6 (S6). Core sediment thickness samples 4, 5, 7-12, and 15-17 fell within (+/-) 1 standard deviation of the mean, while samples 3, 6, and 18 were greater than (+/-) 1 standard deviation of the mean, and sample 1, 2, 13, and 14 were less than (+/-) 1 standard deviation of the mean. UVOST sediment thickness samples 2, 3, 5, 7-12, and 14-18 fell within (+/-) 1 standard deviation of the mean, while samples 4 and 6 were greater than (+/-) 1 standard deviation of the mean, and samples 1 and 13 were less than (+/-) 1 standard deviation of the mean. These results indicate that there was slight variation on a local scale of sediment thicknesses in the sampled area (S6). To determine the significance of the variation noted between sampling techniques (sediment gravity core vs UVOST), cluster six (S6) have been further assessed statistically using the t-test.

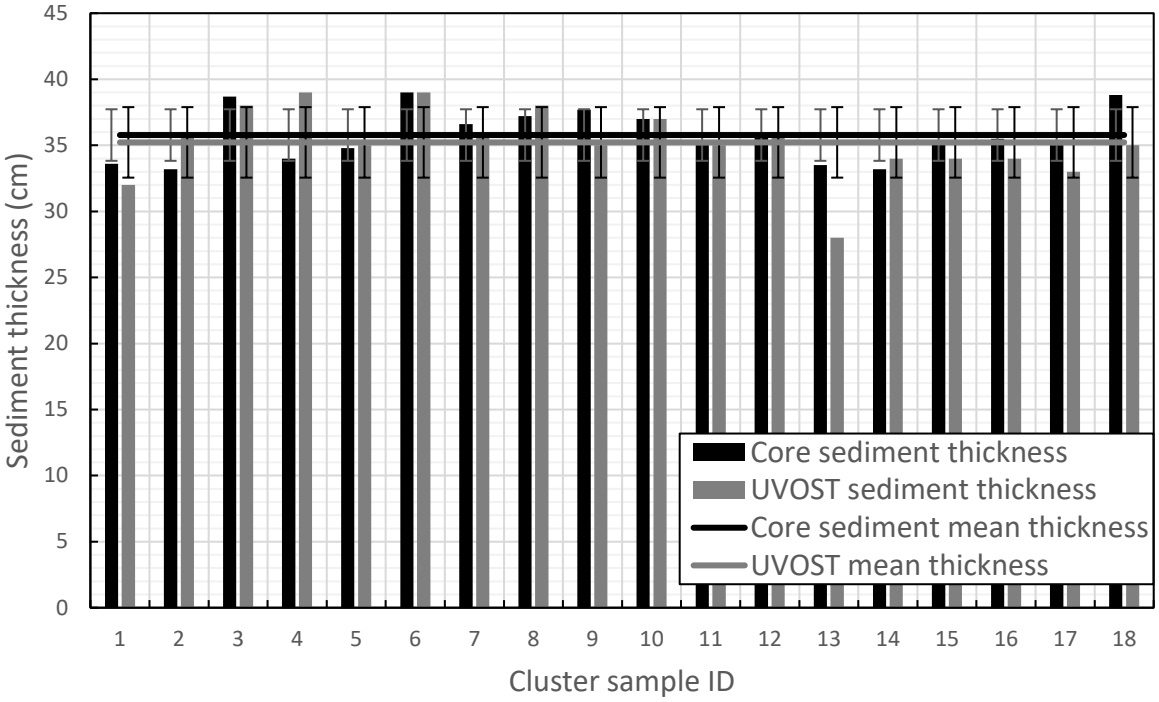

Figure 46: Cluster 6 samples bar graph comparison (error bars are mean +/- 1 standard deviation (n = 18) for both UVOST and core measured thicknesses).

Cluster 6 t-Test results indicate that as t Stat is less then t critical two tail, and greater than -t critical two tail, we accept the null hypothesis (Table 21). The mean difference between the paired observations of sediment gravity core and UVOST sediment thicknesses are equal and are not significantly different at alpha = 0.05.

Table 21: Cluster 6 t-Test: paired two sample for means.

Cluster 6		
	Core sediment thickness (cm)	***UVOST sediment thickness (cm)***
Mean	35.78	35.22
Variance	3.81	7.12
Observations	18.00	18.00
Pearson Correlation	0.53	
Hypothesized Mean Difference	0.00	
df	17.00	

Cluster 6		
	Core sediment thickness (cm)	***UVOST sediment thickness (cm)***
t Stat	1.01	
P(T<=t) one-tail	0.16	
t Critical one-tail	1.74	
P(T<=t) two-tail	0.33	
t Critical two-tail	2.11	
P-value	0.32	
Result	**1.01 < 2.11 and 1.01 > -2.11**	**Accept Ho**

Measured BEIS thicknesses for cluster 7 show a range of thickness readings from 36 cm to 48.5 cm (Figure 47). UVOST sediment readings were noted to range from 31 cm to 54 cm. The difference in UVOST measurements from sediment gravity core results ranged from -9 cm to +9.3 cm, with an average difference of +2.16 cm of variation for the sampling methods at cluster 7 (S7). Core sediment thickness samples 1-3, 5-11, 13, and 16-18 fell within (+/-) 1 standard deviation of the mean, while sample 4 was greater than (+/-) 1 standard deviation of the mean, and samples 12, 14, 15, and 19 were less than (+/-) 1 standard deviation of the mean. UVOST sediment thickness samples 1, 3-14, 16, 17, and 19 fell within (+/-) 1 standard deviation of the mean, while sample 2 was greater than (+/-) 1 standard deviation of the mean, and samples 15 and 18 were less than (+/-) 1 standard deviation of the mean. These results indicate that there was slight variation on a local scale of sediment thicknesses in the sampled area (S7). To determine the significance of the variation noted between sampling techniques (sediment gravity core vs UVOST), cluster seven (S7) has been further assessed statistically using the t-test.

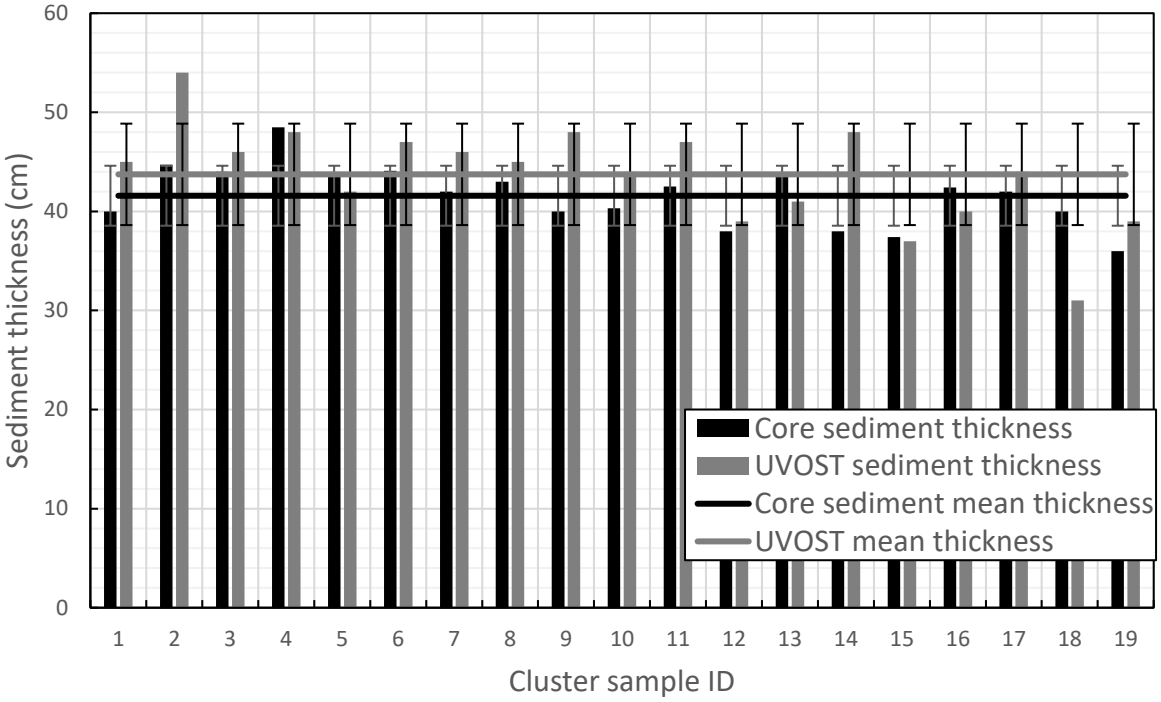

Figure 47: Cluster 7 samples bar graph comparison (error bars are mean +/- 1 standard deviation (n = 19) for both UVOST and core measured thicknesses).

Cluster 7 t-Test results indicate that as t Stat is less then t critical two tail, and greater than -t critical two tail, we accept the null hypothesis (Table 22). The mean difference between the paired observations of sediment gravity core and UVOST sediment thicknesses are equal and are not significantly different at alpha = 0.05.

Table 22: Cluster 7 t-Test: paired two sample for means.

Cluster 7		
	Core sediment thickness (cm)	***UVOST sediment thickness (cm)***
Mean	41.58	43.74
Variance	9.16	26.20
Observations	19.00	19.00
Pearson Correlation	0.49	
Hypothesized Mean Difference	0.00	

Cluster 7		
	Core sediment thickness (cm)	***UVOST sediment thickness (cm)***
df	18.00	
t Stat	-2.09	
P(T<=t) one-tail	0.03	
t Critical one-tail	1.73	
P(T<=t) two-tail	0.05	
t Critical two-tail	2.10	
P-value	0.05	
Result	**-2.09 < 2.10 and -2.09 > -2.10**	**Accept Ho**

As can be seen in the side by side comparison of UVOST and sediment gravity core thickness results, the interpreted thickness of each testing method is similar. When visually assessed, UVOST interpreted sediment thicknesses closely compare to that of sediment gravity core thickness measurements. The majority of samples within clusters 1-7 (S1-S7) fell within (+/-) 1 standard deviation of the mean. This means that within a given sample area, collected results are similar for both UVOST and sediment gravity core samples. Further pairing that with the t-test (paired two sample for means), it appears that the UVOST is able to collect results which are comparable to that of a physical collection method (i.e. sediment gravity core) (Tables 16 to 22). The results of the cluster samples t-Test analyses indicate that the means of the two datasets do not differ significantly for all clusters. The null hypothesis was accepted at each cluster, and as such, no statistically significant difference (using a 95% confidence interval) was detected between the means of the two datasets.

4.4.2.3 Comparing Paired Sediment Gravity Core Results to UVOST Results Using Linear Regression Analysis

The similarities between all UVOST interpreted measurements and sediment gravity core thicknesses were further compared using regression analysis (Table 23 and

Table 24) and linear regression (Figure 48). Data collected from sediment gravity core 1-100 and UVOST sample logs 1-100 (excluding 22, 23, 44, and 45) were used for this interpretation. Shown below, is the linear regression of the complete dataset which includes the 99% confidence interval range (Figure 48). The comparison between UVOST and sediment gravity core thicknesses has a strong positive correlation with an R^2 of 0.91.

Table 23: Sediment gravity core and UVOST sediment thickness regression analysis.

SUMMARY OUTPUT	
Regression Statistics	
Multiple R	0.95
R Square	0.91
Adjusted R Square	0.91
Standard Error	3.73
Observations	96

Table 24: Sediment gravity core and UVOST sediment thickness regression analysis (continued).

	Coefficients	***Standard Error***	***t Stat***	***P-value***	***Lower 95%***	***Upper 95%***	***Lower 99.0%***	***Upper 99.0%***
Intercept	0.31	1.02	0.30	0.76	-1.71	2.33	-2.37	2.99
X Variable 1	0.95	0.03	30.58	0.00	0.89	1.02	0.87	1.04

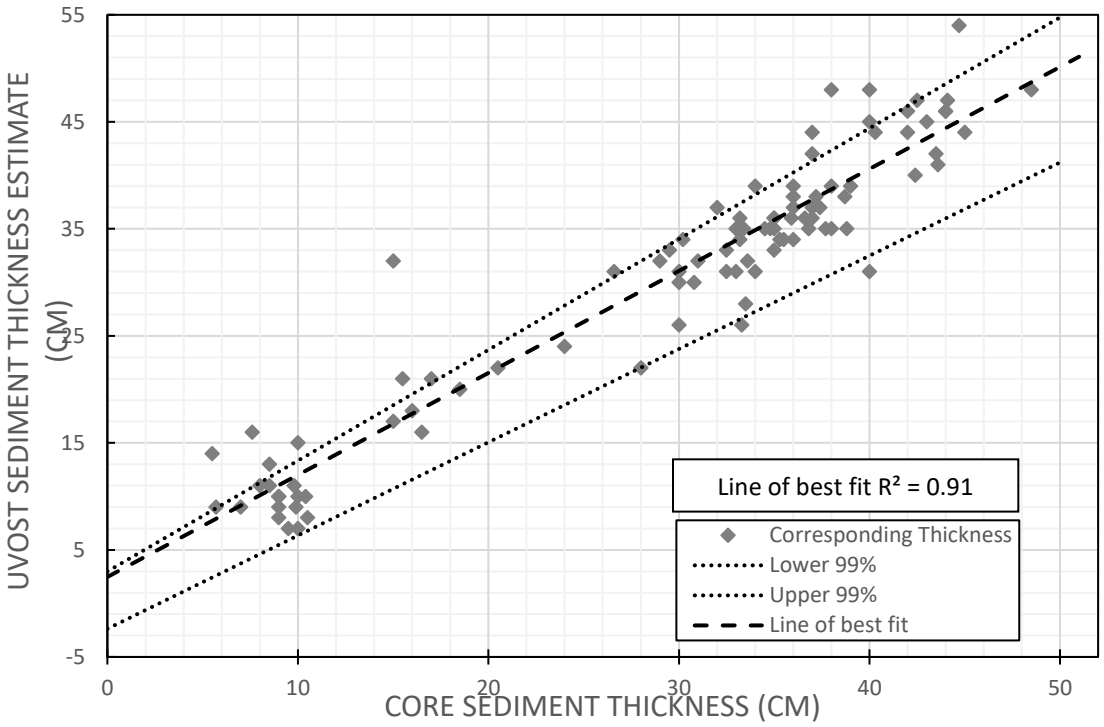

Figure 48: Linear regression of measured core thickness and interpreted UVOST sediment thickness for all cluster samples (S1-S7).

4.4.3 Summary of Field Trials

Methods which were developed throughout the laboratory and pilot study stages of this thesis were used to interpret UVOST logs collected during field trials. The parameters of interest included %RE, conductivity, and wavelength ratios, which were used to delineate the observed mediums (air, water, BEIS, GEIS) at 100 UVOST sample locations. These results were paired with sediment gravity core samples, to examine the reliability of the delineation method which was previously developed. By comparing the differences observed in duplicate samples, it was shown that slight variation on a local scale is to be expected between each sampling method (core-core, UVOST-UVOST, UVOST-core). The statistical analysis at each cluster site (S1-S7), indicated that the means of the data sets at each cluster were equal (95% CI, alpha = 0.05). The variation between sampling methods was therefore not statistically significant. Pooling the data to produce a linear regression

model indicated that sediment gravity core thickness measurements and UVOST measurements are positively correlated (R^2 = 0.91). When UVOST derived sediment thickness data is compared to a physical method of thickness determination (i.e. sediment gravity core), the UVOST can delineate the contacts of stratigraphic units with a level of accuracy that is comparable to that of a measured sediment gravity core.

Chapter 5 Summary and Conclusion

This study addresses knowledge gaps in the application of the UVOST to detect contaminated sediment in freshwater aquatic environments. Through the design and application of a four phase proof-of-concept, this thesis has determined: 1) The ability of the UVOST to detect optical differences of unique sediments in a laboratory setting; 2) The ability of the UVOST to detect optical differences of unique mediums in a field setting; 3) The capability of the UVOST to delineate an organic-rich, freshwater-covered, contaminated sediment layer, where hydrocarbons are not the main contaminant of concern; 4) The accuracy of the UVOST's thickness measurements using the method developed during this thesis.

A proof-of-concept consisted of the following four phases: 1) obtain the sediments of interest; 2) show that the two sediments are distinct from one another in terms of their organic matter; 3) develop a preliminary method of interpretation using the UVOST in a laboratory setting; 4) refine the developed method of interpretation using the UVOST in a field setting.

After obtaining the sediment and consulting the literature, this study confirmed that both BEIS and GEIS were distinct from one another physically and chemically. The BEIS has high water and terrestrial organic content. The GEIS consists primarily of silt, contains a variety of marine fauna, and has organics which were derived from a marine source. As both the chemical and physical nature of each sediment type differed significantly, the UVOST was hypothesized to be capable of distinguishing between them.

Laboratory trials were conducted on the BEIS and GEIS individually, as well as on a mock core which was fabricated to resemble a field sample. In this setting the BEIS was

noted to have a relatively higher %RE compared to the GEIS when tested ex-situ. The GEIS was noted to have a higher conductivity then that of the BEIS. Differential ratios between the various wavelengths observed using the UVOST show that the green, orange, and red wavelengths emitted by the GEIS show more variation when compared to the blue wavelength, then that of the BEIS. The mock core also showed these relations and further demonstrated the UVOST's ability to delineate between the sediments. These results posed a further question, being whether or not the UVOST would be able to delineate the sediment in a field setting.

UVOST data gathered during the field trials allowed for the identification of 4 distinct mediums present at Boat Harbour. The detected mediums were interpreted as air, fresh water, BEIS, and GEIS from top to bottom respectively. These mediums were distinguishable by examining %RE, conductivity and the differential ratios of wavelengths detected by the UVOST within each layer. To summarize these results, the mediums of the BHSL bore the following relations:

- **(%RE) %RE water > %RE BEIS > %RE GEIS**
- **(conductivity) mS/m water < mS/m BEIS < mS/m GEIS.**
- **(differential ratios) the wavelength ratios of green: blue, orange: blue, red: blue in water > wavelength ratios of green: blue, orange: blue, red: blue in BEIS:**
- **(differential ratios) the wavelength ratios of green: blue, orange: blue, red: blue in GEIS > wavelength ratios of green: blue, orange: blue, red: blue in BEIS.**

All three methods proved effective in delineating the mediums within the UVOST logs. The accuracy of the thickness estimates which were obtained using the UVOST logs were then tested by directly comparing the results to a physical collection method (i.e. sediment gravity core). Through the collection of 100 sediment gravity core and UVOST samples, it

was determined that these two collection methods showed a positive correlation (R=0.91) with one another. The methods discussed throughout this thesis have shown to be an effective means of delineating a contaminated sediment layer.

The following question was posed at the beginning of this study,

"Can UVOST technology be used to delineate an organic-rich, water-covered, contaminated sediment layer, where hydrocarbons are not the main contaminant of concern."

The results of this study indicate that the capabilities of the UVOST can be expanded beyond that of a PAH detecting device. At freshwater aquatic sites where organic-rich sediment overlays an impermeable or semi-impermeable clastic sediment layer, the UVOST has the potential to accurately delineate these layers. If the physical and chemical nature of the sediments prove to be different, then it is likely that the sediments produce unique fluorescent signatures when examined with the UVOST. This in turn, however, presents a limitation of the device, in that if PAH's are not present, and the chemical nature of fluorophores within the sediments are not distinct, then the UVOST may be unable to delineate these layers.

This application of the UVOST device can provide both a cost and time effective means of obtaining accurate volume estimates of sediment in freshwater aquatic environments. These data can be used to create sediment isopach maps and 3D models of water-covered contaminated sites which inform post remediation decisions and assist in post- remediation monitoring and compliance. UVOST technology can provide a means of project quality control and quality assurance. The methods developed in this study have the potential to be further automated to expedite the delineation process for projects which require a larger scale analysis to be conducted. By connecting the base variations and

relationships between the individual wavelengths associated with different sediment types to a sorting program, one can rapidly characterize a variety of sediments. Future studies should be conducted on a variety of sediment types in various settings to further establish the transportability of this technology for sediment characterization in aquatic environments

References

Alimohammadi, M., Tackley, H., Holmes, B., Davidson, K., Lake, C. B., Spooner, I. S., Jamieson, R. C., & Walker, T. R. (2019). Laboratory and Field Physical Property Characterization for a Contaminated Sediment for Bench Scale Dewatering Purposes. *Geo-Environmental Engineering*.

Becker, R. S. (1969). *Theory and interpretation of fluorescence and phosphorescence*. Wiley Interscience.

Bero, B. N., von Braun, M. C., Knowles, C. R., & Hammel, J. E. (1995). Further studies using X-ray fluorescence to sample lead contaminated carpeted surfaces. *Environmental Monitoring and Assessment*, *36*(2), 123–138. https://doi.org/10.1007/BF00546785

Bidmanova, S., Kotlanova, M., Rataj, T., Damborsky, J., Trtilek, M., & Prokop, Z. (2016). Fluorescence-based biosensor for monitoring of environmental pollutants: From concept to field application. *Biosensors and Bioelectronics*, *84*, 97–105. https://doi.org/10.1016/j.bios.2015.12.010

Brodie, C. R., Casford, J. S. L., Lloyd, J. M., Leng, M. J., Heaton, Tim. H. E., Kendrick, C. P., & Yongqiang, Z. (2011). Evidence for bias in C/N, δ13C and δ15N values of bulk organic matter, and on environmental interpretation, from a lake sedimentary sequence by pre-analysis acid treatment methods. *Quaternary Science Reviews*, *30*(21), 3076–3087. https://doi.org/10.1016/j.quascirev.2011.07.003

Bromley, J. E. C. (1985). *Keys to the fauna and flora of Minas Basin*. National Research Council of Canada.

Burrows, Hugh. D., Azenha, M., & Monteiro, Carlos. J. P. (2008). *Catalysis from Theory to Application. An Integrated Course*. ResearchGate. https://www.researchgate.net/publication/236212474_Catalysis_from_Theory_to_Application_An_Integrated_Course

Christensen, J. H., Hansen, A. B., Mortensen, J., & Andersen, O. (2005). Characterization and Matching of Oil Samples Using Fluorescence Spectroscopy and Parallel Factor Analysis. *Analytical Chemistry*, *77*(7), 2210–2217. https://doi.org/10.1021/ac048213k

Creaden, E. (2015). *Light-Induced Fluorescence (LIF) and Integrated Site Visualizations (ISV)*. WCEC.

Davidson, K. (2018). *Spatiotemporal assessment of metal concentrations of pre-effluent estuarine sediments in a freshwater Kraft Pulp Mill tailings pond using paleolimnological methods, A'se'k, Pictou, Nova Scotia* [Honours thesis]. Acadia University.

Donaldson, L. (2013). Softwood and Hardwood Lignin Fluorescence Spectra of Wood Cell Walls in Different Mounting Media. *IAWA Journal / International Association of Wood Anatomists*, *34*, 3–19. https://doi.org/10.1163/22941932-00000002

Donaldson, L., Link to external site, this link will open in a new window, & Williams, N. (2018). Imaging and Spectroscopy of Natural Fluorophores in Pine Needles. *Plants (Basel,Switzerland)*,*7*(1). http://dx.doi.org.ezproxy.library.dal.ca/10.3390/plants7010010

Gagnon, C., Pelletier, É., & Mucci, A. (1997). Behaviour of anthropogenic mercury in coastal marine sediments. *Marine Chemistry*, *59*, 159–176.

Galimov, E. (2012a). *The Biological Fractionation of Isotopes*. Elsevier.

Garron, C., Gagne, F., Ernst, W., Julien, G., Bernier, M., & Caldwell, C. (2005). Mercury contamination of marine sediments and blue mussels (Mytilus edulis) in the vicinity of a mercury cell chlor-alkali plant in Dalhousie, New Brunswick, Canada. *Water Quality Research Journal of Canada*, *40*, 1–15.

GHD Limited. (2017). *Phase I Environmental Site Assessment Boat Harbour Remediation Planning and Design* (Technical Report No. 3; Project 11148275). Nova Scotia Lands Inc.

GHD Limited. (2018a). *Phase 2 Environmental Site Assessment Boat Harbour Remediation Planning and Design Pictou County, Nova Scotia* (Technical Report No. 6; Project 11148275). Nova Scotia Lands Inc.

GHD Limited. (2018b). *Remedial Option Decision Document* (Technical Report No. 5; Project 11148275). Nova Scotia Lands Inc.

Glew, J. R. (1989). A new trigger mechanism for sediment samplers. *Journal of Paleolimnology*, *2*(4), 241–243. https://doi.org/10.1007/BF00195474

Gobeil, C., & Cossa, D. (1993). Mercury in sediments and sediment pore water in the Laurentian Trough. *Canadian Journel of Fisheries and Aquatic Sciences*, *50*, 1794–1800.

Guilbault, G. G. (1990). *Practical Fluorescence, Second Edition*. CRC Press.

Hoffman, E., Alimohammadi, M., Lyons, J., Davis, E., Walker, T. R., & Lake, C. B. (2019). Characterization and spatial distribution of organic contaminated sediment derived from historical kraft pulp mill effluent. *Journal of Environmental Science and Pollution Research*.

Hoffman, E., Lyons, J., Boxall, J., Robertson, C., Lake, C. B., & Walker, T. R. (2017). Spatiotemporal assessment (quarter century) of pulp mill metal(loid) contaminated sediment to inform remediation decisions. *Environmental Monitoring and Assessment*, *189*(6), 257. https://doi.org/10.1007/s10661-017-5952-0

Holmes, B. (2018a). *Application of the paleolimnological method in the environmental assessment of effluent-influenced freshwater sediment: An example from Northern Nova Scotia* [Honours thesis]. Acadia University.

Hudson, N., Baker, A., & Reynolds, D. (2007). Fluorescence analysis of dissolved organic matter in natural, waste and polluted waters—A review. *River Research and Applications*, *23*(6), 631–649. https://doi.org/10.1002/rra.1005

Jabłoński, A. (1935). Über den Mechanismus der Photolumineszenz von Farbstoffphosphoren. *Zeitschrift für Physik*, *94*(1), 38–46. https://doi.org/10.1007/BF01330795

JWEL, & Beak. (1992). *An Investigation of Sediment Characteristics at Boat Harbour Treatment Facilities* (No. 8109).

Kallithrakas-Kontos, N., Foteinis, S., Paigniotaki, K., & Papadogiannakis, M. (2016). A robust X-ray fluorescence technique for multielemental analysis of solid samples. *Environmental Monitoring and Assessment*, *188*(2), 120. https://doi.org/10.1007/s10661-016-5127-4

Kotzick, R., & Niessner, R. (1996). Application of time-resolved, laser-induced and fiber-optically guided fluorescence for monitoring of a PAH-contaminated remediation site. *Fresenius' Journal of Analytical Chemistry*, *354*(1), 72–76. https://doi.org/10.1007/s002169600012

Lakowicz, J. R. (2006). *Principles of Fluorescence Spectroscopy* (3rd ed.). Springer US. //www.springer.com/gp/book/9780387312781

Mackie, E. A. V., Leng, M. J., Lloyd, J. M., & Arrowsmith, C. (2005). Bulk organic δ13C and C/N ratios as palaeosalinity indicators within a Scottish isolation basin. *Journal of Quaternary Science*, *20*(4), 303–312. https://doi.org/10.1002/jqs.919

Martin, T., & St. Germain, R. (2008, January 16). *Direct Push Site Characterization of NAPL with Laser-Induced Fluorescence (LIF)* [Powerpoint]. 2008 North American Environmental Field Conference & Exposition, Tampa, FL.

Meyers, P. A., & Lallier-Vergès, E. (1999a). Lacustrine Sedimentary Organic Matter Records of Late Quaternary Paleoclimates. *Journal of Paleolimnology*, *21*(3), 345–372. https://doi.org/10.1023/A:1008073732192

Parsons, M. B., & Cranston, R. E. (2006). Influence of lead smelter emissions on the distribution of metals in marine sediments from Chaleur Bay, eastern Canada. *Geochemistry: Exploration, Environment, Analysis*, *6*, 259–276.

Pettersen, R. C. (1984). The Chemical Composition of Wood. In *The Chemistry of Solid Wood* (Vol. 207, pp. 57–126). American Chemical Society. https://doi.org/10.1021/ba-1984-0207.ch002

Sawidis, T., Mitrovic, M., Pavlovic, P., & Tsigaridas, K. (2011). Trees as bioindicator of heavy metal pollution in three European cities. *Environmental Pollution (Barking, Essex : 1987)*, *159*, 3560–3570. https://doi.org/10.1016/j.envpol.2011.08.008

SCG Industries Limited. (2019). *Boat Harbour LIF Pilot Program Results* (p. 17) [Results].

Schaller, Chris. P. (2020). *14.7: Fluorescence and Phosphorescence*. Chemistry LibreTexts. https://chem.libretexts.org/Bookshelves/Physical_and_Theoretical_Chemistry_Textbook_Maps/Map%3A_Physical_Chemistry_for_the_Biosciences_(Chang)/14%3A_Spectroscopy/14.7%3A_Fluorescence_and_Phosphorescence

Song, X. (2020). *Evaluating 50 plus years of contaminant migration into a marine sediment* [MASc Thesis]. Dalhousie University.

Spooner, I. S., & Dunnington, D. W. (2016). *Boat Harbour Gravity Core Sediment Survey* (p. 11).

St. Germain, R. (2019). *UltraViolet Optical Screening Tool (UVOST) Training* [Training session].

Stea, R. R., Conley, H., & Brown, Y. (1992). *Surficial Geology of the Province of Nova Scotia* (Map 92-3) [Map]. Nova Scotia Department of Natural Resources. https://novascotia.ca/natr/meb/data/mg/MAP/pdf/map_1992-003_front_600_cln.pdf

Tackley, H. (2019). *The Fate of Metals During Geotextile Filtration of a Contaminated Sediment* [Masters Thesis]. Dalhousie University.

United Nations Environment Programme (UNEP). (2008). *The global atmospheric mercury assessment: Sources, emissions and transport*. http://www.unep.org/

Verhoeven, J. W. (1996). Glossary of terms used in photochemistry (IUPAC Recommendations 1996). *Pure and Applied Chemistry*, *68*(12), 2223–2286. https://doi.org/10.1351/pac199668122223

Wagner, A. M., & Barker, A. J. (2019). Distribution of polycyclic aromatic hydrocarbons (PAHs) from legacy spills at an Alaskan Arctic site underlain by permafrost. *Cold Regions Science and Technology*, *158*, 154–165. https://doi.org/10.1016/j.coldregions.2018.11.012

Walker, T. R. (2016a). Mercury concentrations in marine sediments near a former mercury cell chlor-alkali plant in eastern Canada. *Marine Pollution Bulletin*, *107*, 398–401.

Walker, T. R. (2016b). Mercury concentrations in marine sediments near a former mercury cell chlor-alkali plant in eastern Canada. *Marine Pollution Bulletin*, *107*(1), 398–401. https://doi.org/10.1016/j.marpolbul.2016.03.033

Walker, T. R., Lake, C. B., Hoffman, E., Lyons, J., Boxall, J., & Robertson, C. (2016). *Review of Metal(loid) Sediment Contamination in A'se'k (Boat Harbour)* (p. 39).

Wentworth, C. K. (1922). A Scale of Grade and Class Terms for Clastic Sediments. *The Journal of Geology*, *30*(5), 377–392. https://doi.org/10.1086/622910

Wilson, R. C. H., & Travers, I. C. (1976). *Mercury in the Atlantic provinces: A report to the Atlantic Regional Board Executive, Fisheries and the Environment Canada* (p. 49). Environment Canada, Environmental Services Branch, Environmental Protection Service.

YSI Incorporated. (2009). *YSI Professional Plus User Manual*. https://www.ysi.com/File%20Library/Documents/Manuals/605596-YSI-ProPlus-User-Manual-RevD.pdf

Appendix A : Additional Figures

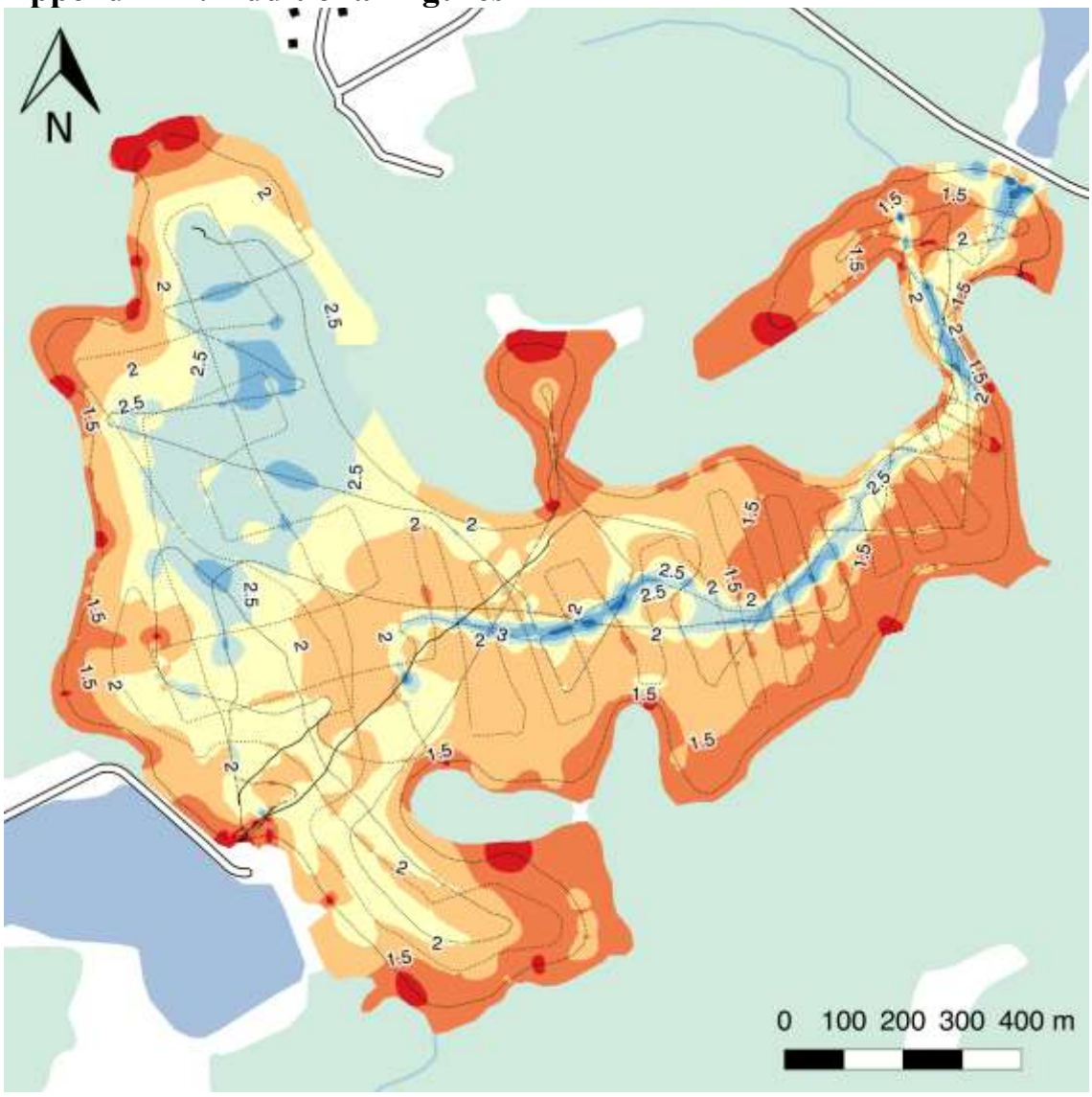

Figure 49: Bathymetric model of the BSHL (Spooner and Dunnington, 2017).

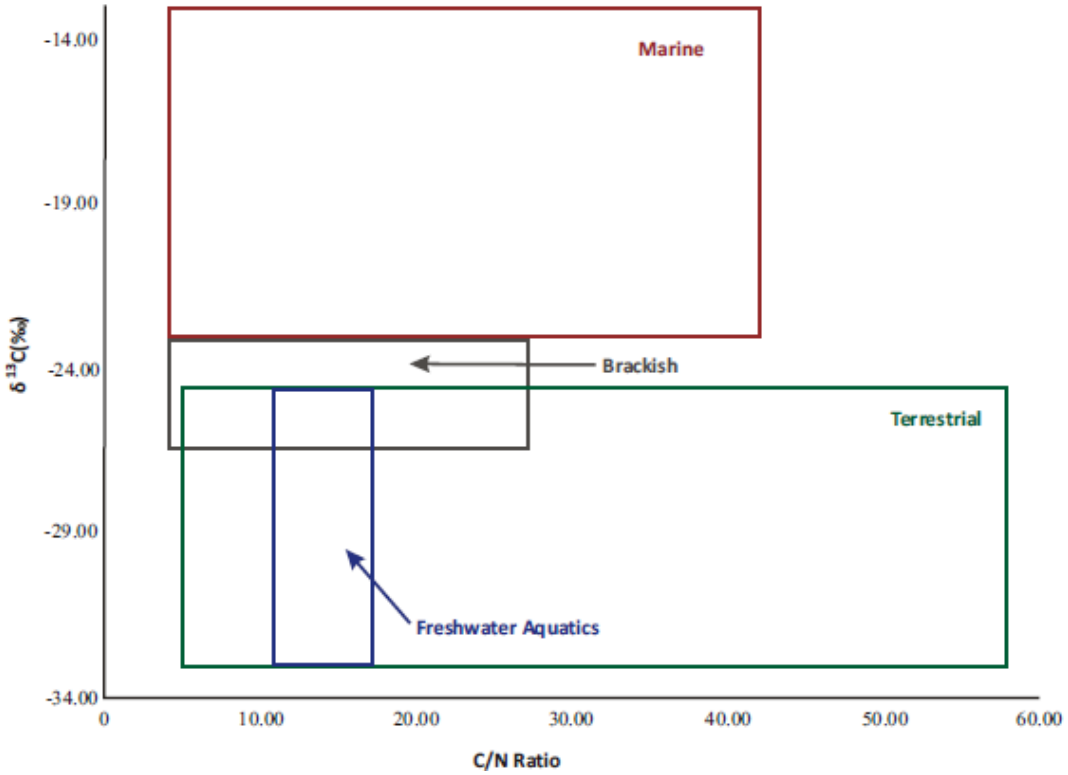

Figure 50: C/N ratio versus δ13C summary (Davidson, 2018; Galimov, 2012; Mackie et al., 2005; Meyers and Lallier-Vergès, 1999).

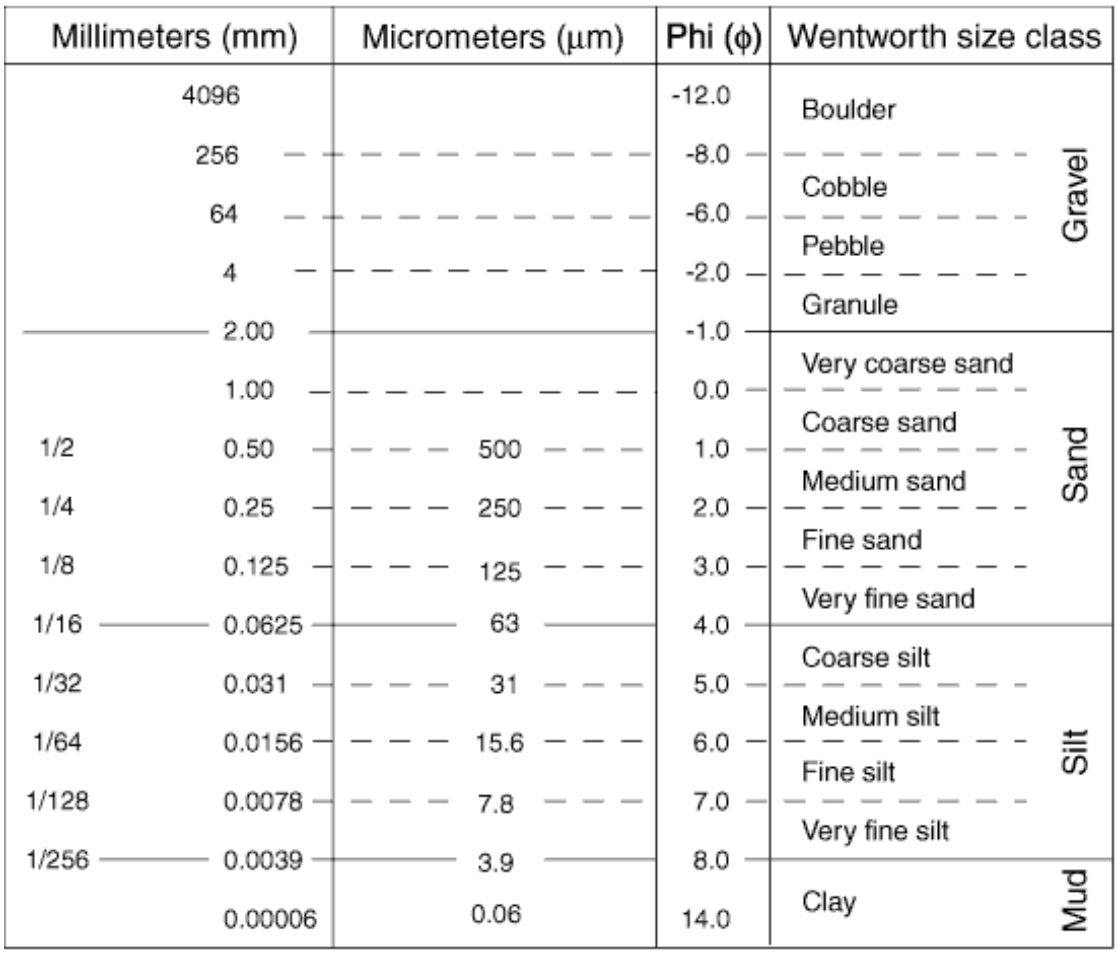

Figure 51: Wentworth classification system for sediment particle sizes (Wentworth, 1922).

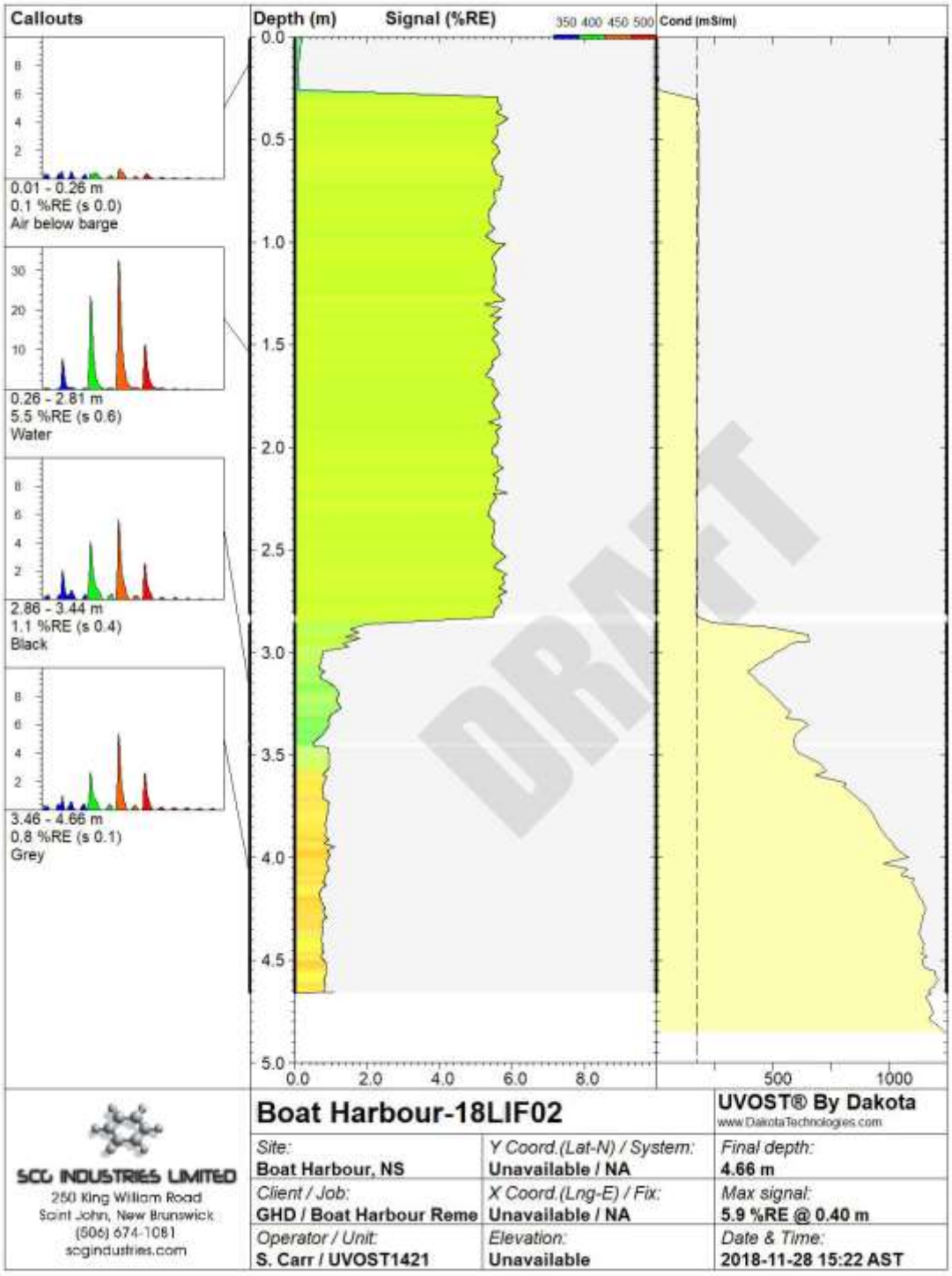

Figure 52: Boat Harbour18-LIF02.

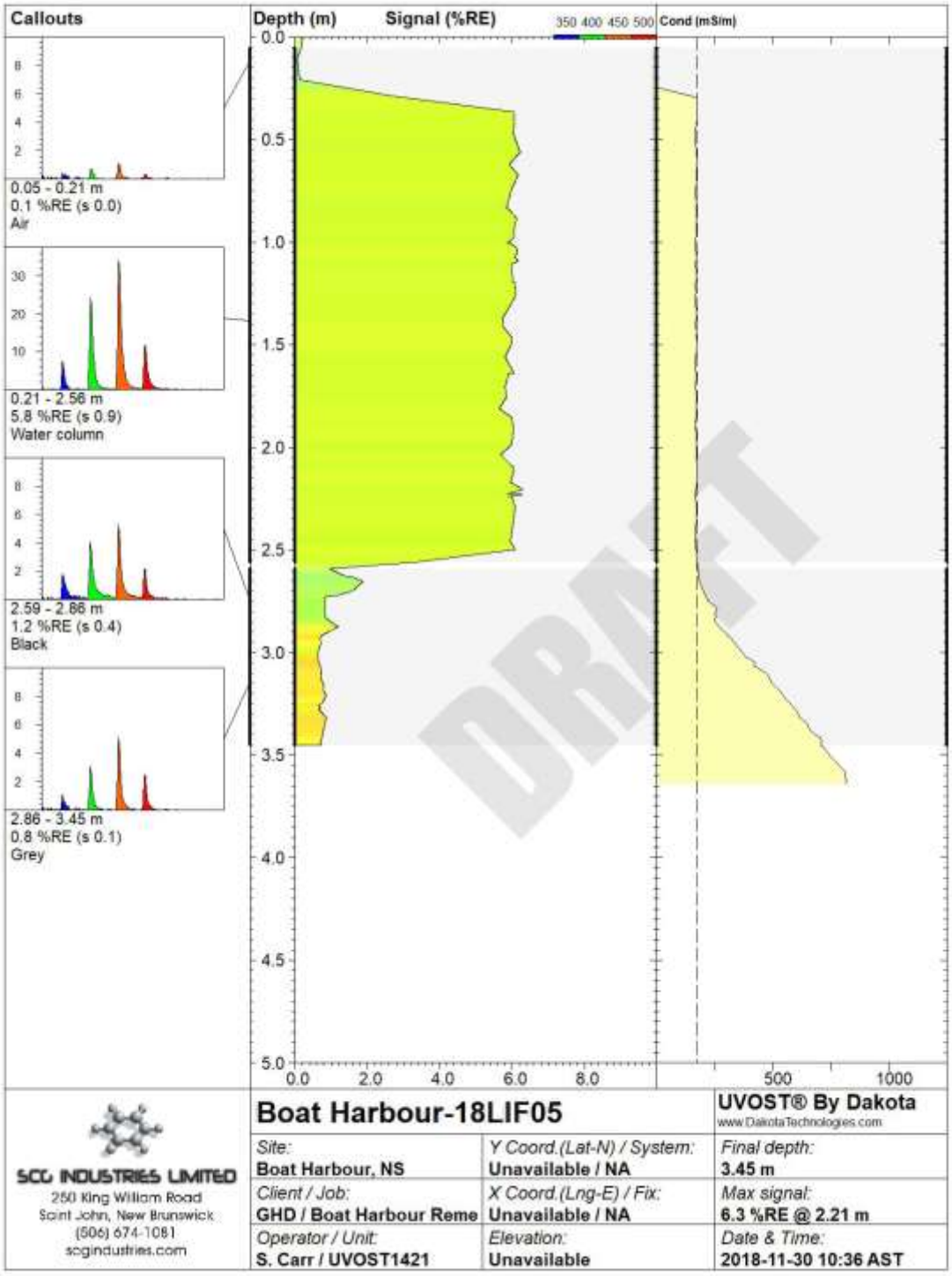

Figure 53: Boat Harbour18-LIF05.

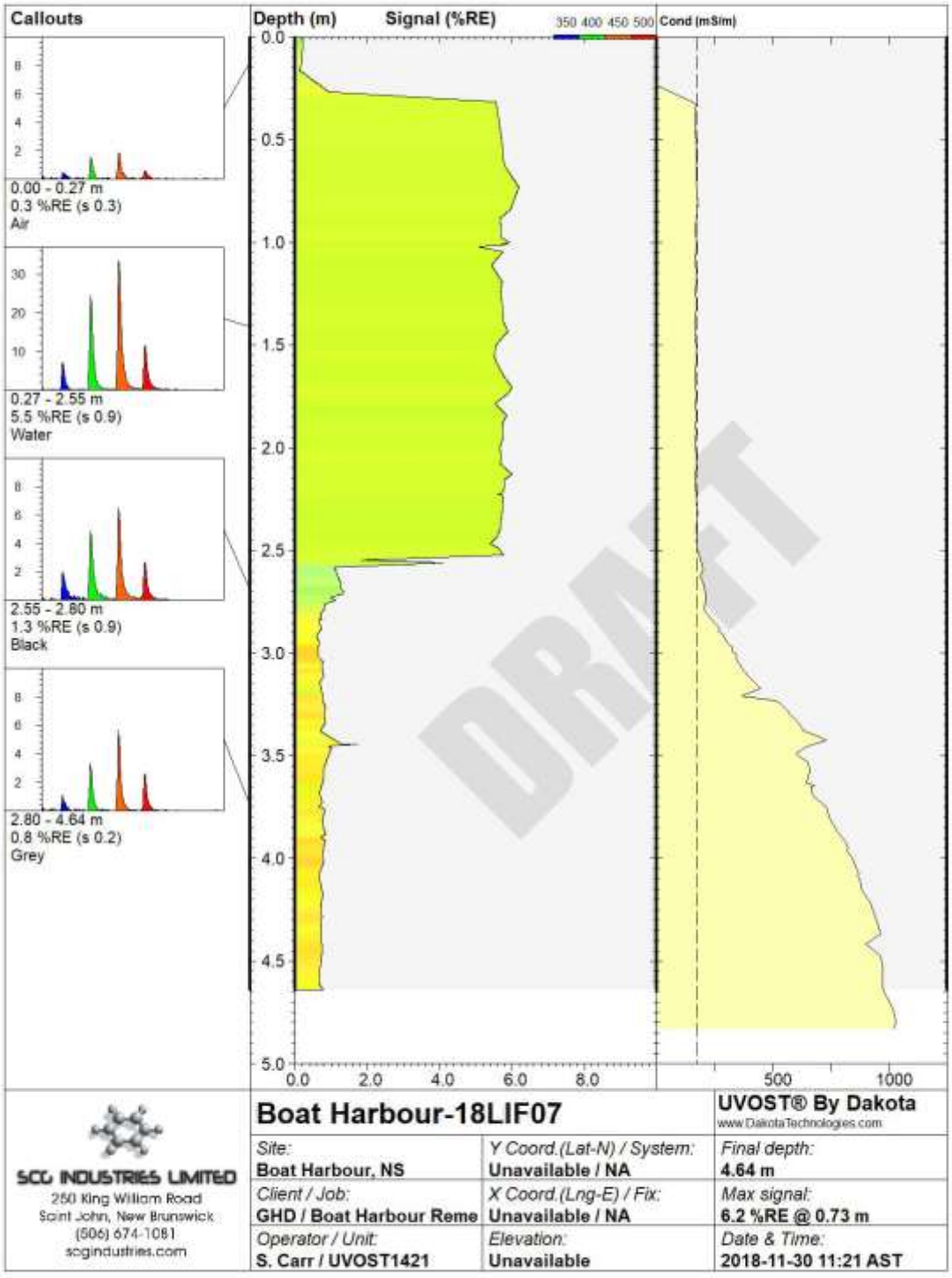

Figure 54: Boat Harbour18-LIF07.

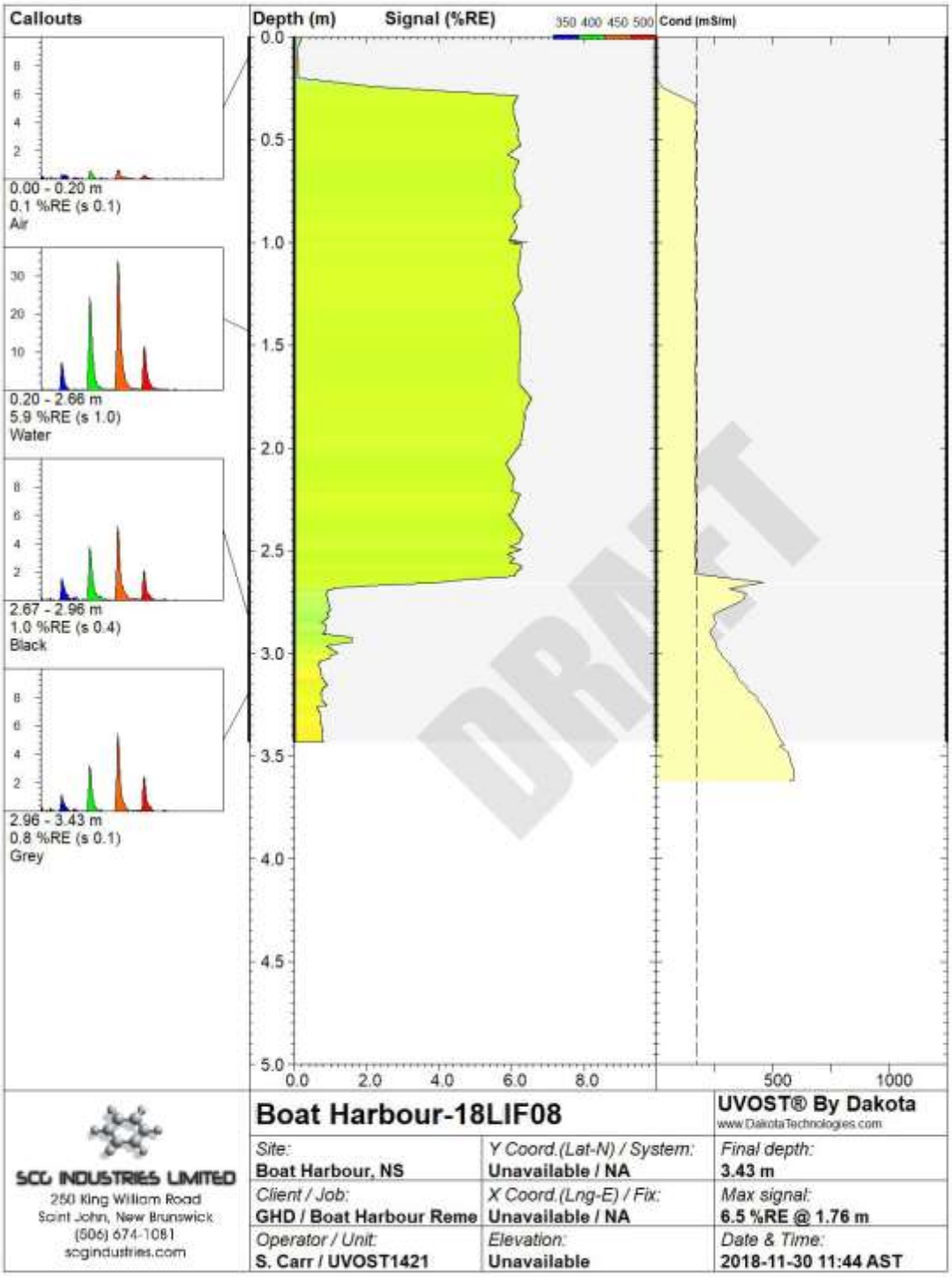

Figure 55: Boat Harbour18-LIF08.

Appendix B: Cluster Sample Datasets

Table 25: UVOST and sediment core identification of location chart (S1-S7, Figure 28).

Cluster	Lat.	Long.	Core	UVOST	Cluster sample I.D.
S1	526787	5056962	BHUV19-0001	19LIF01	1
	526785	5056957	BHUV19-0002	19LIF02	2
	526781	5056955	BHUV19-0003	19LIF03	3
	526783	5056939	BHUV19-0004	19LIF04	4
	526786	5056938	BHUV19-0005	19LIF05	5
	526787	5056945	BHUV19-0006	19LIF06	6
	526784	5056945	BHUV19-0007	19LIF07	7
	526778	5056944	BHUV19-0008	19LIF08	8
S2	527837	5056907	BHUV19-0009	19LIF09	1
	527841	5056906	BHUV19-0010	19LIF10	2
	527848	5056906	BHUV19-0011	19LIF11	3
	527845	5056912	BHUV19-0012	19LIF12	4
	527844	5056910	BHUV19-0013	19LIF13	5
	527839	5056909	BHUV19-0014	19LIF14	6
	527836	5056906	BHUV19-0015	19LIF15	7
	527843	5056908	BHUV19-0016	19LIF16	8
	527850	5056909	BHUV19-0017	19LIF17	9
	527846	5056912	BHUV19-0018	19LIF18	10
S3	527953	5056900	BHUV19-0019	19LIF19	1
	527962	5056903	BHUV19-0020	19LIF20	2
	527962	5056900	BHUV19-0021	19LIF21	3
	527956	5056909	BHUV19-0024	19LIF24	4
	527954	5056907	BHUV19-0025	19LIF25	5
	527952	5056903	BHUV19-0026	19LIF26	6
	527951	5056900	BHUV19-0027	19LIF27	7
	527957	5056900	BHUV19-0028	19LIF28	8
	527958	5056903	BHUV19-0029	19LIF29	9
S4	527315	5056692	BHUV19-0030	19LIF30	1
	527313	5056690	BHUV19-0031	19LIF31	2
	527313	5056686	BHUV19-0032	19LIF32	3
	527317	5056689	BHUV19-0033	19LIF33	4
	527322	5056690	BHUV19-0034	19LIF34	5
	527318	5056697	BHUV19-0035	19LIF35	6
	527315	5056697	BHUV19-0036	19LIF36	7
	527313	5056692	BHUV19-0037	19LIF37	8
	527315	5056689	BHUV19-0038	19LIF38	9
	527322	5056689	BHUV19-0039	19LIF39	10

Cluster	Lat.	Long.	Core	UVOST	Cluster sample I.D.
	527319	5056693	BHUV19-0040	19LIF40	11
	527316	5056697	BHUV19-0041	19LIF41	12
	527315	5056696	BHUV19-0042	19LIF42	13
	527321	5056685	BHUV19-0043	19LIF43	14
	526668	5056414	BHUV19-0046	19LIF46	15
S5	526648	5056488	BHUV19-0047	19LIF47	1
	526650	5056488	BHUV19-0048	19LIF48	2
	526651	5056491	BHUV19-0049	19LIF49	3
	526653	5056491	BHUV19-0050	19LIF50	4
	526654	5056495	BHUV19-0051	19LIF51	5
	526651	5056499	BHUV19-0052	19LIF52	6
	526650	5056498	BHUV19-0053	19LIF53	7
	526646	5056494	BHUV19-0054	19LIF54	8
	526649	5056492	BHUV19-0055	19LIF55	9
	526646	5056493	BHUV19-0056	19LIF56	10
	526644	5056493	BHUV19-0057	19LIF57	11
	526643	5056493	BHUV19-0058	19LIF58	12
	526644	5056493	BHUV19-0059	19LIF59	13
	526645	5056493	BHUV19-0060	19LIF60	14
	526645	5056491	BHUV19-0061	19LIF61	15
	526646	5056490	BHUV19-0062	19LIF62	16
	526646	5056488	BHUV19-0063	19LIF63	17
S6	526667	5056824	BHUV19-0064	19LIF64	1
	526668	5056820	BHUV19-0065	19LIF65	2
	526673	5056826	BHUV19-0066	19LIF66	3
	526673	5056826	BHUV19-0067	19LIF67	4
	526674	5056828	BHUV19-0068	19LIF68	5
	526674	5056828	BHUV19-0069	19LIF69	6
	526675	5056828	BHUV19-0070	19LIF70	7
	526676	5056829	BHUV19-0071	19LIF71	8
	526675	5056832	BHUV19-0072	19LIF72	9
	526671	5056832	BHUV19-0073	19LIF73	10
	526674	5056834	BHUV19-0074	19LIF74	11
	526671	5056831	BHUV19-0075	19LIF75	12
	526669	5056831	BHUV19-0076	19LIF76	13
	526665	5056839	BHUV19-0077	19LIF77	14
	526665	5056832	BHUV19-0078	19LIF78	15
	526663	5056830	BHUV19-0079	19LIF79	16
	526666	5056828	BHUV19-0080	19LIF80	17
	526667	5056827	BHUV19-0081	19LIF81	18
S7	526703	5057215	BHUV19-0082	19LIF82	1
	526702	5057214	BHUV19-0083	19LIF83	2

Cluster	Lat.	Long.	Core	UVOST	Cluster sample I.D.
	526708	5057211	BHUV19-0084	19LIF84	3
	526707	5057210	BHUV19-0085	19LIF85	4
	526705	5057207	BHUV19-0086	19LIF86	5
	526703	5057205	BHUV19-0087	19LIF87	6
	526701	5057205	BHUV19-0088	19LIF88	7
	526701	5057207	BHUV19-0089	19LIF89	8
	526699	5057209	BHUV19-0090	19LIF90	9
	526697	5057212	BHUV19-0091	19LIF91	10
	526699	5057212	BHUV19-0092	19LIF92	11
	526700	5057214	BHUV19-0093	19LIF93	12
	526703	5057216	BHUV19-0094	19LIF94	13
	526706	5057216	BHUV19-0095	19LIF95	14
	526708	5057211	BHUV19-0096	19LIF96	15
	526702	5057208	BHUV19-0097	19LIF97	16
	526698	5057207	BHUV19-0098	19LIF98	17
	526696	5057212	BHUV19-0099	19LIF99	18
	526705	5057215	BHUV19-0100	19LIF100	19

Table 26: UVOST and sediment core thickness and measurement difference results by cluster.

Core	LIF	Core Sediment Thickness (cm)	UVOST Sediment Thickness (cm)	Difference in reading (UVOST - gravity) (cm)
BHUV19-0001	19LIF01	44	46	**2**
BHUV19-0002	19LIF02	37	36	**-1**
BHUV19-0003	19LIF03	33	31	**-2**
BHUV19-0004	19LIF04	36	38	**2**
BHUV19-0005	19LIF05	34.5	35	**0.5**
BHUV19-0006	19LIF06	37	42	**5**
BHUV19-0007	19LIF07	35	36	**1**
BHUV19-0008	19LIF08	32.5	33	**0.5**
BHUV19-0009	19LIF09	24	24	**0**
BHUV19-0010	19LIF10	20.5	22	**1.5**
BHUV19-0011	19LIF11	16	18	**2**
BHUV19-0012	19LIF12	17	21	**4**
BHUV19-0013	19LIF13	15	17	**2**
BHUV19-0014	19LIF14	30	26	**-4**
BHUV19-0015	19LIF15	28	22	**-6**
BHUV19-0016	19LIF16	18.5	20	**1.5**
BHUV19-0017	19LIF17	16.5	16	**-0.5**
BHUV19-0018	19LIF18	15.5	21	**5.5**
BHUV19-0019	19LIF19	10	15	**5**
BHUV19-0020	19LIF20	9	8	**-1**

Core	LIF	Core Sediment Thickness (cm)	UVOST Sediment Thickness (cm)	Difference in reading (UVOST - gravity) (cm)
BHUV19-0021	19LIF21	8.5	11	**2.5**
BHUV19-0024	19LIF24	10	10	**0**
BHUV19-0025	19LIF25	10.5	8	**-2.5**
BHUV19-0026	19LIF26	9.5	7	**-2.5**
BHUV19-0027	19LIF27	9.8	11	**1.2**
BHUV19-0028	19LIF28	9.9	9	**-0.9**
BHUV19-0029	19LIF29	8	11	**3**
BHUV19-0030	19LIF30	8.5	13	**4.5**
BHUV19-0031	19LIF31	9	9	**0**
BHUV19-0032	19LIF32	15	32	**17**
BHUV19-0033	19LIF33	38	35	**-3**
BHUV19-0034	19LIF34	5.5	14	**8.5**
BHUV19-0035	19LIF35	7	9	**2**
BHUV19-0036	19LIF36	5.7	9	**3.3**
BHUV19-0037	19LIF37	10.4	10	**-0.4**
BHUV19-0038	19LIF38	33.3	26	**-7.3**
BHUV19-0039	19LIF39	9	10	**1**
BHUV19-0040	19LIF40	9	10	**1**
BHUV19-0041	19LIF41	10	7	**-3**
BHUV19-0042	19LIF42	7.6	16	**8.4**
BHUV19-0043	19LIF43	45	44	**-1**
BHUV19-0046	19LIF46	37	44	**7**
BHUV19-0047	19LIF47	36	37	**1**
BHUV19-0048	19LIF48	32	37	**5**
BHUV19-0049	19LIF49	30.8	30	**-0.8**
BHUV19-0050	19LIF50	31	32	**1**
BHUV19-0051	19LIF51	36.8	35	**-1.8**
BHUV19-0052	19LIF52	33	35	**2**
BHUV19-0053	19LIF53	35	36	**1**
BHUV19-0054	19LIF54	29.5	33	**3.5**
BHUV19-0055	19LIF55	33.4	35	**1.6**
BHUV19-0056	19LIF56	30	31	**1**
BHUV19-0057	19LIF57	32.5	31	**-1.5**
BHUV19-0058	19LIF58	26.6	31	**4.4**
BHUV19-0059	19LIF59	30	30	**0**
BHUV19-0060	19LIF60	30.2	34	**3.8**
BHUV19-0061	19LIF61	36	34	**-2**
BHUV19-0062	19LIF62	34	31	**-3**
BHUV19-0063	19LIF63	29	32	**3**
BHUV19-0064	19LIF64	33.6	32	**-1.6**
BHUV19-0065	19LIF65	33.2	36	**2.8**

Core	LIF	Core Sediment Thickness (cm)	UVOST Sediment Thickness (cm)	Difference in reading (UVOST - gravity) (cm)
BHUV19-0066	19LIF66	38.7	38	**-0.7**
BHUV19-0067	19LIF67	34	39	**5**
BHUV19-0068	19LIF68	34.8	35	**0.2**
BHUV19-0069	19LIF69	39	39	**0**
BHUV19-0070	19LIF70	36.6	36	**-0.6**
BHUV19-0071	19LIF71	37.2	38	**0.8**
BHUV19-0072	19LIF72	37.7	35	**-2.7**
BHUV19-0073	19LIF73	37	37	**0**
BHUV19-0074	19LIF74	35	35	**0**
BHUV19-0075	19LIF75	35.9	36	**0.1**
BHUV19-0076	19LIF76	33.5	28	**-5.5**
BHUV19-0077	19LIF77	33.2	34	**0.8**
BHUV19-0078	19LIF78	35.3	34	**-1.3**
BHUV19-0079	19LIF79	35.5	34	**-1.5**
BHUV19-0080	19LIF80	35	33	**-2**
BHUV19-0081	19LIF81	38.8	35	**-3.8**
BHUV19-0082	19LIF82	40	45	**5**
BHUV19-0083	19LIF83	44.7	54	**9.3**
BHUV19-0084	19LIF84	44	46	**2**
BHUV19-0085	19LIF85	48.5	48	**-0.5**
BHUV19-0086	19LIF86	43.5	42	**-1.5**
BHUV19-0087	19LIF87	44.1	47	**2.9**
BHUV19-0088	19LIF88	42	46	**4**
BHUV19-0089	19LIF89	43	45	**2**
BHUV19-0090	19LIF90	40	48	**8**
BHUV19-0091	19LIF91	40.3	44	**3.7**
BHUV19-0092	19LIF92	42.5	47	**4.5**
BHUV19-0093	19LIF93	38	39	**1**
BHUV19-0094	19LIF94	43.6	41	**-2.6**
BHUV19-0095	19LIF95	38	48	**10**
BHUV19-0096	19LIF96	37.4	37	**-0.4**
BHUV19-0097	19LIF97	42.4	40	**-2.4**
BHUV19-0098	19LIF98	42	44	**2**
BHUV19-0099	19LIF99	40	31	**-9**
BHUV19-0100	19LIF100	36	39	**3**

Appendix C: BH18-LIF01 Datasets

Table 27:Boat Harbour18LIF-01 UVOST log with wavelength measurements.

Boat Harbour18-LIF01						
			Wavelength channel (%RE)			
Medium	**Depth**	**Signal**	**Ch1: Blue**	**Ch2: Green**	**Ch3: Orange**	**Ch4: Red**
Air	0.0038	0.107	0.05	0.105	0.061	-0.109
	0.0475	0.213	0.037	0.098	0.092	-0.014
	0.0813	0.062	0.007	0.052	0.041	-0.039
	0.195	-0.001	-0.011	0.038	0.048	-0.075
	0.2682	0.103	0.021	0.063	0.054	-0.035
	0.2782	0.101	-0.008	0.073	0.049	-0.014
Water	0.2957	2.609	0.196	0.782	1.234	0.398
	0.2994	2.384	0.171	0.81	1.077	0.327
	0.3044	6.426	0.513	2.053	2.784	1.075
	0.3069	6.568	0.479	1.987	3.054	1.049
	0.3082	6.668	0.518	2.056	3.026	1.068
	0.3701	6.673	0.569	2.061	3.011	1.031
	0.4345	6.526	0.528	1.996	2.991	1.011
	0.5232	6.642	0.509	2.132	2.963	1.039
	0.6482	6.724	0.513	2.096	3.035	1.08
	0.6889	6.48	0.539	2.063	2.907	0.971
	0.7214	6.822	0.555	2.137	3.066	1.064
	0.8208	6.534	0.495	2.073	3	0.965
	0.8783	6.809	0.534	2.064	3.119	1.092
	0.9252	7.012	0.552	2.192	3.142	1.126
	0.9746	6.909	0.536	2.15	3.162	1.061
	1.0071	6.929	0.516	2.177	3.176	1.061
	1.0077	6.835	0.475	2.074	3.202	1.084
	1.0089	7.027	0.534	2.204	3.14	1.149
	1.0164	7.073	0.585	2.2	3.125	1.163
	1.0214	6.872	0.556	2.119	3.087	1.11
	1.0387	6.896	0.598	2.092	3.086	1.12
	1.0693	6.955	0.581	2.105	3.208	1.061
	1.0881	7.176	0.574	2.248	3.173	1.181

Boat Harbour18-LIF01						
			Wavelength channel (%RE)			
Medium	**Depth**	**Signal**	**Ch1: Blue**	**Ch2: Green**	**Ch3: Orange**	**Ch4: Red**
	1.11	6.813	0.522	1.965	3.25	1.075
	1.1112	6.816	0.561	1.979	3.166	1.109
	1.2256	6.89	0.56	2.17	3.14	1.02
	1.2944	7.053	0.532	2.241	3.174	1.107
	1.3319	6.93	0.555	2.161	3.181	1.033
	1.3794	6.903	0.541	2.204	3.088	1.07
	1.4038	6.977	0.602	2.112	3.128	1.136
	1.4432	6.731	0.533	2.039	3.118	1.041
	1.4819	6.913	0.526	2.077	3.226	1.084
	1.5088	6.745	0.554	2.144	3.027	1.021
	1.5232	6.741	0.549	2.119	3.107	0.965
	1.5944	6.751	0.569	2.076	3.095	1.011
	1.6132	6.553	0.495	2.089	2.981	0.988
	1.6695	6.493	0.501	2.062	2.859	1.072
	1.7107	6.665	0.514	2.042	3.152	0.957
	1.7332	6.922	0.536	2.2	3.182	1.004
	1.7901	6.83	0.559	2.117	3.202	0.952
	1.8257	6.825	0.585	2.117	3.041	1.082
	1.8951	7.1	0.544	2.187	3.299	1.071
	1.9414	7.107	0.571	2.181	3.207	1.148
	1.9539	6.855	0.595	2.181	3.098	0.983
	1.9689	6.727	0.499	2.109	3.086	1.033
	1.977	6.986	0.547	2.106	3.225	1.108
	1.997	6.663	0.504	2.034	3.109	1.016
	2.0545	6.691	0.531	1.979	3.159	1.022
	2.0739	6.697	0.53	2.052	3.055	1.06
	2.1383	6.854	0.548	2.111	3.122	1.073
	2.1527	7.045	0.566	2.222	3.131	1.126
	2.1646	6.72	0.516	2.192	2.998	1.015
	2.1814	7.111	0.592	2.231	3.182	1.107
	2.2008	7.041	0.586	2.154	3.169	1.132
	2.2096	6.967	0.561	2.176	3.191	1.039
	2.2127	6.941	0.572	2.031	3.163	1.175
	2.2133	6.895	0.539	2.115	3.158	1.082
	2.2352	6.909	0.524	2.212	3.128	1.045
	2.2377	6.938	0.557	2.102	3.235	1.045

Boat Harbour18-LIF01						
			Wavelength channel (%RE)			
Medium	**Depth**	**Signal**	**Ch1: Blue**	**Ch2: Green**	**Ch3: Orange**	**Ch4: Red**
	2.2383	6.788	0.53	2.079	3.093	1.086
	2.2402	6.785	0.555	2.051	3.095	1.084
	2.2481	7.077	0.592	2.144	3.193	1.149
	2.25	6.94	0.552	2.152	3.155	1.081
	2.2518	6.86	0.514	2.048	3.206	1.092
	2.3112	6.982	0.577	2.216	3.202	0.987
	2.3656	7.168	0.562	2.166	3.345	1.095
	2.4475	7.067	0.538	2.193	3.205	1.131
	2.4875	7.181	0.591	2.271	3.218	1.101
	2.5238	7.274	0.566	2.206	3.387	1.115
	2.5419	7.209	0.511	2.266	3.303	1.129
	2.5619	7.281	0.562	2.386	3.209	1.124
	2.6007	7.311	0.507	2.333	3.314	1.156
	2.6263	6.977	0.545	2.191	3.136	1.105
	2.645	7.108	0.583	2.232	3.221	1.072
	2.6713	7.056	0.601	2.238	3.166	1.051
	2.6975	7.068	0.56	2.163	3.222	1.124
	2.7288	7.29	0.588	2.228	3.306	1.166
	2.7463	7.316	0.548	2.173	3.374	1.222
	2.7719	7.295	0.574	2.257	3.351	1.112
	2.7988	7.098	0.602	2.21	3.154	1.132
	2.8144	6.999	0.587	2.197	3.149	1.066
	2.8363	7.013	0.507	2.224	3.163	1.12
BEIS	2.8638	3.076	0.333	1.024	1.281	0.437
	2.8813	6.337	0.524	2.022	2.836	0.955
	2.8938	6.884	0.557	2.152	3.11	1.064
	2.9026	6.142	0.455	1.991	2.779	0.916
	2.9107	4.989	0.423	1.583	2.237	0.746
	2.9251	3.43	0.306	1.066	1.554	0.504
	2.9438	1.572	0.178	0.508	0.683	0.204
	2.952	1.007	0.096	0.35	0.409	0.153
	2.9676	1.146	0.141	0.328	0.513	0.164
	2.9926	0.997	0.133	0.311	0.439	0.113
	3.0214	0.991	0.143	0.3	0.418	0.131
	3.042	1.033	0.156	0.354	0.399	0.124
	3.0714	0.948	0.125	0.326	0.417	0.08

Boat Harbour18-LIF01						
			Wavelength channel (%RE)			
Medium	**Depth**	**Signal**	**Ch1: Blue**	**Ch2: Green**	**Ch3: Orange**	**Ch4: Red**
	3.087	1.012	0.126	0.31	0.444	0.131
	3.1026	0.947	0.138	0.314	0.39	0.104
	3.1251	1.502	0.238	0.496	0.596	0.172
	3.1414	1.708	0.278	0.586	0.638	0.206
	3.162	2.15	0.359	0.756	0.732	0.304
	3.1789	2.126	0.33	0.778	0.717	0.302
	3.1876	1.886	0.346	0.678	0.64	0.222
	3.202	2.165	0.418	0.784	0.682	0.281
	3.2133	2.198	0.387	0.847	0.671	0.293
	3.2345	2.192	0.398	0.774	0.706	0.313
	3.2589	2.086	0.4	0.804	0.66	0.222
	3.2758	1.871	0.346	0.679	0.605	0.241
	3.2895	1.837	0.342	0.656	0.624	0.216
	3.3033	2.031	0.338	0.664	0.788	0.241
	3.3258	2.864	0.43	1.004	1.042	0.388
	3.3352	2.87	0.44	1.06	1.024	0.345
	3.3452	2.823	0.421	0.999	1.043	0.36
	3.3583	3.079	0.504	1.125	1.075	0.376
	3.3783	2.96	0.452	1.078	1.065	0.365
	3.3902	3.18	0.546	1.127	1.078	0.429
	3.4252	2.221	0.377	0.794	0.774	0.275
	3.4271	1.709	0.336	0.589	0.584	0.201
	3.4458	1.471	0.242	0.536	0.53	0.163
	3.4502	1.114	0.171	0.38	0.449	0.114
	3.4527	1.163	0.218	0.369	0.413	0.162
	3.4583	1.238	0.19	0.426	0.476	0.147
	3.4596	1.141	0.17	0.365	0.481	0.125
	3.4602	1.14	0.131	0.371	0.478	0.16
	3.4687	0.992	0.131	0.313	0.454	0.094
	3.47	0.937	0.101	0.331	0.402	0.104
	3.4712	1.073	0.115	0.356	0.469	0.133
	3.4725	1.015	0.136	0.305	0.423	0.151
GEIS	3.5137	0.864	0.085	0.256	0.404	0.119
	3.5531	0.967	0.079	0.275	0.479	0.135
	3.6031	0.929	0.074	0.247	0.441	0.166
	3.6494	0.765	0.052	0.224	0.38	0.109

Boat Harbour18-LIF01						
			Wavelength channel (%RE)			
Medium	**Depth**	**Signal**	**Ch1: Blue**	**Ch2: Green**	**Ch3: Orange**	**Ch4: Red**
	3.6806	0.877	0.075	0.25	0.415	0.137
	3.6994	0.754	0.066	0.236	0.347	0.105
	3.7313	0.88	0.049	0.242	0.441	0.148
	3.76	0.982	0.046	0.281	0.509	0.147
	3.7606	0.84	0.073	0.261	0.405	0.102
	3.8238	0.835	0.057	0.24	0.405	0.133
	3.855	0.777	0.053	0.199	0.403	0.123
	3.8869	0.925	0.062	0.261	0.47	0.133
	3.9207	0.865	0.04	0.255	0.451	0.118
	3.9444	0.844	0.049	0.226	0.417	0.152
	3.9694	0.946	0.081	0.284	0.42	0.161
	3.9913	0.881	0.06	0.271	0.409	0.141
	4.0132	1.002	0.089	0.286	0.469	0.157
	4.0369	0.911	0.066	0.229	0.45	0.165
	4.0563	0.874	0.074	0.258	0.419	0.124
	4.0876	0.887	0.056	0.246	0.448	0.137
	4.1163	0.853	0.06	0.242	0.42	0.13
	4.1282	0.879	0.088	0.251	0.429	0.111
	4.147	1.007	0.06	0.299	0.474	0.174
	4.1601	1.017	0.064	0.27	0.474	0.209
	4.1851	0.901	0.057	0.259	0.447	0.139
	4.212	0.93	0.052	0.271	0.433	0.173
	4.2257	0.881	0.082	0.228	0.432	0.14
	4.247	0.941	0.063	0.275	0.454	0.149
	4.2851	1.067	0.082	0.279	0.532	0.174
	4.3107	0.909	0.063	0.233	0.446	0.166
	4.337	1.076	0.069	0.294	0.517	0.197
	4.3608	1.014	0.095	0.268	0.488	0.163
	4.3895	0.915	0.07	0.269	0.453	0.123
	4.4139	0.825	0.053	0.233	0.405	0.135
	4.4376	0.923	0.057	0.226	0.473	0.167
	4.4539	0.884	0.041	0.258	0.447	0.139
	4.4764	1.003	0.074	0.26	0.49	0.179
	4.4977	0.991	0.074	0.28	0.448	0.188
	4.5164	1.003	0.081	0.234	0.507	0.18
	4.5352	0.898	0.055	0.252	0.419	0.172

Boat Harbour18-LIF01						
			Wavelength channel (%RE)			
Medium	**Depth**	**Signal**	**Ch1: Blue**	**Ch2: Green**	**Ch3: Orange**	**Ch4: Red**
	4.5489	0.98	0.053	0.291	0.474	0.162
	4.5595	0.907	0.067	0.251	0.449	0.141
	4.5702	0.946	0.031	0.273	0.496	0.147
	4.5783	0.951	0.052	0.248	0.489	0.162
	4.5871	0.899	0.049	0.243	0.481	0.126
	4.5952	0.901	0.051	0.233	0.478	0.139
	4.6052	0.91	0.056	0.244	0.461	0.148
	4.6171	0.843	0.054	0.238	0.431	0.12
	4.6202	0.842	0.063	0.201	0.447	0.131
	4.6321	0.908	0.043	0.247	0.44	0.177
	4.6433	0.904	0.055	0.226	0.467	0.157
	4.6539	0.92	0.059	0.25	0.451	0.161
	4.6796	0.778	0.027	0.243	0.387	0.12
	4.6808	0.763	0.048	0.218	0.375	0.122

Table 28: Boat Harbour18LIF-01 UVOST log electrical conductivity (EC) readings with depth.

Boat Harbour18-LIF01		
	Conductivity	
Medium	**EC Depth**	**EC Value**
Air	0.194	-4.533
	0.238	-2.36
	0.272	-3.447
Water	0.386	160.627
	0.459	159.555
	0.469	158.482
	0.486	159.555
	0.49	158.482
	0.495	157.41
	0.497	160.627
	0.499	159.555
	0.561	157.41
	0.625	157.41
	0.714	160.627
	0.839	161.7
	0.879	156.337
	0.912	159.555

Boat Harbour18-LIF01		
	Conductivity	
Medium	EC Depth	EC Value
	1.011	158.482
	1.069	156.337
	1.116	161.7
	1.165	157.41
	1.198	159.555
	1.198	158.482
	1.199	164.916
	1.207	157.41
	1.212	159.555
	1.229	161.7
	1.26	159.555
	1.279	157.41
	1.3	157.41
	1.302	157.41
	1.416	157.41
	1.485	159.555
	1.522	156.337
	1.57	157.41
	1.594	159.555
	1.634	159.555
	1.672	163.844
	1.699	159.555
	1.714	159.555
	1.785	157.41
	1.804	159.555
	1.86	155.264
	1.901	158.482
	1.924	159.555
	1.981	157.41
	2.016	157.41
	2.086	160.627
	2.132	157.41
	2.144	159.555
	2.159	158.482
	2.168	153.119
	2.188	157.41
	2.245	160.627

Boat Harbour18-LIF01		
	Conductivity	
Medium	**EC Depth**	**EC Value**
	2.264	156.337
	2.329	158.482
	2.343	157.41
	2.355	158.482
	2.372	159.555
	2.391	156.337
	2.4	161.7
	2.403	157.41
	2.404	153.119
	2.426	159.555
	2.428	156.337
	2.429	155.264
	2.431	156.337
	2.439	172.418
	2.44	159.555
	2.442	158.482
	2.502	158.482
	2.556	158.482
	2.638	159.555
	2.678	159.555
	2.714	156.337
	2.732	160.627
	2.752	157.41
	2.791	158.482
	2.817	160.627
BEIS	2.836	206.653
	2.862	271.65
	2.888	320.434
	2.919	340.527
	2.937	480.236
	2.962	473.969
	2.989	406.91
	3.005	391.138
	3.027	367.968
	3.054	354.256
	3.072	348.977
	3.084	348.977

Boat Harbour18-LIF01		
	Conductivity	
Medium	**EC Depth**	**EC Value**
	3.093	355.311
	3.101	355.311
	3.116	367.968
	3.134	376.399
	3.142	389.034
	3.158	407.961
	3.183	420.562
	3.212	456.194
	3.232	464.562
	3.262	464.562
	3.277	448.867
	3.293	445.725
	3.316	505.271
	3.332	503.187
	3.353	492.76
	3.369	493.803
	3.378	471.879
	3.393	469.789
	3.404	466.653
	3.425	496.932
	3.449	421.612
	3.466	469.789
GEIS	3.48	568.661
	3.494	580.055
	3.516	591.438
	3.526	604.876
	3.536	619.33
	3.549	632.736
	3.569	652.3
	3.581	653.328
	3.616	693.377
	3.618	694.402
	3.636	700.551
	3.641	711.814
	3.643	722.043
	3.649	729.198
	3.65	726.132

Boat Harbour18-LIF01		
	Conductivity	
Medium	EC Depth	EC Value
	3.651	728.176
	3.659	761.849
	3.66	765.924
	3.662	766.942
	3.663	764.905
	3.704	788.307
	3.744	810.646
	3.794	820.785
	3.84	865.287
	3.871	872.35
	3.89	879.409
	3.922	886.463
	3.951	906.592
	3.951	908.603
	4.014	940.726
	4.046	962.756
	4.077	978.749
	4.111	1005.684
	4.135	932.704
	4.16	1009.668
	4.182	1019.623
	4.204	1017.633
	4.227	1028.575
	4.247	1024.597
	4.278	1011.66
	4.307	974.753
	4.319	942.731
	4.337	1012.656
	4.351	1054.392
	4.376	1122.602
	4.402	1122.602
	4.416	1140.323
	4.437	1143.273
	4.476	1159.977
	4.501	1181.554
	4.528	1185.473
	4.551	1192.326

Boat Harbour18-LIF01		
	Conductivity	
Medium	EC Depth	EC Value
	4.58	1142.29
	4.604	1093
	4.628	1148.189
	4.644	1198.197
	4.667	1200.153
	4.688	1198.197
	4.707	1206.997
	4.726	1210.905
	4.739	1212.859
	4.75	1208.951
	4.761	1209.928
	4.769	1193.305
	4.778	1183.514
	4.786	1197.219
	4.796	1203.087
	4.808	1204.064
	4.811	1224.573
	4.823	1225.549
	4.834	1231.401
	4.844	1237.249
	4.87	1247.963
	4.871	1247.963